Arnold Schwarzenegger
Governor

THE USE OF A CLOUD PHYSICS AIRCRAFT FOR THE MAPPING OF POLLUTION AEROSOLS DETRIMENTAL TO WINTER OROGRAPHIC PRECIPITATION OVER THE CALIFORNIA SIERRA NEVADA

PIER PROJECT REPORT

Prepared For:
California Energy Commission
Public Interest Energy Research Program

Prepared By:
Woodley Weather Consultants
and
Dr. Daniel Rosenfeld

December 2005
CEC-500-2005-205

California Climate Change Center
Report Series Number 2005-021

Prepared By:

Dr. William L. Woodley, President
Woodley Weather Consultants
11 White Fir Court
Littleton, Colorado 80127

and

Dr. Daniel Rosenfeld, Professor
Department of Atmospheric Sciences
The Hebrew University of Jerusalem
Jerusalem, Israel

Contract No. 500-99-013

Prepared For:

California Energy Commission

Public Interest Energy Research (PIER) Program

Guido Franco,
Contract Manager

Kelly Birkinshaw,
Program Area Team Lead
Energy-Related Environmental Research

Martha Krebs, Ph.D.
Deputy Director
ENERGY RESEARCH AND DEVELOPMENT DIVISION

B. B. Blevins
Executive Director

Acknowledgements

The following individuals contributed greatly to the success of the research effort:

- Mr. Duncan Axisa of the Southern Ogallala Aquifer Rainfall (SOAR) Program, who ably served as flight meteorologist and meteorological technician for the SUPRECIP effort.
- Dr. David Prentice, M.D., who piloted the Cheyenne cloud physics aircraft throughout the program.
- Mr. Gary Walker, Manager of the SOAR program of the Sandyland Underground Water Conservation District and occasional pilot for the Cheyenne cloud physics aircraft.
- Crystal Reed of the Department of Atmospheric Sciences of Texas A&M University for her work with the DMA/TDMA instrument.
- The enthusiastic encouragement of Mr. Guido Franco, of the California Energy Commission's Public Interest Energy Research (PIER) program, is gratefully acknowledged.
- Dr. Masao Kanamitsu, Research Meteorologist of the Climate Research Division of the Scripps Institution of Oceanography of the University of California, San Diego, for providing the high-resolution California wind data presented in Figures 4, 7, and 12.

Please cite this report as follows:

Woodley Weather Consultants. 2005. *The Use of a Cloud Physics Aircraft for the Mapping of Pollution Aerosols Detrimental to Winter Orographic Precipitation over the California Sierra Nevada.* California Energy Commission, PIER Energy-Related Environmental Research. CEC-500-2005-205.

Preface

The Public Interest Energy Research (PIER) Program supports public interest energy research and development that will help improve the quality of life in California by bringing environmentally safe, affordable, and reliable energy services and products to the marketplace.

The PIER Program, managed by the California Energy Commission (Energy Commission), annually awards up to $62 million to conduct the most promising public interest energy research by partnering with Research, Development, and Demonstration (RD&D) organizations, including individuals, businesses, utilities, and public or private research institutions.

- PIER funding efforts are focused on the following RD&D program areas:
- Buildings End-Use Energy Efficiency
- Energy-Related Environmental Research
- Energy Systems Integration
- Environmentally Preferred Advanced Generation
- Industrial/Agricultural/Water End-Use Energy Efficiency
- Renewable Energy Technologies

The California Climate Change Center (CCCC) is sponsored by the PIER program and coordinated by its Energy-Related Environmental Research area. The Center is managed by the California Energy Commission, Scripps Institution of Oceanography at the University of California at San Diego, and the University of California at Berkeley. The Scripps Institution of Oceanography conducts and administers research on climate change detection, analysis, and modeling; and the University of California at Berkeley conducts and administers research on economic analyses and policy issues. The Center also supports the Global Climate Change Grant Program, which offers competitive solicitations for climate research.

The California Climate Change Center Report Series details ongoing Center-sponsored research. As interim project results, these reports receive minimal editing, and the information contained in these reports may change; authors should be contacted for the most recent project results. By providing ready access to this timely research, the Center seeks to inform the public and expand dissemination of climate change information; thereby leveraging collaborative efforts and increasing the benefits of this research to California's citizens, environment, and economy.

The work described in this report was conducted under The Use of a Cloud Physics Aircraft for the Mapping of Pollution Aerosols Detrimental to Winter Orographic Precipitation over the California Sierra Nevada contract, contract number 500-99-013, by Woodley Weather Consultants and Dr. Daniel Rosenfeld.

For more information on the PIER Program, please visit the Energy Commission's website www.energy.ca.gov/pier/ or contract the Energy Commission at (916) 654-5164.

Table of Contents

List of Figures

List of Tables

Abstract

Woodley Weather Consultants is engaged in a highly focused research effort for the Climate Change Research Subprogram of the Public Interest Energy Research (PIER) Program of the California Energy Commission to document and model the effects of urban and industrial air pollution in California on clouds, precipitation, and stream flows in mountainous terrain downwind of the pollution sources. An important component of the overall effort was the use of a cloud physics aircraft, based in Sacramento, California, during February and March 2005 to reach two objectives:

- Use a cloud physics aircraft to measure atmospheric aerosols in pristine and polluted clouds. Analyze these data to determine the impact of the aerosols on cloud-base microstructure, on the evolution with height of the cloud drop-size distribution, and on the development of precipitation under warm and mixed-phase processes.
- Validate the multi-spectral satellite inferences of cloud structure and the effect of pollutants on cloud processes—especially precipitation suppression.

The project

- documented the regional aerosols (including pollutants from urban and industrial sources) and the effects of these aerosols on cloud structure and behavior,
- suggested, based on the limited data, that cloud condensation nuclei (CCN) aerosols, on which cloud droplets form, constitute about 10% of the overall regional atmospheric aerosols,
- documented that the Sierra Nevada often receives precipitation from shallow pristine clouds as long as they do not ingest pollutants from the atmospheric boundary layer,
- demonstrated that high concentrations of tiny CCN aerosols inhibit precipitation when they are ingested from the boundary layer, due to either convective transport or orographic lift,
- validated the satellite inferences of cloud microstructure using the in-cloud measurements from the cloud physics aircraft on two days of measurement (February 7 and March 4, 2005), and
- verified that pollution aerosols are instrumental in altering the internal structure of the clouds and their resultant precipitation.

Thus, the aircraft component of the overall investigation showed the negative impact of pollutants on cloud processes and precipitation and made the linkages much more credible. Pollution is certainly affecting Sierra clouds and precipitation detrimentally.

Executive Summary

Introduction

Woodley Weather Consultants (WWC) is engaged in a highly focused, exploratory research effort for the Climate Change Research Subprogram of the Public Interest Energy Research (PIER) Program of the California Energy Commission. The purpose of this research is to document and model the effects of urban and industrial air pollution in California on clouds, precipitation, and stream flows in mountainous terrain downwind of the pollution sources. This research involves hydrological analyses, satellite-based cloud analyses and numerical modeling in order to obtain insights into the recently documented detrimental impacts of air pollution on precipitation in several locations in the world, most recently in California. Complicating this research is the knowledge that glaciogenic cloud seeding to enhance the snow pack has been underway over large portions of the California Sierra Nevada since the early 1950s. Thus, cloud seeding likely has confounded the assessment of pollution on precipitation. If seeding has enhanced the precipitation and runoff as intended, it would imply that the documented loss of precipitation due to pollution has been masked to some extent by the offsetting positive effects of cloud seeding. This apparently has been the case in Israel, where seeding has taken place for many years. If so, this would have serious ramifications for the management of water resources in California.

Purpose

An obvious focus of the overall investigation of the effect of pollution on Sierra Nevada winter precipitation ultimately must be on the nature and source of the pollutants that are apparently decreasing the orographic component of the precipitation over the portions of the Sierra Nevada that are climatologically downwind of known pollution sources such as the San Francisco/Oakland/San Jose metropolis and Southern California, including Los Angeles and San Diego. The pollution aerosols are apparently tiny cloud condensation nuclei (CCN) that result in a very narrow spectrum of small drops that inhibit precipitation-forming coalescence processes and ultimately the riming of ice crystals in the clouds. A program, called the Suppression of Precipitation (SUPRECIP) Experiment, was conducted during February and the first week in March 2005 from Sacramento, California, to provide the needed documentation. The number, sizes, and concentrations of ingested aerosols, and the resulting internal cloud microphysical structure, were documented.

Project Objectives

SUPRECIP had two objectives:

1. Use a cloud physics aircraft to measure atmospheric aerosols in pristine and polluted clouds. Analyze these data to determine the impact of the aerosols on cloud-base microstructure, on the evolution with height of the cloud drop-size distribution, and on the development of precipitation under warm and mixed-phase processes.
2. Use the cloud microphysical measurements to validate the multi-spectral satellite inferences of cloud structure and the effect of pollutants on cloud processes especially the suppression of precipitation.

The main precipitation suppression is postulated to occur during westerly flow that captures anthropogenic CCN that are incorporated in certain orographic clouds that form over the Sierra Nevada—those that are sufficiently shallow so that their tops do not fully glaciate before crossing the mountain crest.

This means that at least some of the water in these clouds remains in the form of cloud droplets that are not converted to precipitation (or at least ice hydrometeors) before crossing the divide, and hence re-evaporate and are lost to precipitation on the downwind side of the crest.

Project Outcomes

The weather during SUPRECIP was highly anomalous for the entire U.S. West Coast, consisting of dry conditions in the Pacific Northwest and flooding rains in Southern California. A high-pressure blocking pattern at the surface and aloft—and the resulting split in the jet-stream flow when it encountered the block—forced some of the weather disturbances to the north and northeast into Canada and Alaska, while some traveled southeastward under the blocking high to the Central and Southern California coast. This persistent region of low pressure under the block produced southerly and southeasterly winds and long periods of middle and high clouds over the Central and Northern Sierra for most of the project. The desired orographic clouds produced by the usual westerly winds into the Sierra were a rarity during SUPRECIP, and the program was extended through the first week in March 2005 in the hope of obtaining orographic storm events. Although the weather was a disappointment during SUPRECIP, much was learned in documenting the effect of pollutants on cloud microstructure and in validating the satellite inferences of cloud structure using the aircraft measurements and the concurrent radar depictions.

The Cheyenne cloud physics aircraft flew 21 flights in California, exclusive of the ferry flights to and from the state. Two flights were for the purposes of instrumentation calibration and the 19-flight balance were research flights. A total of 43 hours 26 minutes were expended during these flights out of a 70-hour flight allotment. Two flights were conducted on five of the 19 flight days, and two of the five were made during the one-week extension of the program into March 2005. Although the Cheyenne II cloud physics aircraft had its share of mechanical problems, no research flight opportunity was lost due to these problems. One research flight was terminated early, however, due to failure of the cloud droplet probe (CDP), which was repaired subsequently.

In addressing Objective 1, the project accomplished the following:

- Documentation of the regional aerosols, including pollutants from urban and industrial sources, and the effects of these aerosols on cloud structure and behavior.
- Demonstration that CCN aerosols, on which cloud droplets form, constitute about 10% of the overall regional atmospheric aerosols
- Documentation that the Sierra Nevada often receives precipitation from shallow clouds that remain pristine as long as they do not ingest pollutants from the atmospheric boundary layer.

- Demonstration that high concentrations of tiny CCN aerosols inhibit precipitation when they are ingested from the boundary layer because of either convective transport or orographic lift.

Despite the many accomplishments, Objective 1 under the contract was not reached fully due to two problems:

- Incomplete documentation of the aerosols in the atmospheric boundary layer, due to the near impossibility of obtaining clearance to conduct flight under instrument flight rules (IFR) in the boundary layer in the San Francisco/Oakland/Sacramento heavily populated urban and industrial areas. A second aircraft flying under visual flight rules (VFR) would have been necessary to obtain the needed documentation.
- The great lack of orographic cloud conditions over the California Sierra due to weak wind flow into the Sierra during virtually all of the period of flight operations. A longer period of operations would have been required to obtain the desired orographic clouds for study.

With respect to Objective 2, the satellite and aircraft inferences of cloud microstructure were made, in terms of the effective diameter. The satellite inferences were made for all of the cloud pixels within a series of boxes along the flight track. Each box was defined such that it encompassed some of the individual aircraft cloud passes. This strategy made it possible to compare the effective diameters for the cloud passes at the height and temperature of the pass with the satellite inferences of the effective diameters at the 50th percentile for the composite cloud for all clouds in the box. Considering the differences in scale (i.e., individual cloud passes vs. the composite cloud within a box that contains the cloud passes) and time, the agreement is remarkably good (linear correlation=0.73), giving increased credibility to the satellite inferences of suppressed precipitation-forming processes associated with pollution. For the purposes of this research effort, this is an extremely important finding.

In addressing Task 2, this project accomplished the following:

- Validation of the satellite inferences of cloud microstructure using the in-cloud measurements from the cloud physics aircraft on two days of measurement (February 7 and March 4, 2005).
- Verification that pollution aerosols are instrumental in altering the internal structure of the clouds and their resultant precipitation.

Despite these accomplishments, Objective 2 was not reached fully, because the sample was too small to justify a claim that the validity of the satellite inferences had been proved.

Conclusions

The use of the cloud physics aircraft has made possible the documentation of dramatic differences in cloud microstructure associated with differences in CCN, measured by the airborne CCN counter that were visibly related to air pollution. The research further determined that these differences were related to the satellite retrievals, which were validated by the aircraft measurements. This is crucial, because previously only the satellite retrievals

were available as indicators of the apparent negative effect of pollution on Sierra precipitation. The new aircraft measurements have provided further "ground truth" for the satellite inferences. Thus, the aircraft component of the overall investigation showed the negative impact of pollutants on cloud processes and precipitation and made the linkages much more credible. Pollution is certainly affecting Sierra clouds and precipitation detrimentally. Through the aircraft and satellite measurements in SUPRECIP it has been noted that much of the Sierra precipitation was produced by surprisingly shallow pristine clouds. This finding suggests that pollution will act detrimentally on such clouds and may help explain the long-term losses in Sierra orographic precipitation.

Recommendations

The results from SUPRECIP support the view that pollution is suppressing California orographic precipitation. Although much was accomplished, further investigation is needed, because it is impossible to characterize the problem in only a five-week measurement program. It is recommended that SUPRECIP be continued for a second year as SUPRECIP-2 in order to focus on the orographic storm events in the Sierra Nevada that were lacking in 2005. Specifically, it is crucial to document the ingestion of the pollution aerosols by the orographic clouds as they move uphill. The satellite imagery already says that this is taking place and the precipitation measurements show the long-term effects of the pollution. Because it was nearly impossible in 2005 to "map" the pollution aerosols at low levels in urban areas with the cloud physics aircraft on an IFR flight plan, it is recommended further that a second aircraft be used to carry the CCN counter for the mapping of the pollution aerosols at low levels during VFR flight. More attention must be focused on the details of the pollution "footprint" as to the sources, kinds and concentrations of the pollution aerosols and on what portions of the Sierra should be most affected by them.

Benefits to California

The California Sierra Nevada is apparently losing orographic precipitation and subsequent runoff because of the suppressive effects of fine pollution aerosols. If validated by this and ancillary research efforts, this finding ultimately will have serious consequences for California's water supply and hydroelectric power generation. Thus, resolving this issue will be highly beneficial to California, because it will be crucial to the development of informed public policy relating to future development and the resulting pollution. Resolution of this issue will also influence priority setting at the state and federal levels.

1.0 Introduction

1.1. Project Rationale

Woodley Weather Consultants (WWC) is engaged in a highly focused, exploratory research effort for the Climate Change Research Subprogram of the Public Interest Energy Research (PIER) Program of the California Energy Commission. The purpose of this research is to document and model the effects of urban and industrial air pollution in California on clouds, precipitation, and stream flows in mountainous terrain downwind of the pollution sources. This research involves hydrological analyses, satellite-based cloud analyses and numerical modeling in order to obtain insights into the recently documented (Givati and Rosenfeld, 2004a) detrimental impacts of air pollution on precipitation in several locations in the world, most recently in California. Complicating this research is the knowledge that glaciogenic cloud seeding to enhance the snowpack has been under way over large portions of the California Sierra Nevada since the early 1950s. Thus, cloud seeding likely has confounded the assessment of pollution on precipitation. If seeding has enhanced the precipitation and runoff as intended, it would imply that the documented loss of precipitation due to pollution has been masked to some extent by the offsetting positive effects of cloud seeding. This apparently has been the case in Israel (Givati and Rosenfeld, 2004b), where seeding has taken place for many years. If so, this would have serious ramifications for the management of water resources in California. Consequently, the separation of the offsetting effects of pollution on precipitation from those due to cloud seeding must ultimately be a focus of this research effort.

An obvious focus of the overall investigation of the effect of pollution on Sierra Nevada winter precipitation ultimately must be on the nature and source of the pollutants that are apparently decreasing the orographic component of the precipitation over the portions of the Sierra Nevada that are climatologically downwind of known pollution sources such as the San Francisco/Oakland/San Jose metropolis and the Southern California basin, including Los Angeles and San Diego. The pollution aerosols are apparently tiny cloud condensation nuclei (CCN) that result in a very narrow spectrum of small drops that inhibits precipitation-forming coalescence processes and ultimately the riming of ice crystals in the clouds. The Suppression of Precipitation (SUPRECIP) Experiment was conducted during February and the first week in March 2005 from Sacramento, California, to provide the needed documentation. The number, sizes, and concentrations of ingested aerosols and the resulting internal cloud microphysical structure were documented.

SUPRECIP was conducted under the umbrella of Woodley Weather Consultants (WWC), which specializes in weather modification studies, with the participation of Professor Daniel Rosenfeld, the Southern Ogallala Aquifer Rainfall (SOAR) program, and Dr. Don Collins. Professor Rosenfeld, of the Hebrew University of Jerusalem in Jerusalem, Israel, is known worldwide for his pioneering studies of the effects of pollutants on clouds. The Southern Ogallala Aquifer Rainfall (SOAR) program, which is managed by the Sandy Land Underground Water Conservation District in Plains, Texas, provided the Cheyenne II, turbo-prop, cloud-physics aircraft, a pilot (Dr. David Prentice, M.D.) and flight meteorologist Duncan Axisa. Dr. Don Collins works at the Atmospheric Aerosol Research Group within the Department of Atmospheric Sciences at Texas A&M University.

1.2. Objectives

SUPRECIP had two objectives: (1) to use a cloud physics aircraft to measure atmospheric aerosols in pristine and polluted clouds, and analyze these data to determine the impact of the aerosols on cloud-base microstructure, on the evolution with height of the cloud drop-size distribution, and on the development of precipitation under warm and mixed-phase processes; and (2) to use the cloud microphysical measurements to validate the multi-spectral satellite inferences of cloud structure and the effect of pollutants on cloud processes—especially precipitation suppression.

The main precipitation suppression is postulated to occur during westerly flow (anywhere from southwesterly to northwesterly) that captures anthropogenic CCN that are incorporated in certain orographic clouds that form over the Sierra Nevada—those that are sufficiently shallow so that their tops do not fully glaciate before crossing the mountain crest. This means that at least some of the water in these clouds remains in the form of cloud droplets that are not converted to precipitation (or at least ice hydrometeors) before crossing the divide, and hence re-evaporate and are lost to precipitation on the downwind side of the ridge. Such conditions prevail mainly in post frontal conditions. The cloud depth gradually decreases after the frontal passage, producing a sequence of cloud depths and natural precipitation efficiencies that should be sampled extensively during the few such synoptic situations that are expected to occur.

2.0 Project Context, Tools, and Flight Procedures

2.1. Project Context

The context and rationale for SUPRECIP is embodied in the processed satellite image at 2050 Greenwich Mean Time (GMT) (1250 PST) on 7 December 2003 (Figures 1a, 1b, and 1c), which shows in three panels the post-frontal cloud field over most of California on this day. The clouds in the image have been "colorized" according to the inputs from the three sensor channels (i.e., visible, 3.7 microns, and infrared) using the method of Rosenfeld (Rosenfeld and Lensky, 1998) as explained in Appendix A. The brightest clouds have the most red, the clouds with the smallest drops have the most green, and the warmest clouds have the most blue. By combining the inputs from the three channels quantitatively, the clouds receive a resultant color.

Thus, very bright (high red) clouds having relatively large particles (no green) and cold (no blue) cloud tops will appear red (i.e., red + no green + no blue = red). On the other hand, relatively bright (some red) clouds with small particles (some green) and relatively warm (some blue) cloud tops will appear yellow-green to orange. One can think of many other color possibilities depending on the input from the three channels—all of this is solely for visualization. Thus, clouds downwind of major pollution sources appear more yellow-orange with some green than those clouds that are downwind of more pristine areas, because the ingested pollution decreases the droplet sizes and the resultant precipitation.

The plots of the "effective radius" (r_e) (the X axis) as a function of temperature (T) (the Y axis) shown in the insets allow a much more quantitative analysis of the apparent effects of pollution on the clouds. The underlying crucial assumption in generating these plots is that the microphysical evolution of a convective cloud can be represented by the composition of the instantaneous values of the tops of convective clouds at different heights or temperatures. This assumption is based on the knowledge that cloud droplets form mainly at the base of convective clouds, and grow with increasing height or decreasing T. The form of dependence of r_e on T contains important information about the cloud and precipitation processes, as explained in Appendix A. The T-r_e relations are obtained from an ensemble of clouds having tops covering a large range of T. Usually many pairs of T-r_e for each 1˚C interval are observed in a region containing a convective cloud cluster. The points with smaller r_e for a given T are typically associated with the younger cloud elements; whereas the larger r_e for the same T are associated with the more mature cloud elements, in which the droplet growth has had more time to progress by coalescence, and ice particles have had more time to develop. Therefore, it is useful to plot not only the median value of T-r_e relation, but also in perhaps 10 percentiles for representing the younger and more mature cloud elements within the measurement region.

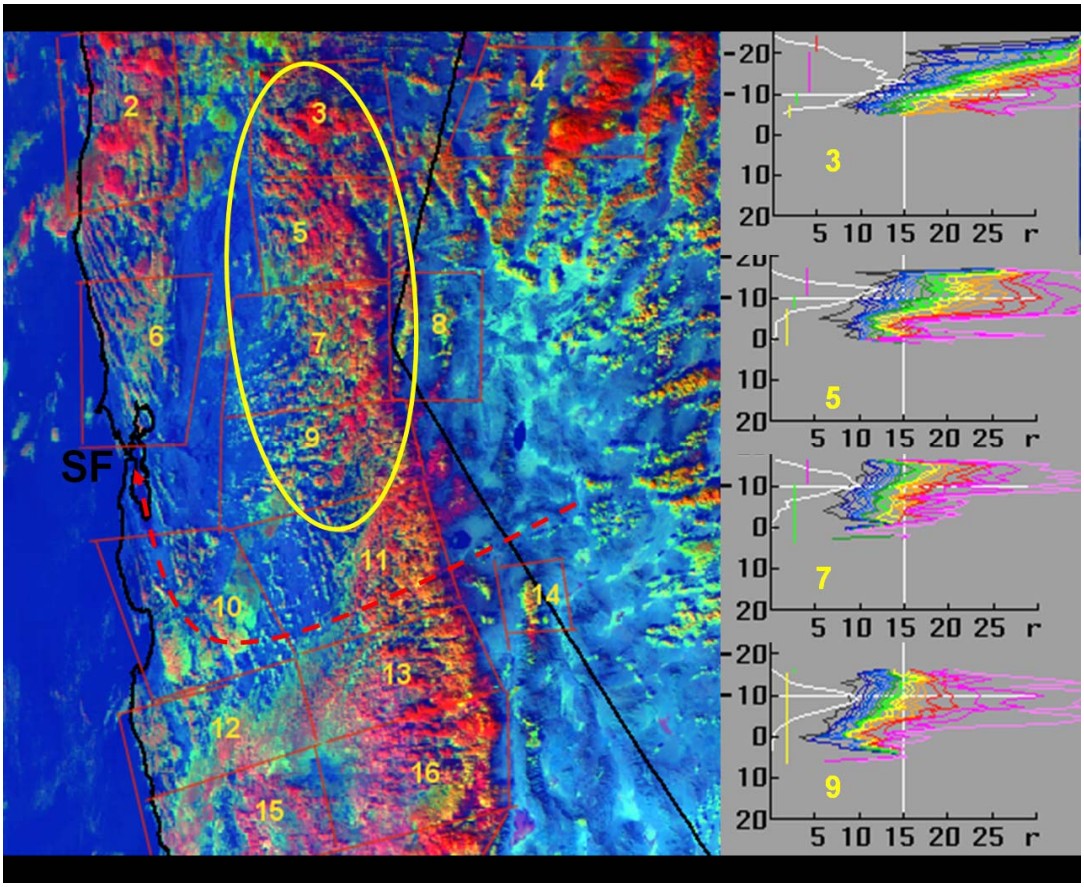

Figure 1a. Processed satellite image at 2050 GMT (1250 PST) on 7 December 2003

Each numbered plot in the insets corresponds to the same number in the colorized image. To generate each plot, the satellite pixels in each numbered area were viewed, giving hundreds to thousands of values, depending on the size of the area. The effective radius results were then presented in percentile intervals from 0% to 10%, 11% to 20%, 21% to 30%, etc. as a function of temperature, as shown by the family of plots in each inset. The colors of the lines in the insets have no relation to the various colors in the satellite image, but have been selected merely for visualization purposes. Thus, the median plot is at the interface of the yellow and green lines. When the family of lines is shifted to the left in the plot, it means that the clouds had rather small particles that grew slowly with decreases in temperature. In some cases the effective radius does not reach the threshold for precipitation (the vertical white line at 15 microns) until very cold temperatures. On the other hand, there are some families of curves for some areas that are shifted to the right at rather warm temperatures, with much of their plot values exceeding the 15-micron (μm) precipitation threshold. The short vertical colored lines on the left in each inset are the microphysical zones as defined by Rosenfeld and Lensky (1998), and the second white line on the extreme left gives the sample size as a function of temperature.

To put the California flight program into a proper context, it is important to examine Figures 1a–c in greater detail—especially the inset plots for the various California areas depicted in the image on 7 December 2003. Working from north to south through areas 3 to 9, note that the r_e

percentile plots move progressively to the left in each inset, indicating increasingly smaller drops sizes as one approaches the latitude of Sacramento and San Francisco. These changes in the clouds may be attributable to the increasing pollutants downwind of these major metropolitan areas.

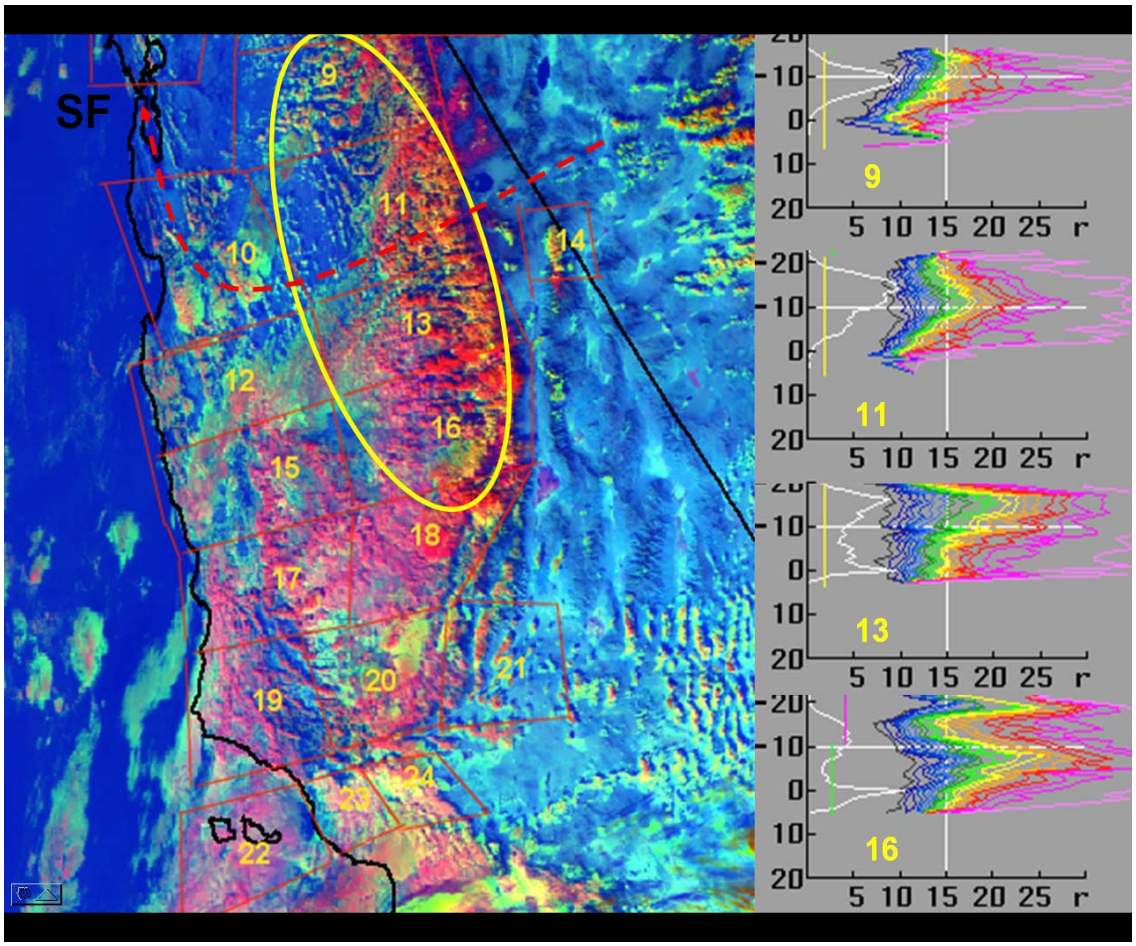

Figure 1b. Processed satellite image at 2050 GMT (1250 PST) on 7 December 2003, focusing on Central California

The plot for area 11 is similar to the plot for area 9 (Figure 1b). Farther south of the latitude of the Bay Area in areas 13 through 18, however, the curves move back to the right, indicating progressively larger drop sizes, indicating less ingested pollution. Looking at the insets for areas 16 and 18, however, note that the yellow and green lines are mostly to the right of the vertical white line that corresponds to the 15 μm precipitation threshold. Thus, the clouds over the Southern Sierra Nevada region that is downwind (i.e., east) of the lightly populated (relatively speaking) coastal region are precipitating. Upon moving farther southward, however, toward the latitude of more heavily populated Southern California, note that the insets for areas 20 and 24 show the yellow-green interface (median effective radius plots as a function of temperature) moving well to the left of the 15 μm precipitation threshold (Figure 1c).

This is true especially for area 24, which corresponds to the mountains to the northeast and east of metropolitan Los Angeles. The clouds in area 24 in the image itself are mostly yellow, indicating highly inefficient precipitation processes. The clouds here are not precipitating.

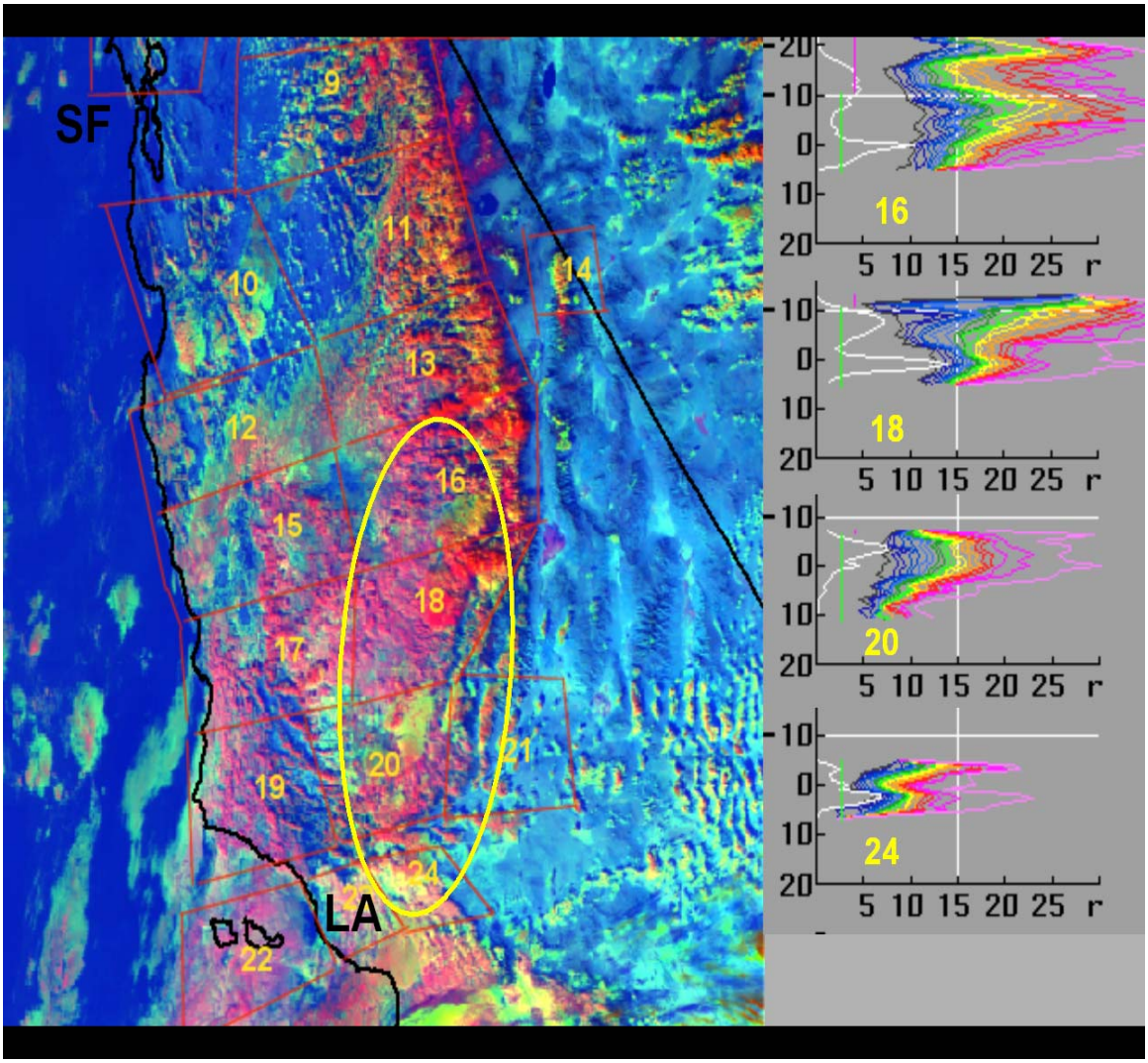

Figure 1c. Processed satellite image at 2050 GMT (1250 PST) on 7 December 2003, focusing on Southern California

The weather situation associated with the satellite images in Figure 1a–c is illustrated in Figure 2, which presents the initial weather conditions for the Medium-Range Forecast (MRF) global model run at 0000 UT on December 8, 2005. The upper left panel has the 850 millibar (mb) wind, temperature, and contour fields; and the upper right panel contains the height and wind fields at 300 mb. The lower left panel is the surface pressure map with 1000 to 500 mb thickness contour superimposed, and the lower right panel gives contours of mean 850 to 500 mb relative humidity and the Lifted Index. Although the upper left panel has the 850 mb winds, they cannot be seen in the figure. To remedy this deficiency, this panel was enlarged and displayed in Figure 3. The view of the wind vectors here is only slightly improved.

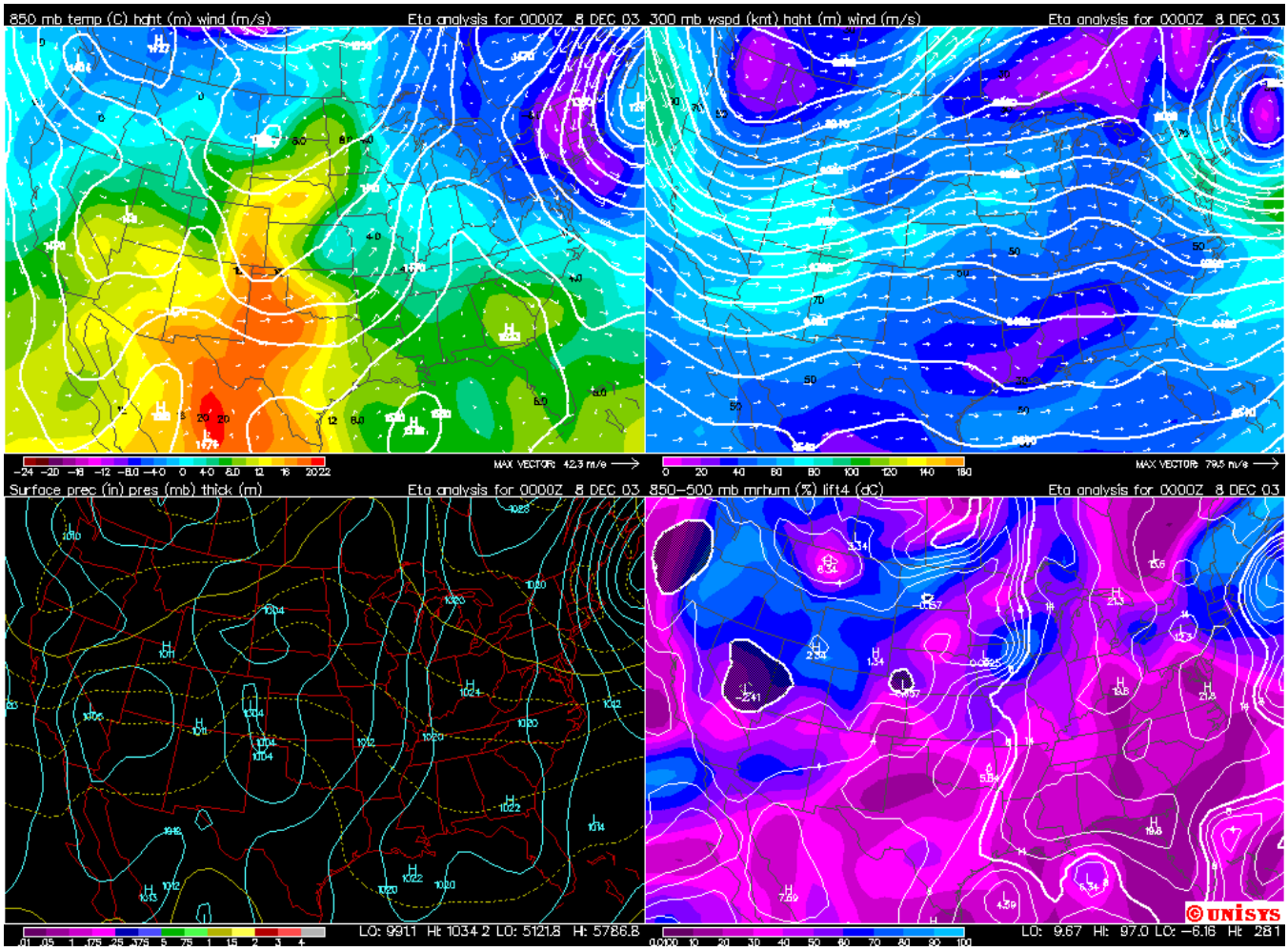

Figure 2. Documentation of the initial weather conditions for the 0000 GMT run of the Eta forecast model

Upon examination of the wind field, it can be seen that the winds were northwesterly in Northern California, and westerly from roughly the latitude of Lake Tahoe southward to the Mexican border. This wind field would have carried the pollutants in the boundary layer (BL) from the heavily urbanized areas to the southeast and east into the Sierra Nevada Mountains in a pattern that is consistent with the cloud microphysical changes evident in the processed satellite imagery of Figure 1a–c. A much closer look at the wind field at 0000 GMT on December 8, 2003 is given in Figure 4, which was provided by Dr. Masao Kanamitsu from the CaRD10 (California Reanalysis Downscaling at 10 km) product (see Kanamitsu, 2005a,b). The depiction again shows northwesterly flow in Northern California, backing to westerly flow in Central and Southern California. This flow pattern would leave Northern California free of pollution, but it would carry the pollutants from the heavily urbanized and industrialized regions into the central and southern Sierra. This pattern is consistent with what was seen in the clouds. Again, this suggests that the reduction of orographic precipitation may be caused by the pollution, serving as numerous small CCN, that increase the cloud droplet concentration, and

subsequently suppress the precipitation by slowing down the coalescence, ice crystal production, and their riming processes.

One case does not prove the effect of pollution on rainfall. PIER is conducting much more analysis to pin this down. The SUPRECIP flight program is an integral component of these investigations. The cloud physics aircraft has been used to measure cloud structure, especially the cloud droplet distribution, for the comparisons with satellite inferences of cloud microstructure, such as those shown in Figure 1a–c. The primary purpose of SUPRECIP, therefore, is to validate the indications of precipitation suppression from the satellite imagery.

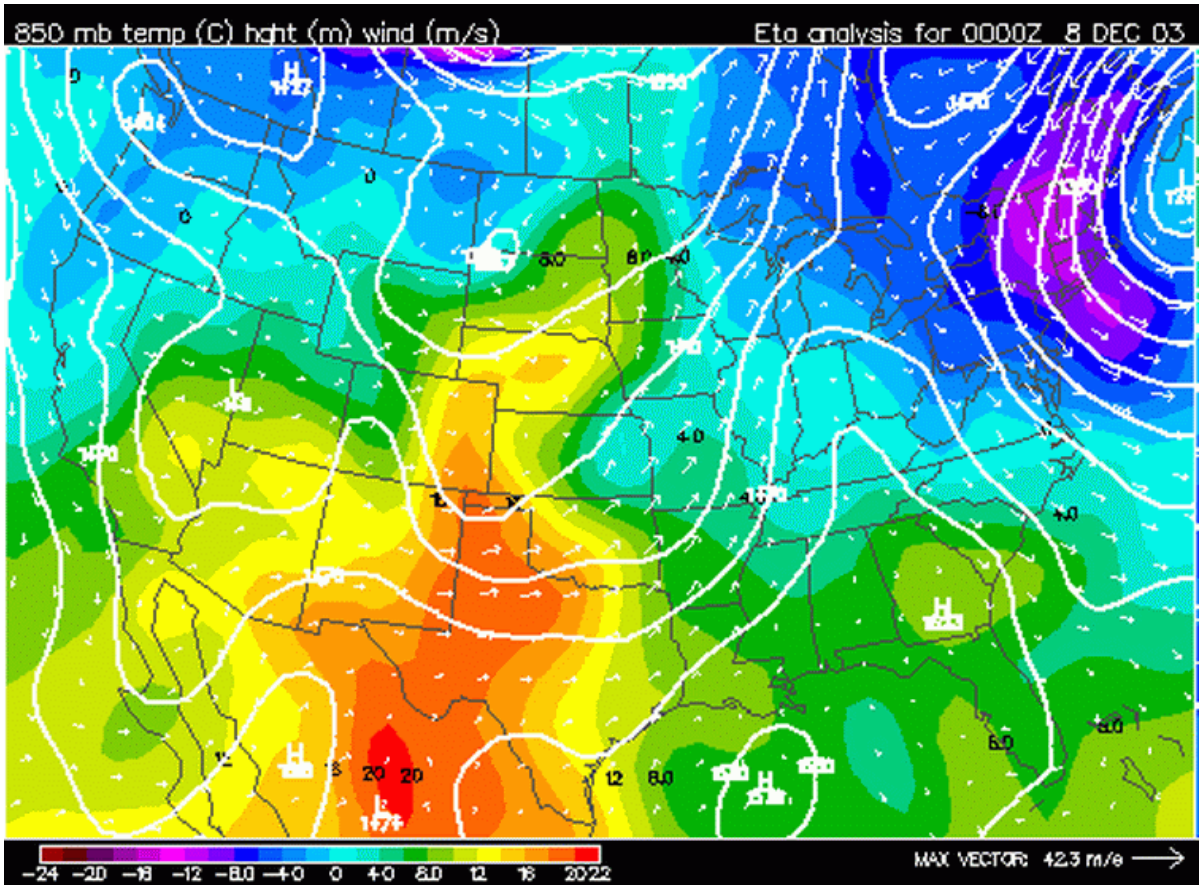

Figure 3. The 850 mb height, temperature contours, and wind field at 0000 GMT on 8 December 2003 that served as input to the Eta forecast model

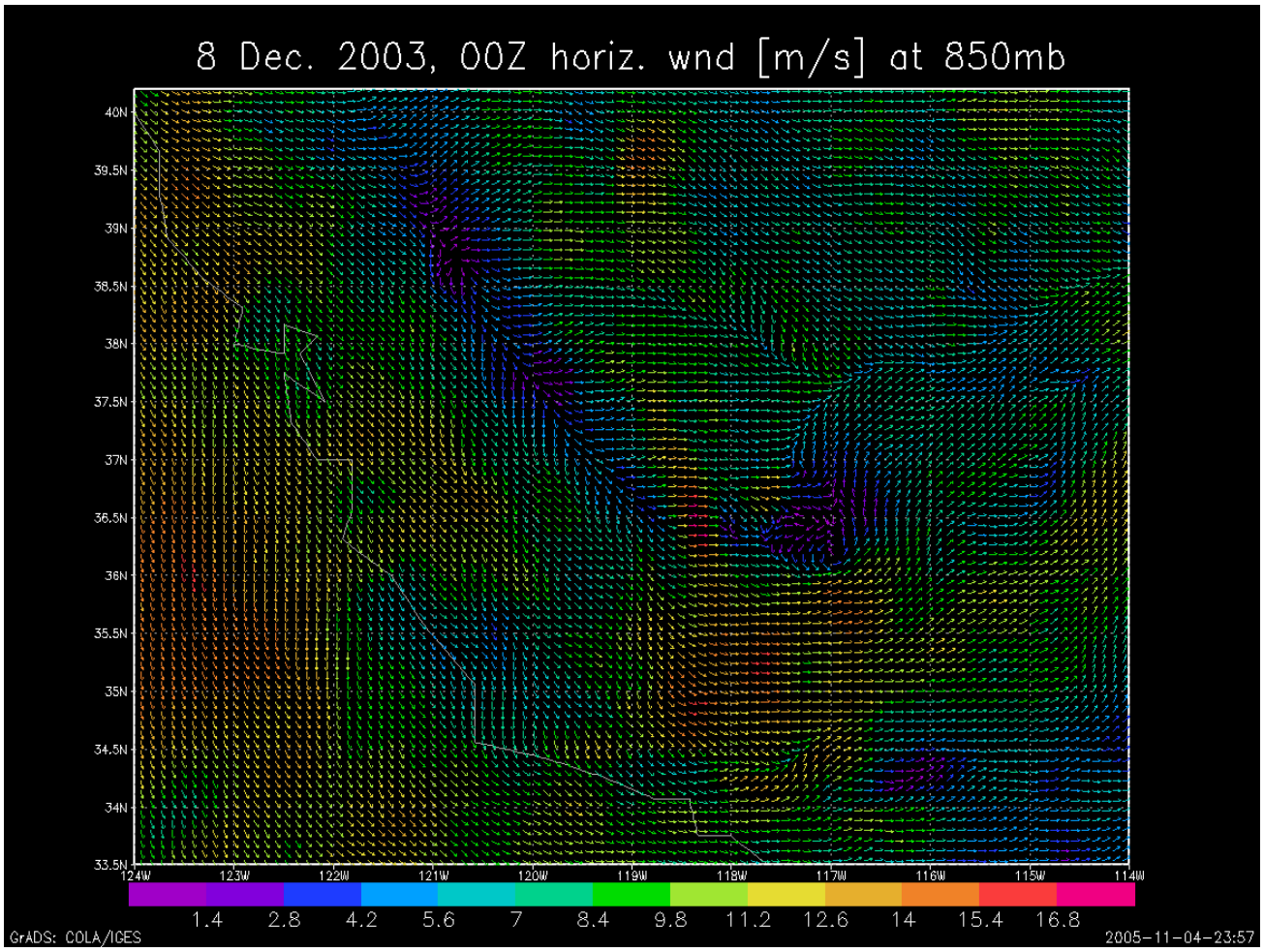

Figure 4. The 850 mb wind field (m s^{-1}) at 10 km resolution at 0000 GMT on December 8, 2003, as provided from the CaRD10 product by Dr. Masao Kanamitsu of the Climate Research Division of the Scripps Institution of Oceanography of the University of California, San Diego. The color coding gives the wind speeds in m s^{-1}. Note that the wind speeds drop to zero in the portions of the Sierra above the 850 mb pressure level.

The example given in Figures 1a–c is but one example of the many applications of the Rosenfeld satellite methodology since its published documentation in 1998 (Rosenfeld and Lensky, 1998). Among the original motivations for its derivation was to provide a research component for the Texas operational cloud-seeding programs (Bomar et al., 1999), to identify seeding opportunities, to document microphysical seeding signatures (Woodley et al., 2000), and to quantify microphysical partitions for the analysis for seeding effects (Woodley and Rosenfeld, 2004).

It was not long, however, before the method was being used to document the worldwide suppressive effect of natural (Rosenfeld, 1999) and anthropogenic (Rosenfeld, 2000) pollution and desert dust (Rosenfeld et al., 2001) on cloud microstructure and rainfall. The method has been used also to document that, when salt from evaporating sea spray is ingested into polluted clouds, their rain-forming processes are restored gradually and they are cleansed ultimately of their pollution burden (Rosenfeld et al., 2002; Rudich et al., 2002). In addition, a current focus is on the climate implications of the suppressive effect of pollution on rainfall and the re-distribution of latent heating (Nober et al., 2003). It is vital also to the SUPRECIP effort.

2.2. Project Tools and their Past Use

The WWC research team has worked together for over 20 years in documenting the effects of deliberate and inadvertent weather modification. During the summer of 2004 the team made measurements in the Houston, Texas, metropolitan area that were similar to what was planned for the SUPRECIP effort in California. The Texas effort involved the use of a state-of-the-art, Piper Cheyenne, turbo-prop, cloud physics aircraft to measure the sizes and concentrations of CCN pollution aerosols throughout the state (Figure 5). This was done in conjunction with Dr. Don Collins of the Atmospheric Aerosol Research Group within the Department of Atmospheric Sciences at Texas A&M University. The aircraft has been provided by the Southern Ogallala Aquifer Rainfall (SOAR) program, which is managed by the Sandy Land Underground Water Conservation District. The aircraft is equipped to measure: temperature, relative humidity, cloud liquid water, updrafts and downdrafts, drop sizes, and ice-particle sizes using special laser probes, aircraft position using a GPS navigation system, and CCN pollution aerosols using two specialized instruments. Documentation of the aircraft's capabilities and instrumentation is provided in Appendix B.

Figure 5. The SOAR Cheyenne II cloud physics aircraft

The first CCN instrument is the Droplet Measurement Technologies (DMT) CCN counter. The CCN counter samples aerosols from outside the aircraft to measure their capability to act as cloud condensation nuclei. The air enters the top center of a 50 cm long vertical cylindrical column in the heart of the CCN counter instrument and is surrounded by an aerosol-free humidified uniform supersaturation flow environment. This provides the environment to activate and grow aerosol particles. As the air sample flows down through the chamber, CCN activate in response to the exposed supersaturation and grow to droplets. An optical particle counter at the base or outlet of the chamber detects all particles with diameters larger than 0.5μm. Particles that grow to 0.7μm are considered as CCN and comprise the CCN concentration.

The second CCN instrument comes from the Atmospheric Aerosol Research Group at Texas A&M University. This instrument is referred to as a *differential mobility analyzer/ tandem differential mobility analyzer* (DMA / TDMA) system on board the Cheyenne II aircraft. This instrument sequentially measures submicron aerosol size distributions and size-resolved hygroscopic growth. These data are coupled to infer the critical supersaturation spectrum of the aerosol. The time resolution of the measurements is dependent upon the number of particle sizes for which hygroscopicity is measured. During most of the flights conducted so far, the time needed for a complete measurement has been about 10 minutes. Further documentation of the instrumentation on the SOAR cloud physics aircraft is provided in Appendix B.

Some of the research flights of the SOAR cloud physics aircraft have focused on the Houston Metropolis, which is one of the most polluted cities in the United States, due primarily to the extensive oil refining in the area. Figure 6 provides a summary of the aerosol measurements from the flight on August 23, 2004. Traverses upwind (to the south of the city) and downwind (on the north side of the city) were made at cloud base to document the aerosols being ingested by the clouds. This was followed by in-cloud measurements at progressively higher elevations to document the effect of the aerosols on the cloud properties. Figure 6 provides the subcloud measurements for this flight.

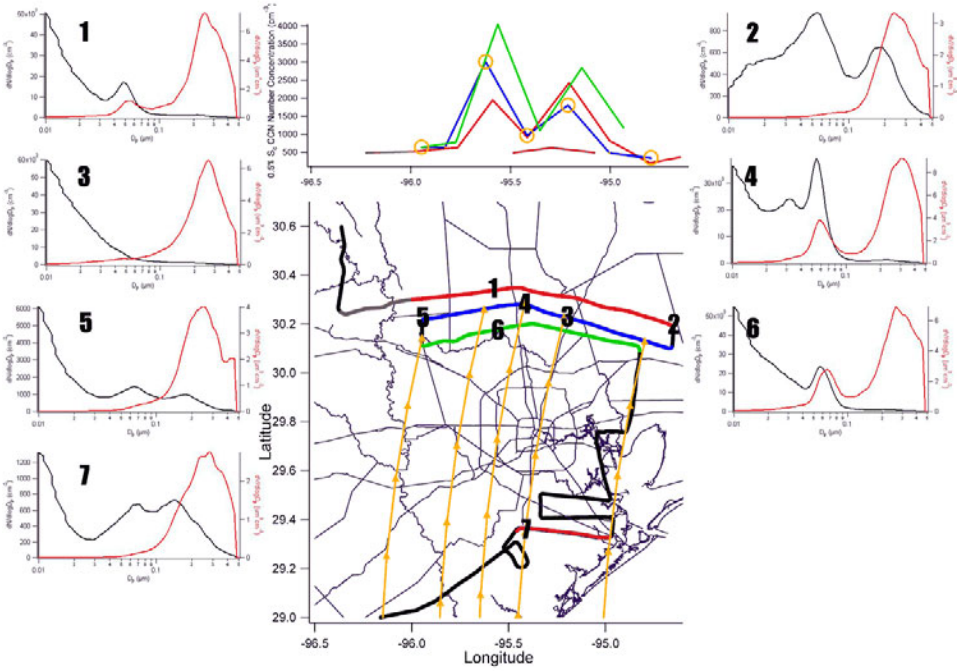

Figure 6. Summary of the Houston measurements, with the aircraft track at the center of the figure and number plots of particle sizes and concentrations shown as insets around it

The uppermost plot is the concentration of CCN at 0.5% supersaturation, measured by the DMT instrument along the five color-coded flight legs identified in Figure 7. Six-hour NOAA Hysplit back trajectories from five separate points are denoted by the orange traces. The ending points for these trajectories are also noted on the DMT CCN concentration plot. The surrounding figures are differential number (black) and volume (red) concentrations, as measured by the Texas A&M University DMA at the numbered points indicated along the flight track. Upon examining all plots and taking into consideration the changing scales on the ordinate, it is obvious that the air passing over Houston to the north is much more polluted than the air approaching from the south. Notice the difference between point 7 and point 3. Point 7, which is upwind of Houston, has a peak differential concentration a little greater than 1200 dN/dlogDp

(cm^{-3}),[1] while point 3, which is downwind of Houston along the same trajectory, has a peak concentration of around 60,000 dN/dlogDp (cm^{-3}). This is hardly a surprise in view of the pollution sources in the region. Some of the plumes appeared to be conserved spatially (e.g., compare the inset plots for position 6 with position 1).

On this day, background CCN concentrations were on the order of 200 to 600 cm^{-3} at 0.25% supersaturation and 400 to 800 cm^{-3} at 0.5% supersaturation. The CCN size distribution was typically broad with a mean diameter around 4μm (Figure 7). When the aircraft approached location 1, the CCN concentration increased to around 4000cm^{-3} with peaks reaching 10000cm^{-3}, indicating that the measurements were being made in the urban pollution plume. At this point, the CCN size distributions were typically narrower, with a mean diameter around 3μm (Figure 8). An interesting feature of these measurements is that two distinct peaks in CCN concentration were apparent (Figure 7).

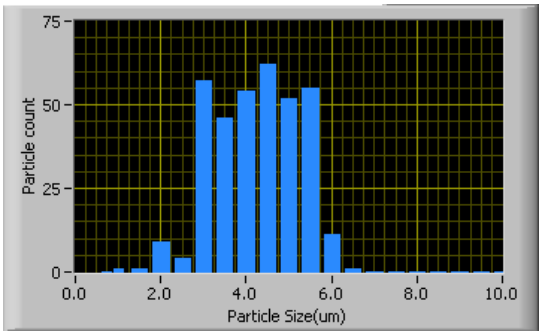

Figure 7. CCN size distributions generally flat from 2 to 6 μm away from the urban plume. CCN number concentration of 565 cm^{-3} at 0.25% supersaturation.

[1] A proper way for presenting particle distributions, and that which is most commonly used in the literature in representing size distributions of aerosols is by plotting in a logarithmic scale dN/dlogDP, dA/dlogDP, and dM/dlogDP, which represent particle number, surface, and mass respectively, per logarithmic interval of size. Normally, concentrations at a specific size are given as dN/dlogDp (cm^{-3}). The important thing is that the number of particles within the narrow size interval selected by an instrument that measures aerosol or droplet sizes is normalized according to the width of the interval. When this normalization is done, it is then possible to compare directly number concentrations (as a function of size) between instruments using different widths. This is normal practice for all size distribution measurements.

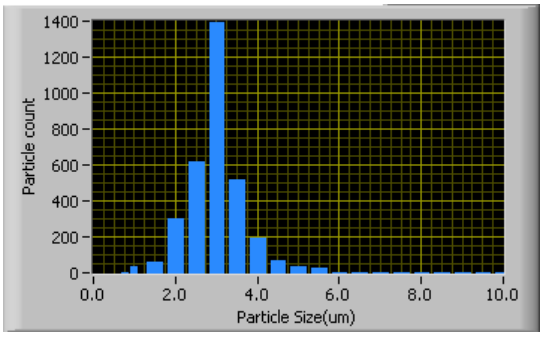

Figure 8. CCN size distributions in the urban plume with a mode around 3 μm. CCN number concentration of 4566 cm^{-3} at 0.25% supersaturation.

The DMA/TDMA system made measurements of the aerosol size distribution from 0.010μm to 0.500 μm. These measurements indicate a very dramatic increase in aerosol concentration that coincides with the increase in CCN concentration. The effect of Houston on aerosol number concentration and size distribution can be clearly seen along the streamline intersecting points 3 and 7 in Figure 6. The dramatic increase in number concentration between measurements at point 3, upwind of Houston, and point 7, downwind of Houston, indicates that large numbers of small particles were added to the air mass as it passed over the Houston area. The change in volume concentration between these points is much less pronounced. This suggests that Houston emissions may have a significant impact on CCN concentrations even when mass concentration measurements, which are more sensitive to larger particles, are largely unaffected.

Once these measurements are made, the researchers can analyze the surface wind features and use back trajectory models to isolate the sources of the anthropogenic emissions that are producing the bimodal distribution of the measurements.

This capability has great implications for the SUPRECIP effort. A *Sacramento Bee* December 18, 2004, front page article reported that the San Joaquin Valley, Los Angeles basin, and San Diego areas were found by the U.S. Environmental Protection Agency (EPA) to exceed limits for fine particulates (Sacramento Bee 2004). SUPRECIP may determine to what extent these fine particles are present in the lower atmosphere and what is the extent of their effect on the precipitation processes and the rainfall amounts.

2.3. Flight Procedures

The cloud physics aircraft, provided by Woodley Weather Consultants through the SOAR program in Texas, was used to measure the aerosols, their impact on cloud-base microstructure, the evolution with height of the cloud drop-size distribution, and the development of precipitation in the warm and mixed phase cloud processes. The project documented background pristine clouds and for polluted clouds, paired to the extent possible with special emphasis whenever possible on the post frontal, relatively shallow orographic clouds over the Sierra Nevada. At the outset of SUPRECIP, it was postulated that the main precipitation suppression would occur during westerly flow that captures anthropogenic CCN that are incorporated in certain orographic clouds that form over the Sierra Nevada—those that are sufficiently shallow so that their tops do not fully glaciate before crossing the mountain crest. This means that at least some of the water in these clouds remains in the form of cloud droplets

that are not converted to precipitation (or at least ice hydrometeors) before crossing the divide, and hence re-evaporate and are lost to precipitation on the downwind side of the ridge. Such conditions prevail mainly after the passage of cold fronts through California. The cloud depth gradually decreases after the frontal passage, producing conditions that should be sampled extensively during the few such synoptic situations that are expected to occur. The case illustrated in Figures 1a–c for December 7, 2003, is an example of what would have been an ideal case to study with the cloud physics aircraft.

The cloud physics aircraft was deployed to the Sacramento Executive Airport in Sacramento, California, which is at the western margins of the Sierra foothills and downwind of major urban pollution sources to the west and southwest. From this location it was possible to identify visually the formation of clouds of interest. When clouds of primary interest appeared to be in place, a flight was scrambled and the following parameters were monitored during the flight:

1. Aerosols: Passive Cavity Aerosol Spectrometer Probe (PCASP) concentrations, CCN at 0.5% and DMA.
2. Cloud base drop size concentrations.
3. Drizzle concentrations, of Cloud Imaging Probe (CIP) > 100 microns.
4. Habits and sizes of hydrometeors from CIP images.
5. Wind direction and speed with height, to be noted every 1000 feet (ft) (305 meters, m) up to 6000 ft (1829 m), and every 2000 ft (610 m) above this height.

A real-time display of these parameters was essential. The values of these parameters were called out by the flight scientist and noted in his log. The ideal flight path is shown schematically in Figure 9. A stepwise ascent through clouds, heading east to the mountains, was made all the way to cloud top level during the documentation of the vertical evolution of cloud properties. The ascent was terminated upon reaching an extensive zone of fully glaciated clouds at the -20°C (-4°F) isotherm or 15,000 ft (4570 m), whichever was the higher.

Upon exiting above cloud tops, the aircraft continued its ascent another 3,000 ft (910 m) or to a height that permitted photographs of the cloud field and an assessment of the situation. From this vantage point this project's researchers evaluated and documented the following cloud properties:

1. **Convective-stratiform degree:** To what extent the cloud tops were flat or broken into convective elements of various top heights.
2. **Orographic extent:** To what extent the cloud cover conformed to the topography, building at the foothills, reaching maximum height at the divide and evaporating on the downslope side of the Sierra crest.
3. **Microstructure appearance:** To what extent the clouds looked hard with all water, had some ice evident, had glaciated patches, or appeared to be fully glaciated. Whether layers of water clouds are visible above lower glaciated clouds.
4. **Along-ridge homogeneity:** To what extent there are similar cloud conditions along the ridge far to the south and/or to the north, so that a similar cross section with different

aerosols can be found there. Whether a trend in the extent of glaciation along the ridge is visible.

After completion of the visual assessment, a decision was made on continuation of the flight mission along the following priorities:

Priority 1

If clouds are:

1. not dominated by convection and have relatively flat tops,
2. orographically generated,
3. mostly not glaciated,
4. have along ridge continuity.

(The case illustrated in Figure 1 for December 7, 2003, satisfies all of these conditions.)

Then:

1. Descend back to cloud tops and continue the flight roughly 500 ft (150 m) below cloud top, flying to the east until emerging from the clouds on their downwind edge.
2. Descend in the clear air to 2000 ft (610 m) above ground level for measuring the aerosols that cross the mountains.
3. Ascend to the minimum height necessary for a safe westward traverse of the mountains in clouds, returning to the foothills at least 2,000 ft (610 m) above the terrain.
4. Descend through the cloud bases of the foothills clouds.
5. Fly along the foothills searching for different aerosols, transiting from polluted to clean or vice versa. This will be done by flying steps below the clouds and in their bases and vice versa. Air trajectories should be useful for guidance. Once substantially different aerosols have been found in the foothills, perhaps along the northern Sierra. This was the case in Areas 3 and 5 on December 7, 2003, where the satellite methodology indicated that much more pristine conditions were present relative to Area 7 that includes the Sierra foothills and crest to the east of Sacramento (see Figure 1a). Upon finding more pristine conditions, repeat the whole cycle of the cross-mountain cloud documentation.
6. After successful documentation of the polluted and pristine pair return through the upslope clouds to the level where the onset of precipitation-sized particles (i.e., > 100 microns diameter) and document the transition of their properties at that fixed altitude when returning to the more polluted segment.
7. From the polluted segment, fly at below-cloud/in-cloud base level upwind (using aircraft wind) in search of the pollution sources, crossing it and flying into the pristine upwind air mass.

8. Re-track and return to base, flying through clouds of opportunity at the height where the onset of precipitation-sized particles is noted. Note how that height rises when moving to the polluted region. It is desirable to take a similar flight westward in the pristine air mass.

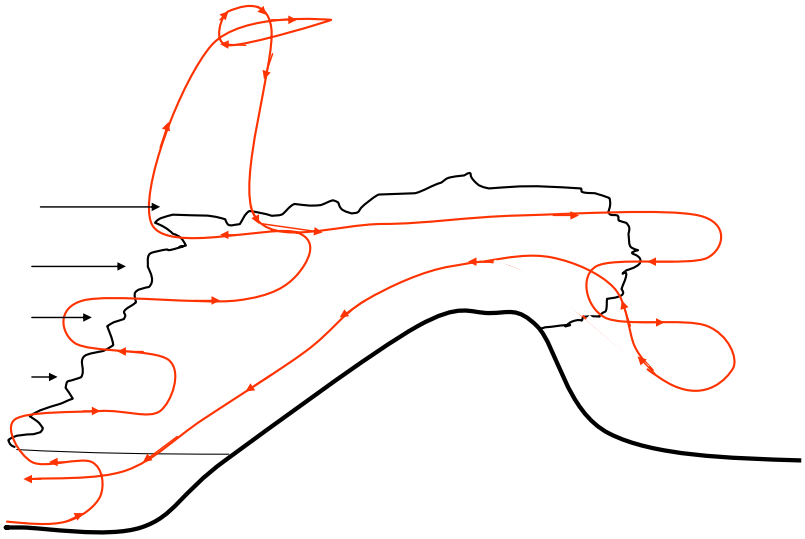

Figure 9. Schematic flight path of the aircraft in an orographic cloud system across the Sierra Nevada. This pattern is done similarly for shallow and deep frontal clouds.

3.0 Results

3.1. Operational Outcome

The weather during SUPRECIP was highly anomalous for the entire U.S. West Coast, consisting of dry conditions in the Pacific Northwest and flooding rains in Southern California. As of the end of February 2005, Los Angeles had had more rainfall for the 2004/2005 rainy season than Seattle, Washington. A high-pressure blocking pattern at the surface and aloft and the resulting split in the jet-stream flow, when it encountered the block, forced some of the weather disturbances to the north and northeast into Canada and Alaska, while some of them traveled southeastward under the blocking high to the Central and Southern California coast. This persistent region of low pressure under the block produced southerly and southeasterly winds and long periods of middle and high clouds over the Central and Northern Sierra for most of the project. The desired orographic clouds produced by the usual westerly winds into the Sierra were a rarity during SUPRECIP, and the program was extended through the first week in March 2005 in the hope of obtaining orographic storm events. Although the weather was a disappointment during SUPRECIP, much was learned nevertheless in documenting the effect of pollutants on the microstructure of the clouds and in validating the satellite inferences of cloud structure using the aircraft measurements and the concurrent radar depictions.

There were 21 flights of the Cheyenne cloud physics aircraft in California, exclusive of the ferry flights to and from the state, as detailed in Table 1 of Appendix C. Two flights were made for instrumentation calibration and the 19 flight balance was research flights. A total of 43 hours 26 minutes were expended during these flights, out of a 70-hour flight allotment. Two flights were conducted on 5 of the 19 flight days, and 2 of the 5 were made during the one-week extension of the program into March 2005. Although the Cheyenne II cloud physics aircraft had its share of annoying mechanical problems, no desired research flight opportunity was lost due to these problems. One research flight was terminated early, however, due to failure of the cloud droplet probe (CDP), which was subsequently repaired.

Table 1 provides a summary of the highlights of the SUPRECIP flights.

Table 1. Summary of the meteorological highlights of the SUPRECIP flights

Date	Flight Commentary
Feb. 7, 2005 First Flight	Four cross-sections through pristine cloud bands wrapped around "polluted" cyclonic circulation NW of Sacramento. The pristine clouds, resembling Hawaiian orographic clouds with drizzle, often had droplet concentrations less than 10 cm^{-3}.
Feb. 7, 2005 Second Flight	Planned to document pollution plume to the east of Fresno. The flight was terminated early because the CDP instrument was not working.
Feb. 11, 2005	Instrumentation and pilot proficiency test flight. The clouds were uninteresting because they were not interacting with the polluted boundary layer.
Feb. 13, 2005	The polluted boundary layer was topped at 2000′ (610 m). Maritime clouds penetrated at the low mid-levels, and were partially modified to 200–270 drops cm^{-3}. These clouds were not nearly as maritime as the clouds of February 7 and 11. They had CCN counts occasionally higher than 1000 cm^{-3}, but mostly somewhat less than 500 cm^{-3}.
Feb. 14, 2005	The CDP appeared to be undercounting and oversizing. The lower level clouds were apparently polluted, but the higher clouds were pristine. This was in line with our expectations, because the upper level clouds that did not appear to interact with the pollution sources on the ground.
Feb. 18, 2005	The low level shallow clouds were polluted, but the mid-level air was clean. The high-level generating clouds consumed their cloud water as fast as it condensed, leaving no susceptibility to aerosols.
Feb. 20, 2005 First flight	The clouds were moderately maritime in nature, developing precipitation and glaciating efficiently when not very vigorous. The small cross mountain component of the flow allowed the clouds time to consume most of the cloud water over the Sierra.
Feb. 20, 2005 Second flight	The meteorological impressions from our first flight were confirmed. The conditions had not changed much microphysically.
Feb. 21, 2005	Vigorous convective clouds formed over the valley, and moved from the SE. They spawned one tornado to the west of Sacramento, while the cloud physics aircraft was flying to the NE. The convection was quite maritime. They had a bimodal drop size distribution (DSD), and readily precipitated when not developing strongly vertically. The cloud water in the strongest updrafts remained to at least 15,000′ (4570 m) with many hydrometeors, but it was exhausted within the main cumulonimbus (Cb) cloud because of interactions with already glaciated clouds. The clouds were efficient precipitators. It was clearly maritime air that was advected into the region through Central California around the low center to the south of Monterey.

Feb. 25, 2005	No notable changes were observed in the DSD over the valley relative to those offshore. The satellite overpass analysis confirmed these data. A look at the DSD plots shows that subtle and interesting differences could be seen in the convective and stratiform clouds.
Feb. 27, 2005	The layer clouds on this day were maritime and they readily precipitated, even when they were very shallow. This was probably because they formed well ahead of the mountains and were very much aged. Their spectrum showed a continuum through the CIP sizes, indicating coalescence that was responsible for drizzle, which then developed ice hydrometeors. In contrast, the wave clouds were very young cloud elements and had a very narrow DSD. The few ice crystals and small graupel that they produced formed a distinctly different and separate population from the cloud droplets.
Feb. 28, 2005 First flight	The flight was made in the dry slot after the cold front but before the arrival of the post frontal convection. The tail of the cold front was receding to the SE. The purpose of the flight was to make morning measurements in the tail of the front. The pollution was trapped in the BL within the stratus and stratocumulus (Sc) clouds. The frontal cloud band of this very weak weather system was shallow, but disconnected from the surface, so that the clouds remained pristine and acted as Hawaiian orographic clouds. There are good pictures documenting the looks of these clouds, as well as good in situ and satellite documentation, all supporting the same impressions.
Feb. 28, 2005 Second flight	The front continued to recede to the SE and dissipated. Weak post frontal convection developed during the day over the northern Sierra and coastal ranges and produced some cellular radar echoes. The cloud droplet concentrations were clearly higher in the vicinity of San Francisco and Sacramento, becoming less than half the urban values some 30 miles to the north. The background concentrations were not maritime, because of the general regional haze that occurred also over the ocean. Evidently the weak front that passed last night did not flush the surface layer. There was a huge contrast between the morning clouds that precipitated very readily, whereas the afternoon clouds over the Sierra did not reach mature precipitation processes, even though they were much thicker. Although the clouds belonged to a very weak system, the contrast in the microphysical and precipitation properties was highly evident, and clearly related to the differences in the aerosols that these clouds were ingesting.
March 2, 2005 First Flight	A front passed into the Sierra overnight and was between Sacramento and Fresno with some cellular structure of the echoes by morning. The cloud tops were not very cold. The trapping of the low level pollution in the BL broke at the foothills and more so with the diurnal warming. The clouds were maritime, but not excessively so, and became quite continental where the convection was able to feed from the BL. There seemed to be some mixing with the pollution effect spreading to the upper clouds. The pollution must have suppressed precipitation considerably on the western slopes.

March 2, 2005 Second flight — The weather stabilized in a hurry after the early morning frontal passage. Only a few cumulus (Cu) clouds remained at the foothills, and the air became stagnant and hazy. The purpose of the flight was to compare the droplet measurements by the CDP with those of the Forward Scattering Spectrometer Probe (FSSP) probe. It was found that the CDP undercounts by a factor of 2 to 4 relative to the FSSP, and it does not tend to undercount worse near cloud base in small drops compared to high in the clouds in larger drops. The effective diameter is over-estimated. This means that the small drops are not lost, but are just under counted with over sizing of all the drops. Therefore, this inter-comparison provides a means to correct the DSD.

March 4, 2005 — The purpose of the flight was to measure clouds over the northern coast, with the hope of characterizing maritime clouds for later comparisons with polluted clouds. The sampled low-level clouds in the valley were polluted up to about 3500′ (1070 m). A disconnected cloud layer with its base at 4000′ (1220 m) had a maritime character. The multilayer maritime clouds precipitated. The clouds over the NW coast were moderately maritime, developing very wide droplet spectra but still containing much cloud water and not producing significant showers.

3.2. Addressing Objective 1: Characterizing the Regional Aerosols, Cloud Condensation Nuclei (CCN) and In-Cloud Droplet Concentrations

This project's first objective was to use a cloud physics aircraft to measure atmospheric aerosols in pristine and polluted clouds, and to analyze these data to determine the impact of the aerosols on cloud-base microstructure, on the evolution with height of the cloud drop-size distribution, and on the development of precipitation under warm and mixed-phase processes. This was done on most flight days of SUPRECIP using the DMA aerosol measurements, the separate measurements of CCN and the observations of cloud droplet sizes and concentrations using the CDP probe. All measurements were plotted as a function of time on each day that the observations were available. Examples are provided in the following subsections.

3.2.1. The Flight on February 14, 2005

Documentation of the SUPRECIP flight on February 14, 2005 is given in Figure 10. The abscissa is in seconds since 0000 GMT. The left ordinate is aircraft altitude in meters (represented by the green line), and the right ordinate is number concentration (in cm^{-3}) for the various particles. The four plotted points in blue at a given time are the overall DMA-measured aerosol concentrations. The top blue square is the overall total aerosol concentration. The next three blue points give the aerosol concentrations for particle sizes larger than the values shown in the legend. The red plotted points are the CCN concentrations which are a small fraction of the total aerosol concentrations (i.e., 10^4 cm^{-3} DMA aerosols vs. < 10^3 CCN aerosols). The black plotted points are the in-cloud measurements of droplet concentrations by the CDP probe. Note that the droplet concentrations are mostly < 100 cm^{-3} and often < 10 cm^{-3}. Although an entire flight can be represented in a single figure, maximum understanding was obtained by studying the flight in individual segments.

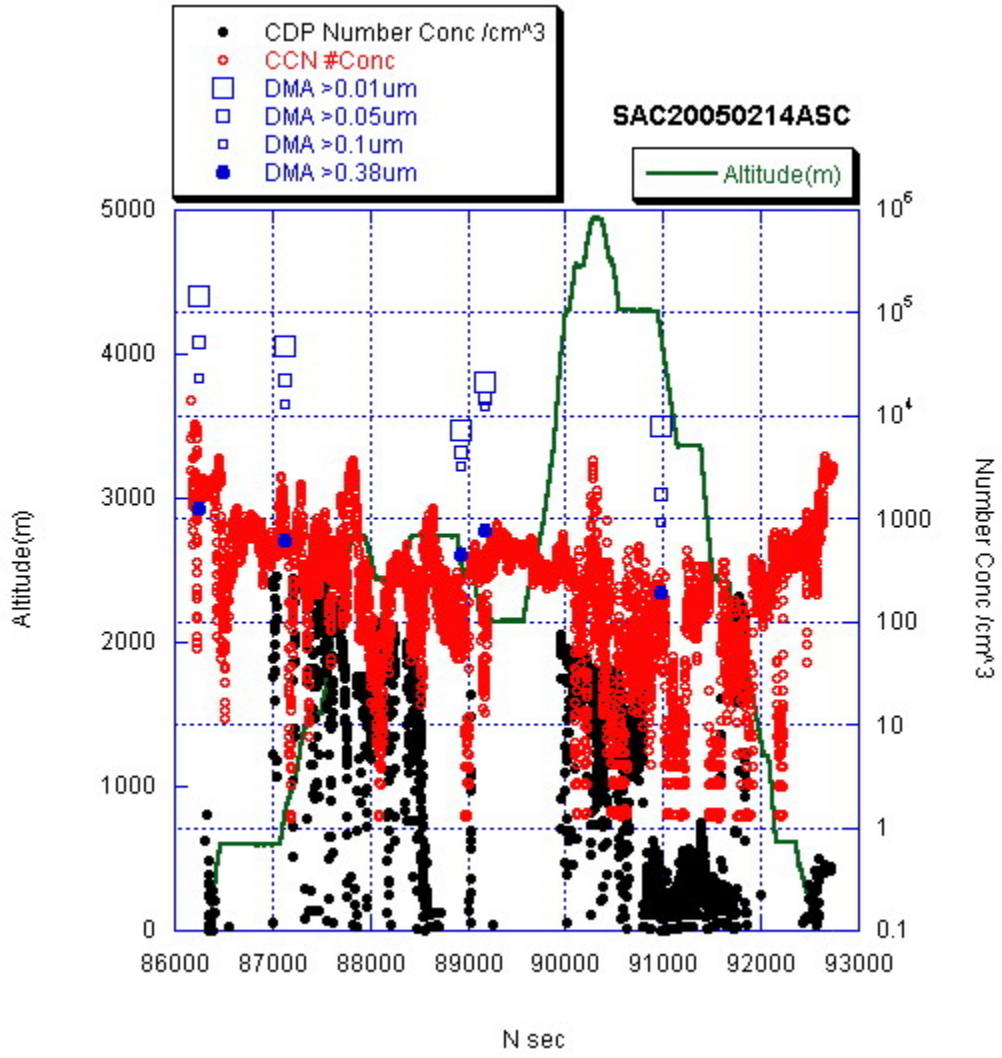

Figure 10. Plots of aerosol and droplet concentrations in cm^{-3} vs. time in seconds, relative to 0000 GMT on February 14, 2005, as measured by the DMA instrument, the CCN counter, and the cloud droplet probe. (N sec = number of seconds)

Upon examining the flight in segments, it was determined that before takeoff the CCN concentrations were about 2000 cm^{-3} and stable. The concentrations decreased to about 800 cm^{-3} above the shallow highly polluted surface layer. A stepwise ascent through a convective cloud feeding from the surface polluted air took place as shown in Figure 11, until t=87800. Droplet concentrations up to 300 cm^{-3} and CCN concentrations up to 1000 cm^{-3} occurred during these passes without any decrease with height.

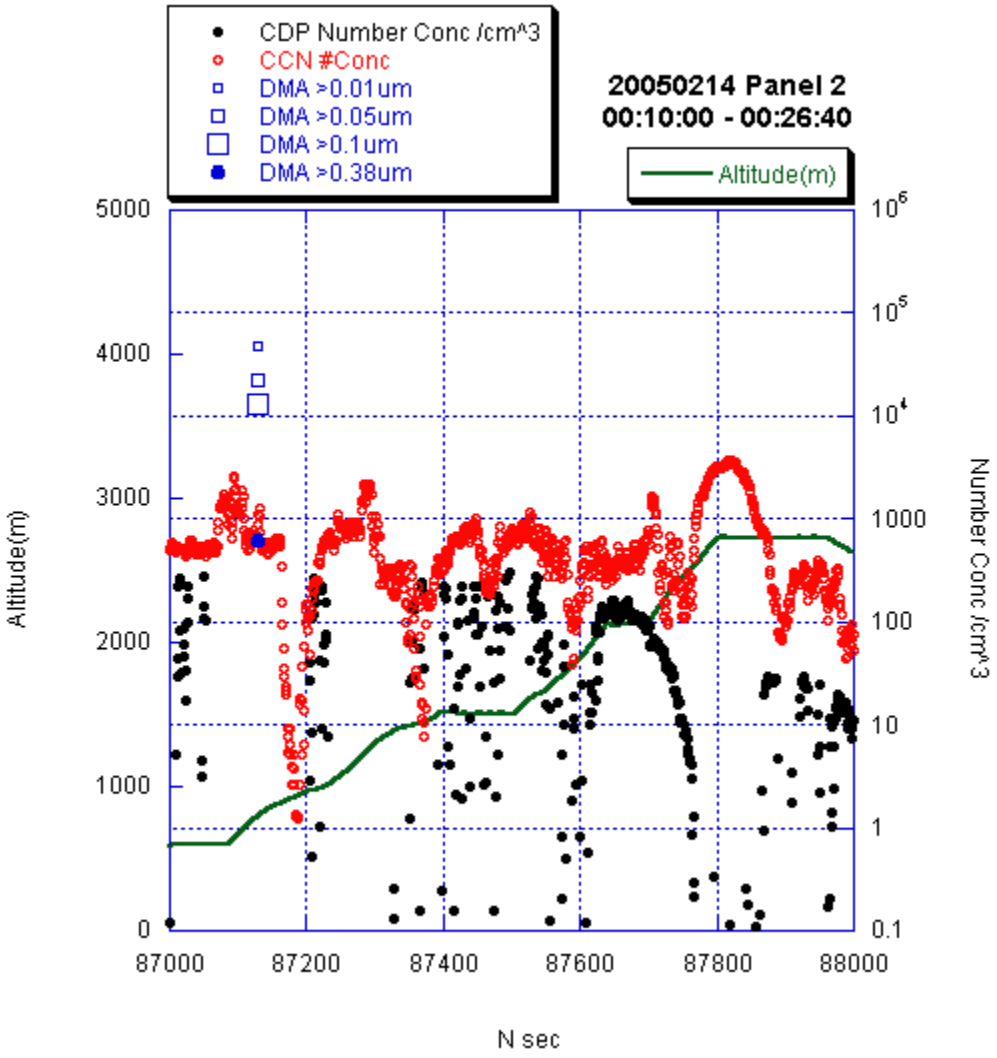

Figure 11. Plots of aerosol and droplet concentrations in cm^{-3} vs. time in seconds, relative to 0000 GMT on February 14, 2005, as measured by the DMA instrument, the CCN counter, and the cloud droplet probe.

The aircraft continued flying to the SE just at the top of the polluted layer, which was marked by the top of the thin layer cloud and, in regions where there was no cloud, by the top of the haze layer. The airplane gently changed heights to monitor the gradient across this border. The CCN concentrations changed from ~100 cm^{-3} above to ~800 cm^{-3} in the hazy air mass below an altitude of 2500 m (8200 ft). The layer clouds below had ~80 drops cm^{-3}, which is much less than the droplet concentrations in the convective clouds, probably because of weaker updraft speeds in the layer clouds.

When approaching the Sierra Nevada the CCN concentrations again became relatively high at 300 to 600 cm^{-3} at t=90,000 seconds, probably because the polluted air layer was rising over the mountains. A new cloud base was encountered near 4000 m (13,120 ft) with drop concentrations of up to 70 cm^{-3} and heavy icing. The DMA aerosol counts matched the CCN counts for particles > 0.38 μm diameter, which means that the aerosols prevented nucleation of the many smaller CCN. This possibly explains the relatively small drop number concentrations

in the relatively modest updraft velocity of these elevated orographic clouds in weak cross mountain flow from 255° at 5 m s^{-1} at an altitude of 4,500 m (14,760 ft).

The CCN concentrations decreased again to 100–200 cm^{-3} when descending to Sacramento, and jumped again to 2000 cm^{-3} at landing. Among the lessons of the day was that there is a ready source of CCN pollution in the boundary layer.

3.2.2. The Two Flights on February 28, 2005

The first flight on this day was made in the dry slot after the cold front but before the arrival of the post frontal convection. The tail of the cold front was receding to the SE. The purpose of the flight was to make morning measurements in the tail of the front. Upon examining the plot for the entire first flight (Figure 12), it was noted that a shallow haze layer was present on the ground in the early morning with CCN particle concentrations of 2,000 cm^{-3}. At a height of 1500 m the CCN decreased to below 100 cm^{-3}, and kept decreasing to about 20–30 cm^{-3} on the way to Fresno. The DMA instrument had the same concentrations for particles having sizes > 0.31 µm. When (by t=60200 seconds) the aircraft sampled shallow maritime heavily drizzling clouds to the NE of Fresno, the CCN concentrations became noisy and increased to around 100 cm^{-3}, but the DMA seemed to have the same concentrations as before. The cloud droplets were very large and had concentrations ranging from 10-40 cm^{-3}, in line with the CCN concentrations when they were stable. Flying above the mountain crest over Yosemite at 5,000 m (16,400) brought the aircraft to air with greater CCN concentrations. At t=63,000 to 64,100 seconds the CCN concentrations dropped just above the cloud layer, as if the clouds had consumed part of the CCN.

When returning to flight altitudes < 1,000 m (< 3280), the CCN concentrations increased to more than 100 cm^{-3}. A cloud feeding from the surface air had about 400 drops cm^{-3}. (See Figure 12) At landing the CCN concentrations had reached 700–800 cm^{-3}, which is in good agreement with that cloud.

The lesson learned from the first flight on this day was that the pristine clouds kept cleansing the air by precipitation, but a strong supply of pollution was available continuously from the local surface as well as at mid-levels by long range transport. Additional insights into this case are provided in Appendix D.

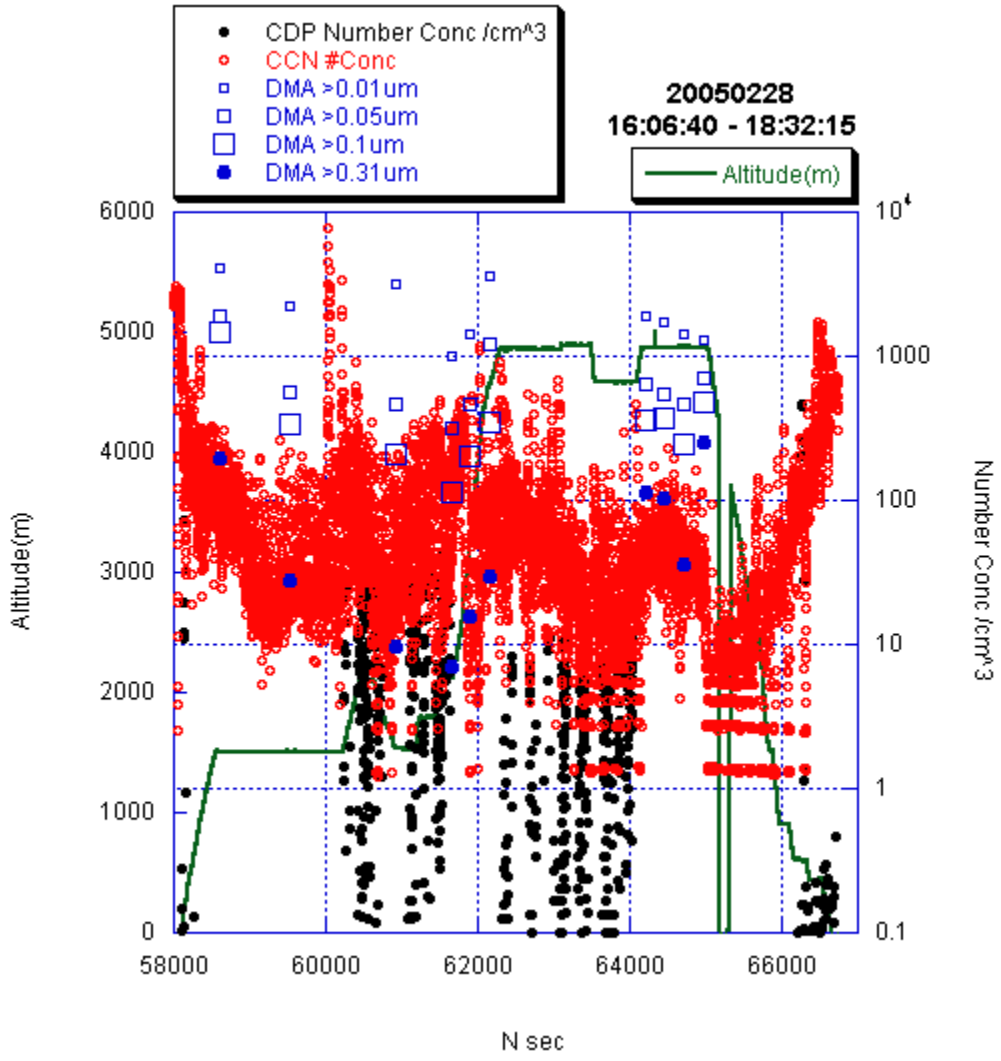

Figure 12. Plots of aerosol and droplet concentrations in cm^{-3} vs. time in seconds, relative to 0000 GMT on February 28, 2005, as measured by the DMA instrument, the CCN counter, and the cloud droplet probe.

The second flight of the day commenced at 2059 GMT. The purpose of the flight was to contrast the clouds growing during the morning hours with those that developed later in the day after prolonged solar heating. The second flight was made through the Central Valley to Chico and then eastward into the Sierra where convective clouds of differing sizes and vigor were encountered (Figure 13). Although the clouds were thicker than the morning clouds, they were less likely to produce precipitation for reasons that can readily be gleaned from the plots in Figure 12, in which it can be seen that the CCN counts and cloud droplet concentrations were clearly higher than during the morning flight (compare Figure 13 with Figure 12). See Appendix D for additional information and discussion of this case, which shows the important role of aerosols in determining cloud structure and whether they will produce precipitation.

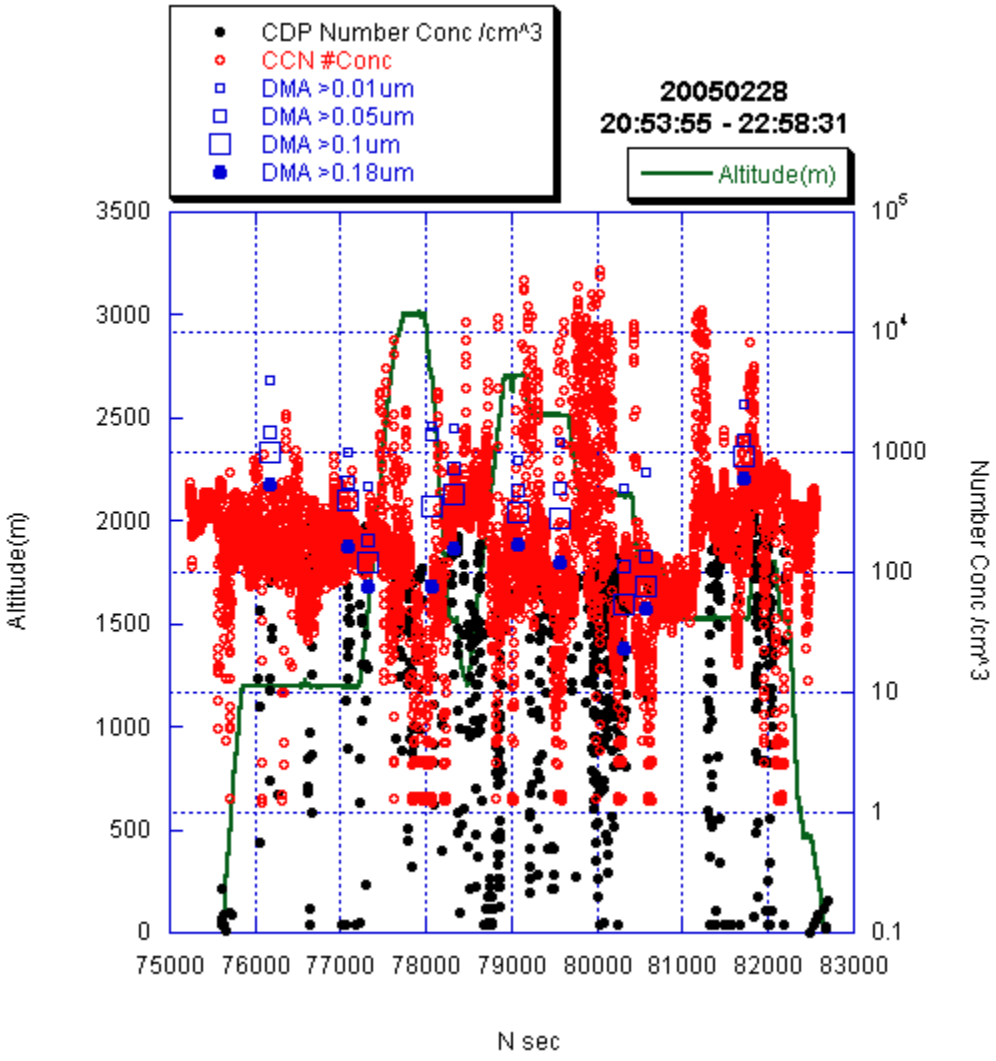

Figure 13. Plots of aerosol and droplet concentrations in cm^{-3} vs. time in seconds, relative to 0000 GMT on February 28, 2005, as measured by the DMA instrument, the CCN counter, and the cloud droplet probe.

3.2.3. Calculations for all days

Comparable analyses, in addition to the two presented here, were made for the other flight days having complete DMA, CCN and CDP data sets. A summary of the measurements by cloud pass is provided in Table 2, which contains a wealth of cloud microphysical information, including time, the altitude and temperature of the cloud pass, the CDP liquid water contents, mean and maximum droplet concentrations, and the median effective radius for the cloud pass. The CIP instrument provided an estimate of the cloud precipitation water. Aerosol information was supplied by the CCN counter operated at 0.5% supersaturation. The total aerosols as a function of size were provided by the DMA instrument. For information about the aircraft instrumentation, see Appendix B.

Table 2. Comparison of selected aircraft aerosol and cloud pass data for segments where the CCN concentrations were not noisy (i.e., not changing within a few seconds by more than a factor of 1.5)

Date	hhmmss (GMT)	N Secs	T °C	Height m	CDP LWC g m^{-3}	CDP N cm^{-3}	CDP Nmax cm^{-3}	CDP R eff μm	Precip LWC D>0.1 mm	CCN 0.5%	DMA >0.01 μm	DMA >0.05 μm	DMA >0.1 μm	DMA >0.2 μm	CCN divided by DMA >0.01 μm
50216	001013	5	9.6	594	0.312	225	266	6.75	0.01	585	48062	22418	13258		0.0122
50216	002139	27	-0.1	2315	0.243	41	96	10.95	0.039	523					
50207	183339	38	7.9	482	0.148	146	271	5.75	0.0	602					
50207	184933	23	-6.9	3254	0.084	11	18	14.55	0.77	82					
50207	192343	9	-15.4	4514	0.420	82	104	10.85	0.109	150					
50207	195359	28	-0.6	1846	0.200	75	170	9.2	0.004	210					
50207	195655	16	-0.5	1860	0.484	132	202	10.0	0.068	439					
50207	210919	26	1.5	1490	0.182	256	342	6.05	0.0	478					
50218	184342	21	2.1	808	0.174	130	180	6.45	0.0	466					
50220	175623	11	2.7	1621	0.461	95	132	10.9	0.025	268					
50220	190842	10	2.0	1526	0.305	109	149	9.3	0.029	927	79021	1645.0	573.57	82.303	0.0117
50221	214449	35	-7.7	3649	0.441	59	112	11.6	0.06	150	3752.0	827.54	482.15	93.254	0.04
50221	222910	16	0.0	2437	0.240	57	103	9.5	0.0	197	8253.9	1532.0	935.22	248.53	0.0239
50225	191231	63	4.6	1138	0.452	274	305	7.7	0.0	788	20465	3597.0	790.50	60.602	0.0385
50225	212627	80	5.7	927	0.187	318	400	5.6	0.0	679	11849	5605.2	2844.0	608.80	0.0573
50225	215648	31	7.0	911	0.219	308	348	5.95	0.0	807					
50228	212436	10	5.3	1192	0.163	193	251	6.05	0.0	230	994.93	574.15	403.03	82.453	0.2312
50228	214503	9	2.6	1511	0.200	178	268	6.65	0.0	304	1573.8	728.99	448.12	79.184	0.1932
50228	220318	14	-2.8	2510	0.439	80	113	11.45	0.1	87	504.19	277.87	29.732	91.114	0.1726
50228	224045	7	3.4	1522	0.098	174	257	5.45	0.0	421	2518.2	1278.6	915.08	566.07	0.1672

Notes: The numbers in the Date column should be read in the following order: year, month, day. The time in the hhmmss column should be read in the following order: hours, minutes, seconds; and the time is Greenwich Mean Time. LWC = liquid water content.

These data were used to address a number of matters of interest. For example, by taking the ratio of the maximum CCN concentration at 0.5% supersaturation to the maximum DMA-determined aerosol concentration for aerosols > 0.01 μm for each cloud pass on each day of flight, it is possible to make a crude estimate of the fraction of the overall aerosols that serve as condensation nuclei. The last column of Table 2 provides these values, ranging from a minimum of 1% to a maximum of 23%. The mean is 9%. Thus, for the period of measurement in California, roughly 10% of the total aerosol population served as CCN activated at 0.5% supersaturation.

In addition, the Table 2 data were used to show an association between the CCN concentrations evident before and after each cloud pass and the in-cloud droplet concentrations. This is shown in Figure 14, which is a scatter plot and regression analysis relating the aircraft-measured droplet concentrations (mean and maximum) to the observed CCN concentrations before and after the cloud penetrations. The figure shows that the greater the CCN around the cloud at the level of its penetration the greater the in-cloud droplet concentrations. Thus, aerosols would appear to have a direct effect on in-cloud structure, suggesting a connection between pollution aerosols and altered cloud processes.

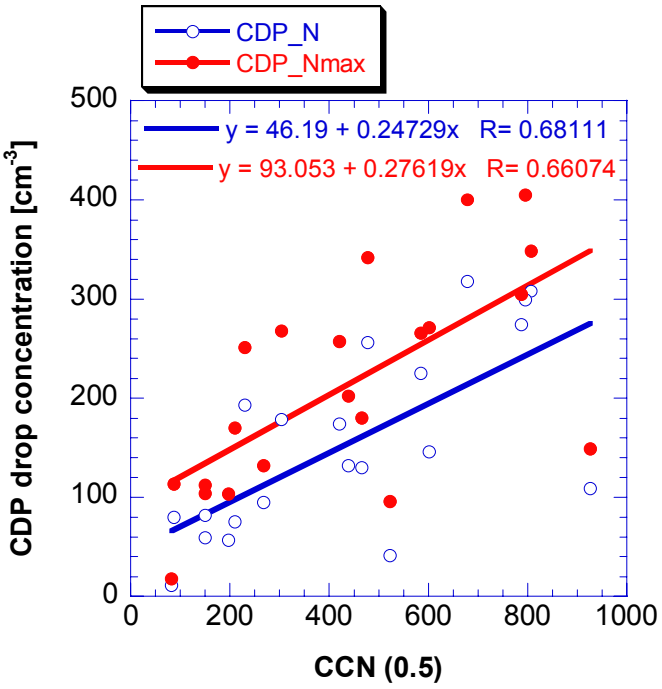

Figure 14. Cloud drop number concentrations as a function of the CCN concentration at supersaturation of 0.5%. Each point represents the average and maximum droplet concentrations for one cloud pass.

The next step in the analysis was to relate the effective diameter[2] of the cloud drops, normalized for the cloud liquid water content by the expression Deff / $LWC^{0.333}$, to the CCN concentrations for each cloud pass, where Deff is the effective diameter. In developing this correction one must understand that for the same CCN, r_e would increase with height above cloud base as would the LWC. The variable cloud-penetration heights above cloud base cause a random variability that would mask the relationships between the CCN and r_e. Because the cloud base height is unknown, we need to normalize with the second best thing, which is LWC. Because droplet diameter depends linearly on the cube root of the volume, the correct normalization form is as used here. The CCN concentrations were taken from the immediate clear air vicinity of the pass. The averaging is just for the cloud drops throughout the pass. Note that the correlation is denoted as unsigned. The negative relation is given by the regression equation. Upon examining the plot in Figure 15 it can be seen that the effective diameter decreases as the CCN aerosol concentration increases. This is the aerosol connection to the drop-size distribution. Thus, as the CCN pollution aerosols increase, the drop sizes decrease.

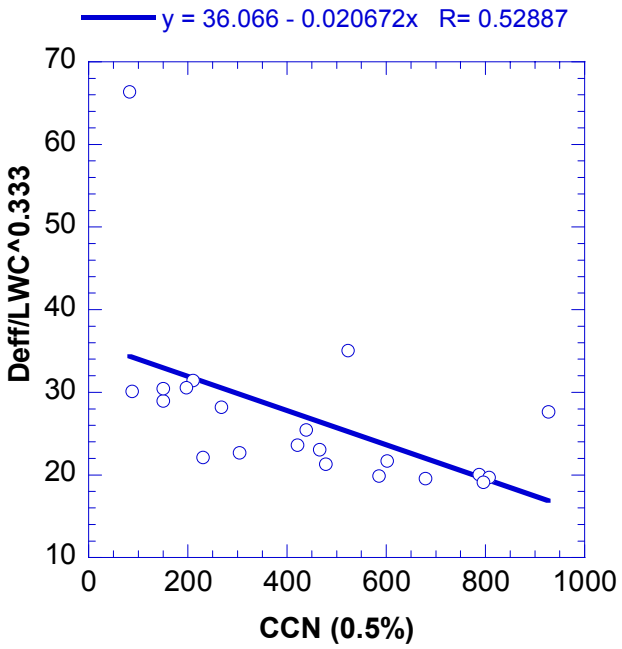

Figure 15. The effective diameter of the cloud drops normalized for the cloud liquid water content by the expression Deff / $LWC^{0.333}$, as a function of the CCN concentrations for each cloud pass

[2] The *effective diameter* is defined as the ratio of the sum of the cube of the droplet diameters to the sum of the square of the droplet diameters.

3.2.4. Status of Objective 1

Comparable analyses, in addition to those presented here, were made for the other flight days having complete DMA, CCN, and CDP datasets. These confirmed the results already presented here. The accomplishments in addressing Objective 1 include:

- documentation of the regional aerosols, including pollutants from urban and industrial sources, and the effects of these aerosols on cloud structure and behavior;
- suggestion, based on the limited data, that the CCN aerosols, on which cloud droplets form, constituted about 10% of the overall regional atmospheric aerosols during the period of study;
- documentation that the Sierra Nevada often receives precipitation from shallow pristine clouds as long as they do not ingest pollutants from the atmospheric boundary layer; and
- demonstration that high concentrations of tiny CCN aerosols inhibit precipitation when they are ingested from the boundary layer, due to either convective transport or orographic lift.

Despite the many accomplishments, Objective 1 was not reached fully, due to two problems:

- Incomplete documentation of the aerosols in the atmospheric boundary layer due to the near impossibility of obtaining clearance to conduct flight under instrument flight rules (IFR) in the boundary layer in the San Francisco/Oakland/Sacramento heavily populated urban and industrial areas. A second aircraft flying under visual flight rules (VFR) would have been necessary to obtain the needed documentation.
- The great lack of orographic cloud conditions over the California Sierra due to weak wind flow into the Sierra during virtually all of the period of flight operations. A longer period of operations would have been required to obtain the desired orographic clouds for study.

3.3. Addressing Objective 2: Validating the Multi-Spectral Satellite Inferences of Cloud Structure and the Effect of Pollutants on Cloud Processes

This project's second objective was to use the aircraft cloud microphysical measurements to validate the multi-spectral satellite inferences of cloud structure and the effect of pollutants on cloud processes—especially the suppression of precipitation. This proved possible on two days having good satellite and aircraft data: February 7, and March 4, 2005. The quantitative comparisons of the aircraft and satellite inferences of cloud microstructure were made after analyzing the aircraft data and after collecting and analyzing the images made by the orbiting Terra, Aqua and NOAA-16 satellites. An unconventional approach, involving multiple figure overlays, was used to illustrate the results.

3.3.1. Quantitative Comparisons on February 7, 2005

Figure 16 provides an overview of the weather pattern on this day. It provides the initial MRF 4-panel documentation of the weather pattern at 0000Z (1600 PST) 8 February 2005, which is the presentation closest in time to the flights on the afternoon of February 7. The upper left and right panels give the 850 mb heights and winds and 300 mb heights and winds, respectively. The lower left panel provides the surface pressure analysis and the surface to 500 mb thickness

contours. The lower right panel gives the mean 850 to 500 mb relative humidity with contours of the Showalter Index. From these graphics one can see that there was a strong northwest current aloft through the Pacific Northwest and through Northern California with a weak front stretching from the San Francisco Bay area northeastward. Considerable light echo activity was associated with the front.

The 850 mb wind field documented in the manner of Kanamitsu (2005a.b) is given in Figure 17. The wind field is somewhat chaotic over much of the region. Note that the closed low-pressure area to the NNE of San Francisco and NNW of Sacramento is resolved nicely in the wind field. The flow to the south of the latitude of San Francisco is northwesterly offshore, and westerly on land, carrying maritime air inland from the Pacific and then into the Sierra Nevada.

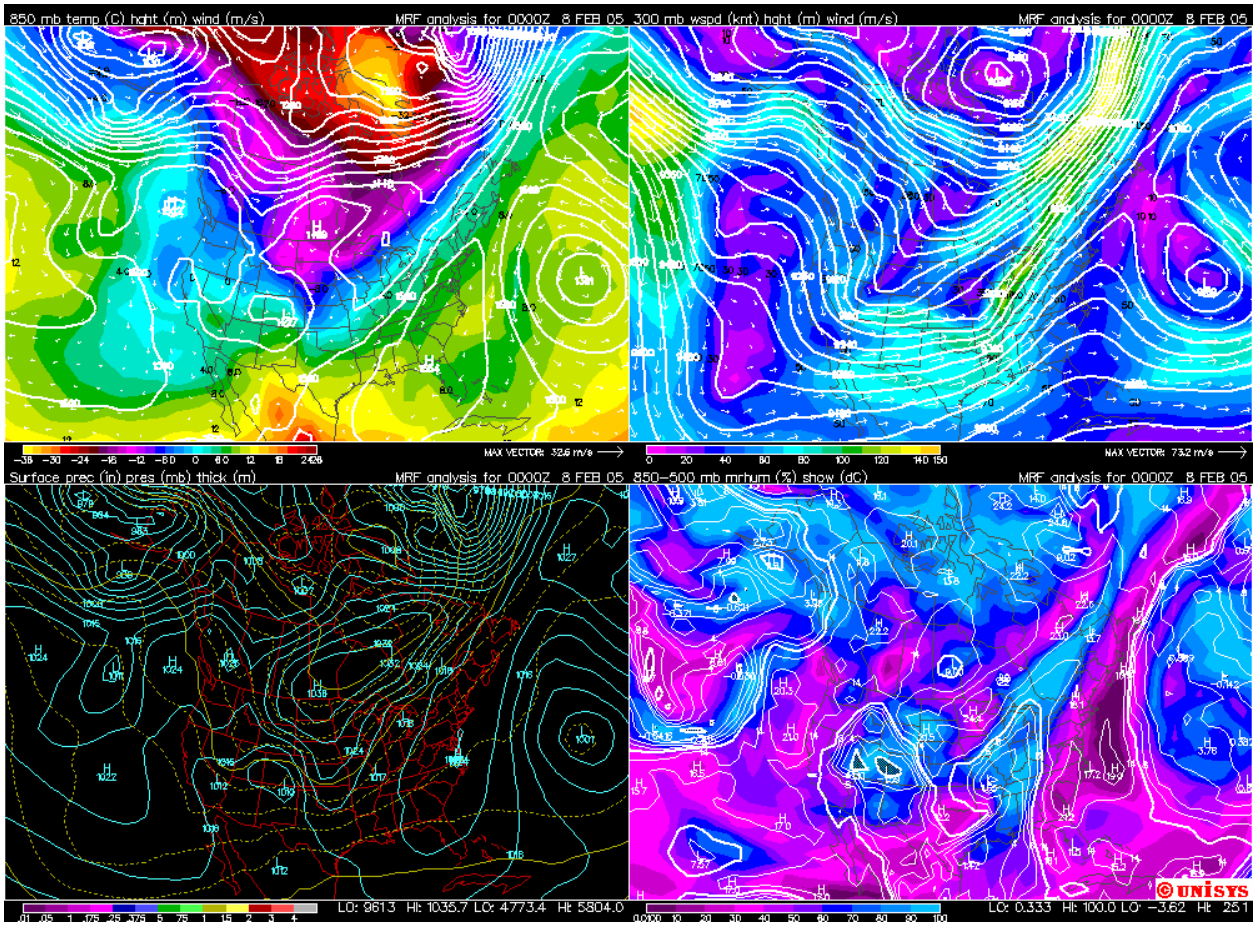

Figure 16. The MRF panel showing the initial conditions at 0000 GMT on February 7, 2005

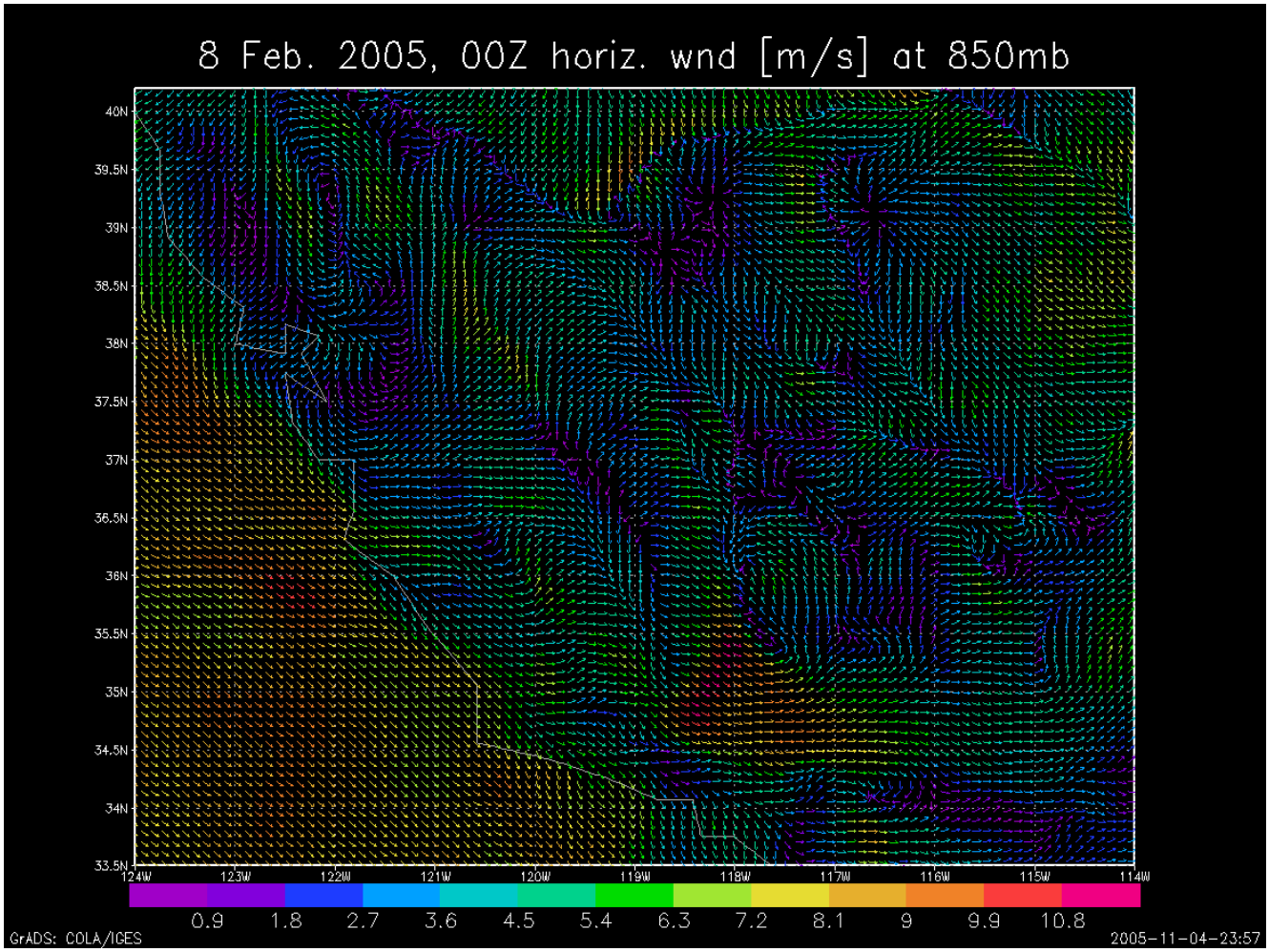

Figure 17. The 850 mb wind field (m s^{-1}) at 10 km resolution at 0000 GMT on February 8, 2005, as provided from the CaRD10 product by Dr. Masao Kanamitsu of the Climate Research Division of Scripps Institution of Oceanography, at the University of California, San Diego.

Figure 18 presents the view of the area at the time of the flight of the cloud physics aircraft, and shows the superposition of the processed Aqua satellite image at 2115 GMT and the NEXRAD radar mosaic at 2104 GMT on February 7, 2005.

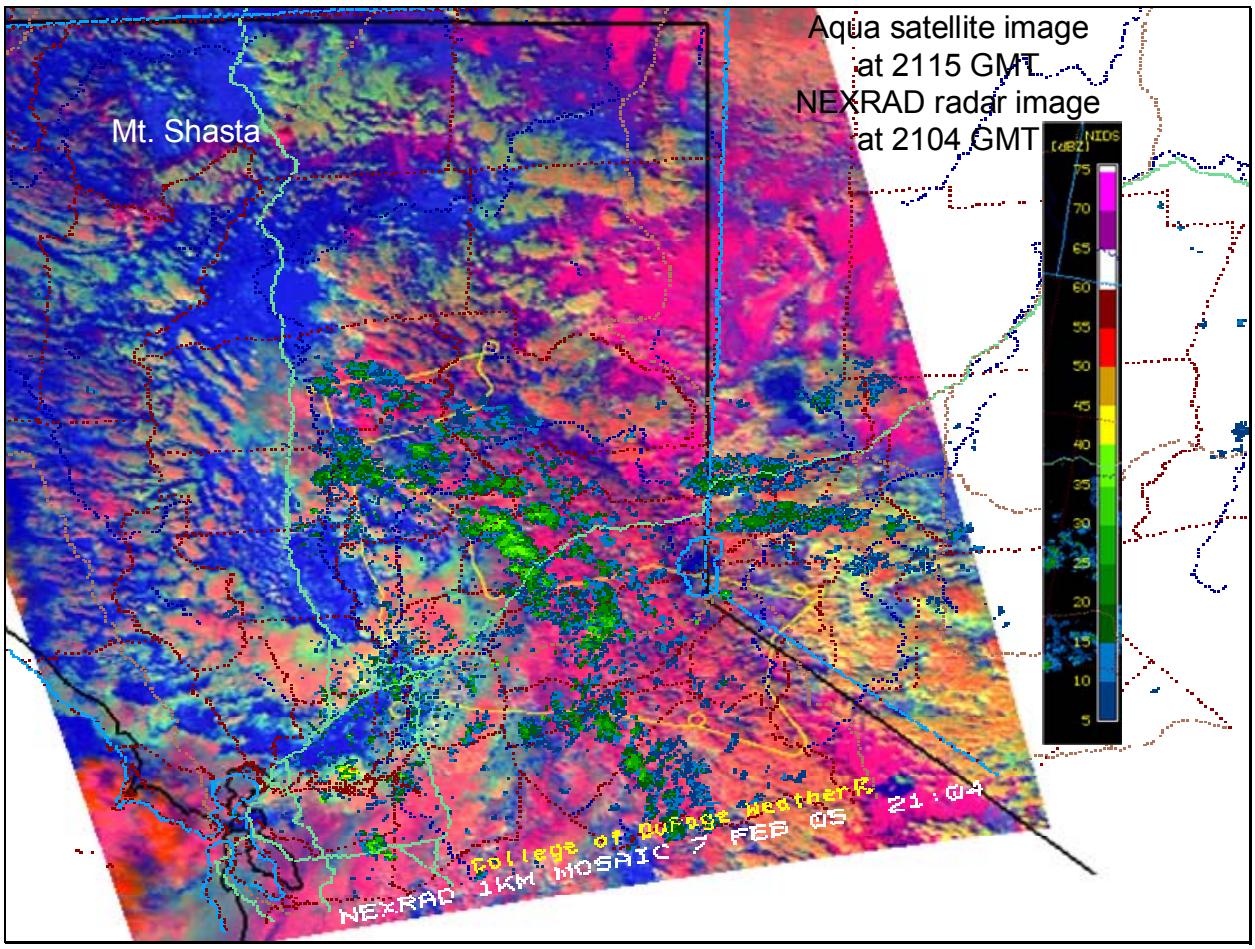

Figure 18. Superposition of the processed Aqua satellite image and the NEXRAD radar mosaic at 2104 GMT on February 7, 2005. The gold line on the satellite image is the track of the cloud physics aircraft that was flying for cloud measurements prior to and immediately after the satellite overpass. The radar echoes are shown in green within the image.

Those familiar with the presentation in Figure 18 know that the colors correspond to different cloud and surface properties. In the infrared channel, a warm surface in the absence of clouds appears blue and a very cold surface, as with the anvil tops of cumulonimbus clouds, would appear white. Likewise, a very bright surface appears red in the visible spectrum; whereas a dim surface would not have any red. Furthermore, clouds having tiny particles would appear green in the 3.7 μm channel; whereas clouds having large particles would not have any green. Upon combining the processed observations from all three sensor channels on the satellite, an image, such as that shown in Figure 18, is the result. Thus, cold (no blue), bright (very red) clouds with large ice particles (no green) would appear red or magenta in the image in roughly the same manner that one would obtain a resultant color by mixing paints of different colors. Clouds having this coloration are most likely to be precipitating. Snow surfaces usually have a magenta coloration, and this can confuse the interpretation of an image. Other resultant colors are obvious possibilities. Relatively warm clouds (some blue) having modest brightness (some

red) and very small particles (some green) might appear yellow, pinkish-yellow or shades of green. Such clouds are not normally precipitating according to the scheme of coloration.

Upon examining the image in Figure 18, note that the clouds with precipitation echoes superimposed are those with red and magenta tones and not those with yellow or green. It should be noted that the echoes in the northern part of the line to the NNE of Sacramento were actually moving north and northwest, suggesting a small low-pressure circulation near the surface. Indeed, the loop of the satellite images clearly showed a closed cyclonic circulation, which drifted slowly to the southwest during the morning hours. Thus, the low-level flow in the Sacramento area was from the west on the southern periphery of the low. In addition, a band of magenta-colored clouds can be seen sweeping inland near Monterey and continuing northeastward and then northward into the Sierra. As has been verified by satellite and cloud physics analyses, the clouds in this band had larger particle sizes than the clouds around the closed low, which was apparently ingesting pollution from the San Francisco Bay area.

Another view of the processed colorized Aqua satellite image at 2115 GMT (GMT = Pacific Standard Time (PST) + 8hrs) on February 7, 2005 is given in the top panel of Figure 19. Appearing also in Figure 19 is a yellow box that encompasses the aircraft position shortly after the aircraft took off from Sacramento, California, and for two subsequent cloud passes. The inset at the middle left gives a plot of the effective radius (r_e) of a composite cloud as a function of temperature.[3]

The 50th percentile plot is at the interface of the sloping green and yellow lines. The vertical yellow and green lines refer to zones of diffusion and coalescence droplet growth, respectively. The vertical white line at 15 microns represents the threshold for the onset of precipitation. The lower-left inset plot gives the relative concentration of drop sizes (diameters) on each of two passes made by the aircraft in clouds within the yellow box. The altitude and time of the cloud pass is shown in the little white inset box within the lower-left inset. Thus, the first cloud pass was made at 335m at 183340 GMT.

Upon examining the two insets it can be seen that the clouds within the overall box have effective diameters (obtained by doubling the radius values in the inset) generally less than 20 μm (i.e., < 20 μm) and the maximum concentration of drop sizes also are less than 20 μm diameter. In making a direct comparison, the calculated effective diameter for the complete pass of the aircraft through the first cloud is 10.49 μm, while that inferred from the satellite plot for the altitude of the aircraft cloud pass is 10 μm. The comparable comparisons for the second aircraft cloud pass are 13.67 μm and 15 μm for the aircraft and satellite, respectively. This is fortuitously good agreement when one considers the difference in scale of the satellite and aircraft measurements.

---

[3] The plots of the effective diameters versus temperature shown in Figure 19 (and the other comparable figures) were calculated from the satellite imagery using the method of Rosenfeld. The median satellite values (i.e., the interface of the yellow and green lines)were extracted from the plots. The corresponding median effective diameters for each cloud pass were calculated from the aircraft data and extracted from the data tabulations. Then the median satellite and the median aircraft effective diameters were compared.

The next area of interest is within the magenta box to the southeast along the track of the aircraft. Note that in this case the coloration of the clouds, having darker magenta shades, is much different from the color of the clouds within the first yellow box, leading one to expect much different cloud structure within the magenta box. Indeed, the inset at the middle right, giving the satellite-inferred effective radius as a function of temperature, gives much larger effective radii, with virtually the entire plot having values > 15 μm in radius, the threshold for precipitation onset. The plots for the passes of the aircraft through four clouds agree with much larger droplet diameters relative to the initial aircraft passes through the first two clouds. The aircraft-inferred effective diameters for these four passes range between 32 and 49 μm diameter, while the effective diameters of the composite cloud within the magenta box from the satellite imagery range between 32 and 36 microns—again very good agreement. The last inset of Figure 19 gives a representative picture of the cloud particles—in this case, small drizzle drops at a temperature of 2°C (36°F). The drops can be sized upon knowing that the width of the black strip in which the drops are shown is 1,500 μm or 1.5 mm. Thus, the drops within the magenta box have reached precipitation size.

The aircraft continued down the track to the next yellow box, where three cloud passes were made (Figure 20). Having climbed to temperatures averaging -11°C (12°F), the aircraft measurements give effective diameters ranging between 26 and 33 μm. Note that the imaged frozen drops are still of precipitation size. The cloud coloration in the satellite image here and the inset plot indicate somewhat smaller cloud particles, ranging between 31 and 34 μm effective diameters for the flight level of the aircraft. This is somewhat greater than was measured by the aircraft during the two cloud passes through clouds in the yellow box.

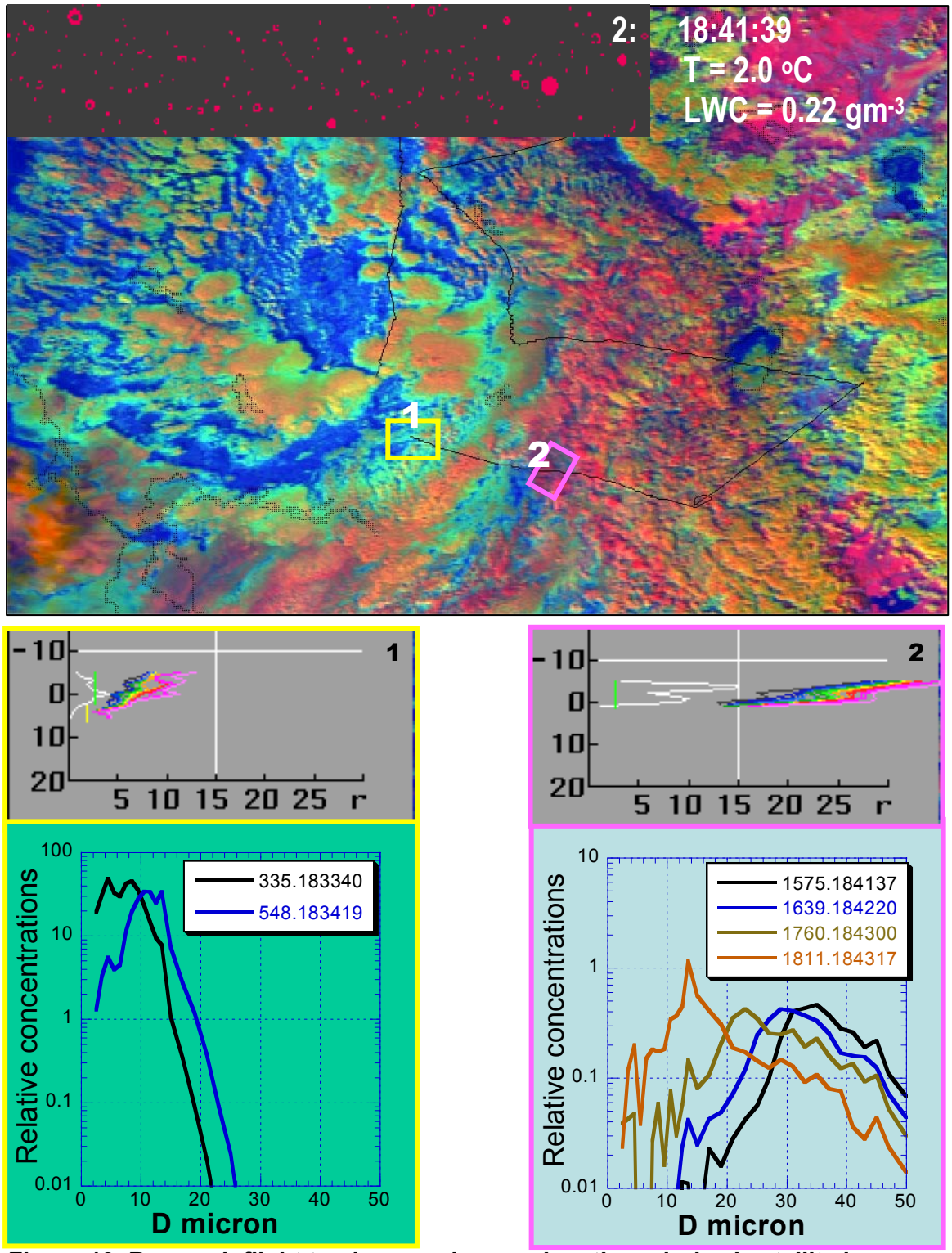

Figure 19. Research flight tracks superimposed on the colorized satellite image on February 7, 2005. The accompanying plots show the T-r_e (0–30 µm droplet radius and the corresponding aircraft cloud penetration data (0–50 µm droplet diameter).

Then the aircraft climbed to 4,514 m (14,810 ft) at a temperature of -15˚C (5˚F) and flew into the area near the California/Nevada border where the satellite clouds have a distinctly yellow coloration that implies small drop sizes (magenta box 4). Indeed, the effective diameters determined from the satellite imagery and aircraft cloud pass are both 24 μm. Despite the cold temperature, the particle sizes are very small, as can be seen in the accompanying inset showing the cloud particles and the maximum cloud water was 0.66 grams per square meter (gm/m^3) during the cloud pass.

The cloud physics aircraft then flew WNW from its previous position into the magenta area again and descended to temperatures between 0˚C (32˚F) and -5˚C (23˚F) (yellow box 5 in Figure 20). The particle images show many frozen drops even though there are substantial quantities of cloud liquid water. The aircraft measurements of effective diameters for the four cloud passes range between 26 and 33 μm whereas the satellite inferred effective diameters range between 38 and 52 μm, which are considerably greater than the aircraft measurements. This disparity is seen typically when the subject clouds contain large ice particles. The agreement between the satellite inferences and the aircraft measurements is best when the clouds have mainly liquid drops. The obvious point to be made here is that the satellite correctly distinguishes between clouds with small and large particles and when those particles have reached precipitation sizes.

The aircraft continued to the northwest, where another magenta box (#6) has been defined to encompass the four cloud passes made between 200233 GMT and 200445 GMT at temperatures slightly < 0˚C (32˚F). The cloud coloration has changed from pink to gold, which should mean smaller particles, and this is what was observed. The ranges of the satellite- and aircraft-inferred effective diameters are 20 to 27 μm and 21 to 25 μm for the aircraft and satellite inferences, respectively. Very little cloud water was observed on the four cloud passes, which was no surprise in view of the large rimmed snowflakes observed during the passes.

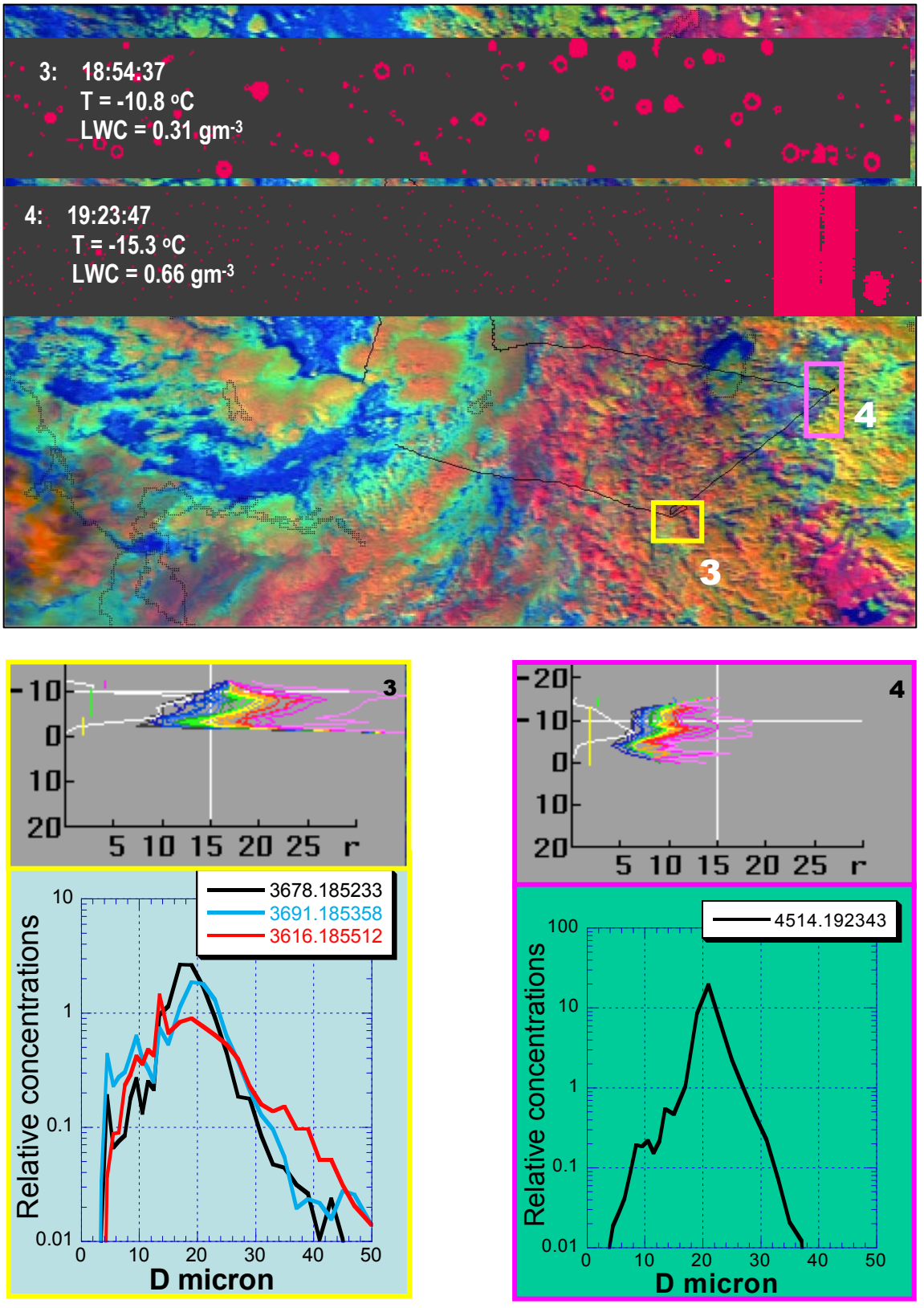

Figure 20. As in Figure 19, but for subsequent cloud passes

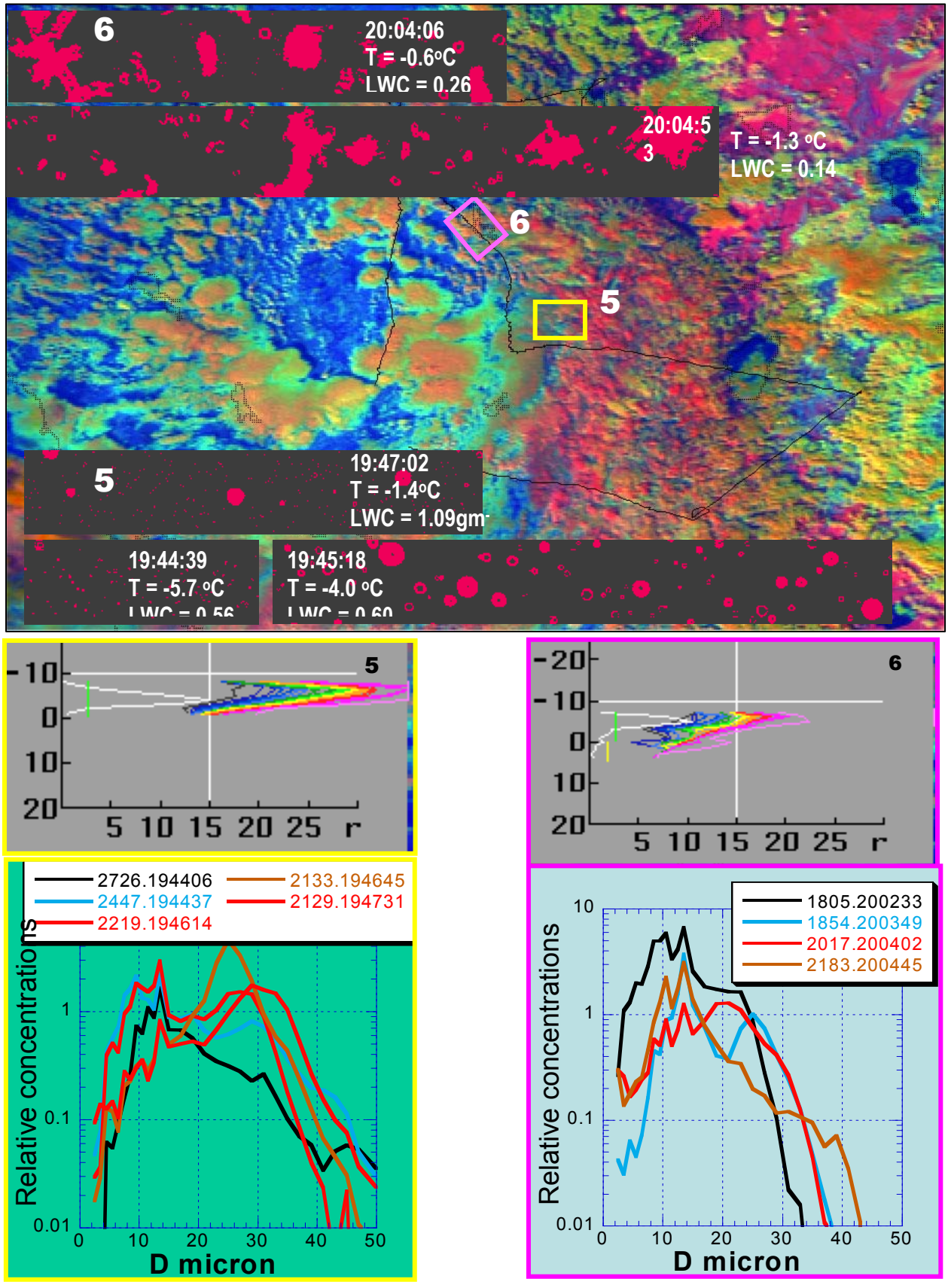

Figure 21. As in Figure 19, but for later cloud passes

The aircraft continued to the northeast, where four additional cloud passes were made in the area indicated by the yellow box (#7) (Figure 21). The coloration of the clouds in the yellow box is yellow, indicating smaller particle sizes and that is what was observed. The effective diameter for the four cloud passes range between 18 and 26 μm and the corresponding range from the satellite imagery is 26 to 28 μm. Again, the clouds contain substantial quantities of cloud water at temperatures between -6˚C (21˚F) and -9˚C (16˚F).

The aircraft then moved to the west, to the area indicated by box 8, where the cloud coloration was magenta. As expected the particles sizes were larger, with effective diameters of 31 μm for the aircraft passes and 42 μm for the satellite inferences. The cloud passes were made near -6˚C (21˚F) and a mixture of ice crystals in columnar form and cloud water contents of slightly over 1.0 gm/m^3.

The next seven aircraft cloud passes were made in the area indicated by the two yellow boxes (#9) on the western portion of the flight track as the aircraft returned to Sacramento airport (Figure 22). The cloud coloration is yellow-green to gold and the droplet effective diameters are quite small, ranging between 14 and 16 μm from the aircraft and between 10 and 12 μm from the satellite. Although clouds here were just to the east of the center of cyclonic circulation, they have no precipitation-sized particles. By extrapolation, that holds for the entire closed cyclonic circulation, and this could be due to pollution effects from San Francisco, Oakland, and Sacramento on this day. This can be visualized by looking at the colorized satellite image without any of the overlays. Although it can not be proven that this is a pollution effect from the data at hand, that is the implication. Certainly the clouds here are the most continental in character, having the smallest particle sizes of any clouds to the west of the Sierra crest.

The great agreement between the satellite inferences of cloud microstructure and the aircraft measurements is very gratifying. It suggests that the satellite inferences of cloud structure, even when aircraft "truth" is absent, can be trusted to give a good representation of actual cloud structure. This corroborates the inferences of the effect of pollutants in mountainous regions downwind of major industrial areas in California that have been discussed elsewhere.

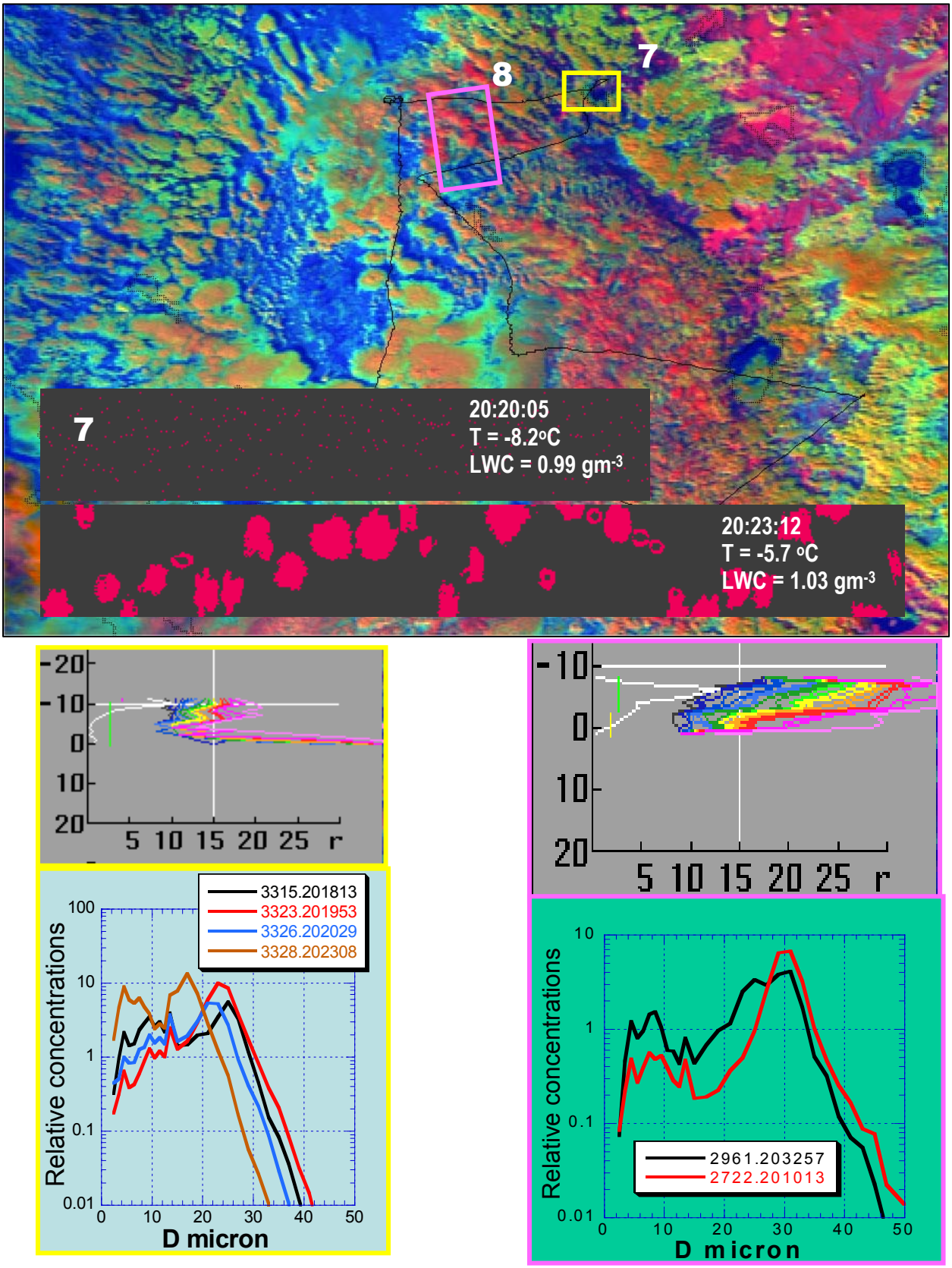

Figure 22. As in Figure 19, but for later cloud passes

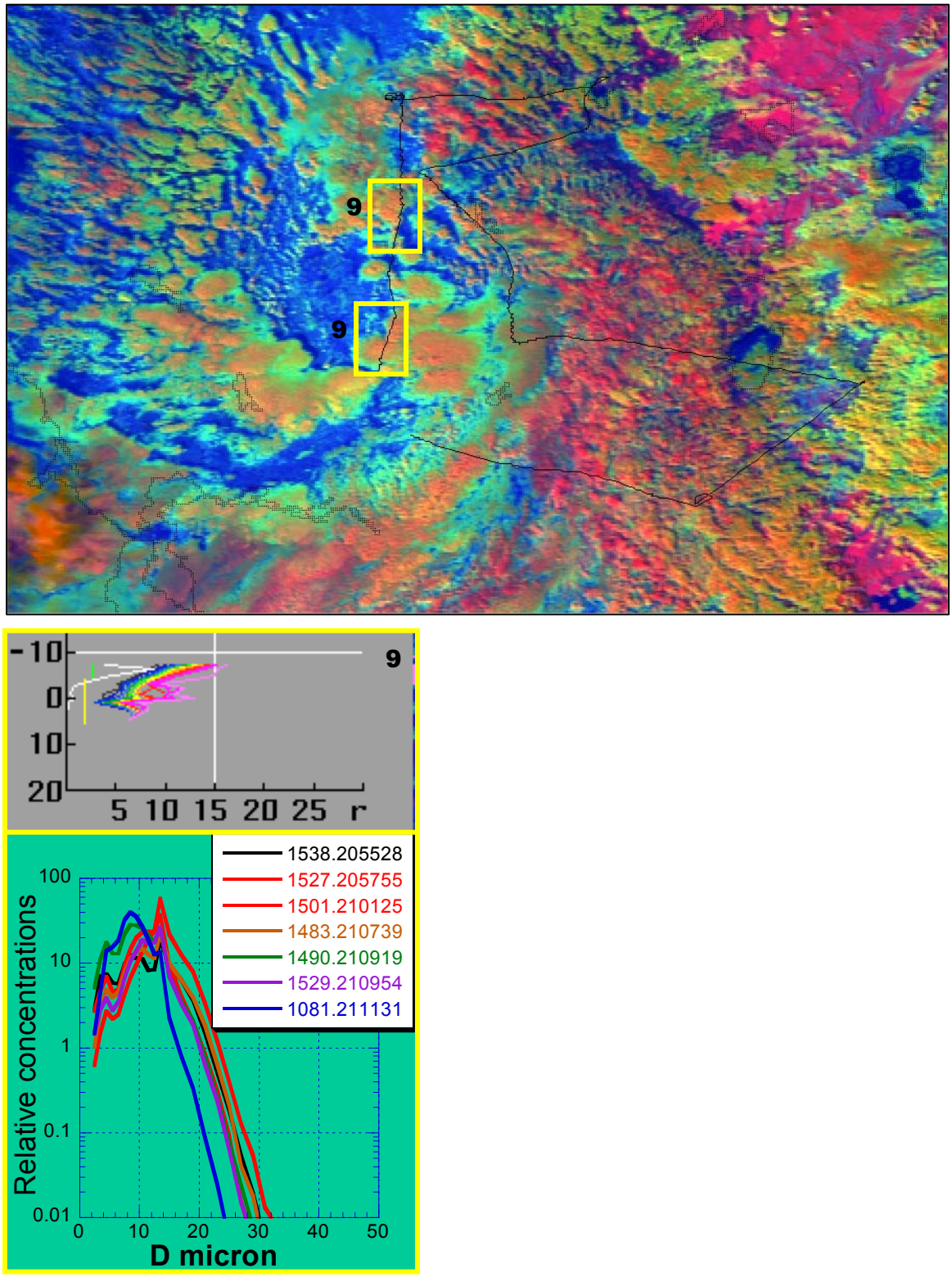

Figure 23. As in Figure 19, but for later cloud passes

The calculations for this case, focusing on the effective radius, are summarized in Table 3. The effective radius is a much more stable property than most might believe. Satellite measurements of r_e are affected by all particles in the clouds; whereas the aircraft cloud droplet spectrometer measures the droplets with diameters < 50 μm. This disparity in measurement scale is one cause for the satellite retrieved effective radius (r_e) to exceed the aircraft measured r_e, especially in rain clouds. The coalescence in clouds with CDP-measured r_e > 10 μm causes larger particles that cause the satellite to see increasingly larger r_e than the aircraft does. This is manifested in Figure 23 below, based on the quantitative analysis of the case of 7 February 2005, presented in Table 3 here.

Other causes for satellite overestimate of the r_e can be:

1. the inhomogeneity of clouds, causing a systematic satellite overestimate of several μm, and/or
2. broken clouds with surface contributions and 3-D effects.

These two problems have been avoided here by applying the Rosenfeld and Lensky (1998) methodology for the clouds selection. Broken and thin clouds are rejected by selecting only clouds with visible reflectance > 0.4 and brightness temperature difference of 10.8–12.0 μm channels < 1.0°C (34°F). Three-dimensional effects are minimal when retrieving the r_e at the highly absorbing wavelength of 3.7 μm. The results of the selection are evident in Figure 23, where there is a close match between the satellite- and aircraft-retrieved re at r_e< 10 μm. The start of the precipitation forming at aircraft r_e > 10 μm drives the satellite retrieved r_e quickly above the 14 μm precipitation threshold for the *satellite*-retrieved r_e.

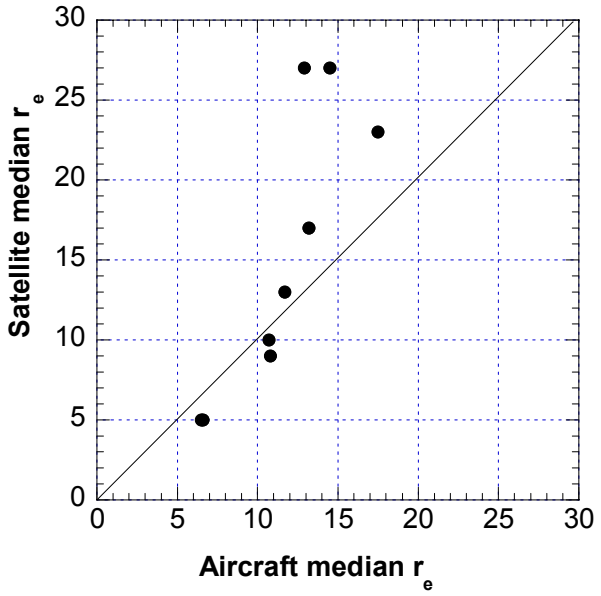

Figure 24. Relation between satellite and aircraft retrieved effective radius, based on the values in Table 3. The line is the 1:1 ratio.

The next step was an investigation of the relationship between the satellite and aircraft-inferred precipitation, as shown in Figure 24, which was derived from the data presented in Table 3, Note from the figure that there was no precipitation water in clouds viewed by the satellite at r_e values < 13 microns. The precipitation water increased at greater satellite-derived r_e. This result is consistent with the study of Rosenfeld and Gutman (1994), in which they used radar and satellite observations to determine that the effective radius of clouds viewed in the satellite imagery had to reach effective radii of 12 to 14 μm for effective coalescence and precipitation. Both results indicate that pollutants will decrease precipitation if it acts to decrease the effective radius.

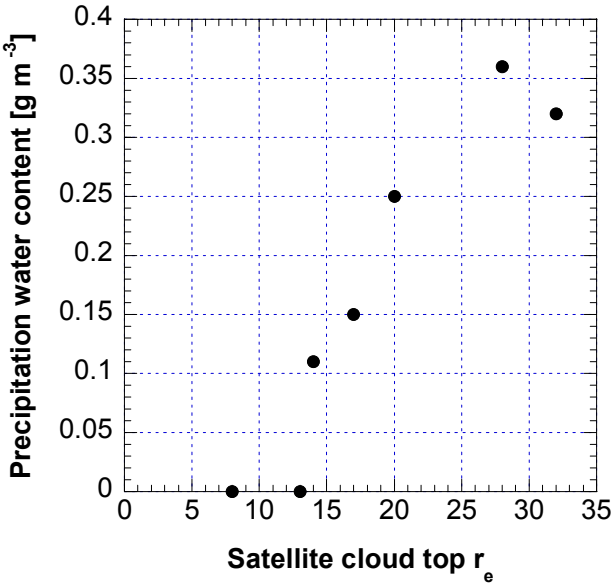

Figure 25. Relation between satellite-retrieved effective radius at the highest cloud tops and aircraft-retrieved precipitation water content, based on the values in Table 3 from data collected by the aircraft in SUPRECIP on February 7, 2005.

Table 3. Comparison of aircraft and satellite retrieved cloud properties for 7 February 2005.

Area	Acft Time	T range	Acft N sec	Satellite15%, 50%, 85% r_e	Sat cld top T	Sat cld top med r_e	Acft min, median, max r_e	Clouds LWC Mean, max	Precip LWC Mean, max
1		2		4, 5, 6	-7	8			
	18:34:33	7.4	6				6.5, 6.6, 6.7	0.21, 0.29	0, 0
2		0		14, 23, 26	-7	32			
	18:41:37	0.8, 2.0	39				12.4, 17.5, 20.1	0.13, 0.20	0.32, 1.14
3		-9		14, 17, 21	-9	20			
	18:52:33	-10, -11	41				9.9, 13.2, 19.0	0.12, 0.27	0.25, 2.49
4		-15		7, 9, 14	-15	14			
	19:23:43	-15, -16	9				10.4, 10.8, 11.1	0.42, 0.54	0.11, 0.26
5		-6		20, 27, 32	-8	28			
	19:44:06	-5, -6	21				11.8, 12.9, 15.0	0.16, 0.49	0.36, 3.00
6		0, -2		7, 10, 12	-8	16			
	20:02:33	0, -2	61				6.0, 10.7, 15.5	0.10, 0.21	SNOW
7		-6, -9		10, 13, 17	-11	17			
	20:18:13	-6, -9	58				6.5, 11.7, 13.8	0.40, 0.82	0.15, 0.77
8		-4, -6		15, 27, 30	-8	31			
	20:32:57	-4, -6	18				13.3, 14.5, 16.0	0.62, 0.93	SNOW
9		1, 2		4, 5, 6	-8	13			
	21:01:25	1, 2	74				3.5, 6.5, 8.0	0.18, 0.43	0.00, 0.01

The columns are:

Area: The area number that corresponds to the area numbers in the report for 7 February 2005.
Acft time: The time [UT] of the first second of aircraft cloud measurement
T range: The temperature or temperature range at which the measurements are reported in this line.
Acft N sec: The number of in-cloud aircraft seconds reported in this line.
Satellite 15%, 50%, 85% r_e: The satellite-retrieved effective radius of the 15, 50, and 85 percentiles of the r_e for the specified temperature range [μm].
Sat cld top T: The coldest cloud top temperature in the satellite window.
Sat cld top med r_e: The satellite retrieved effective radius of the coldest clouds.
Acft min, median, max r_e: The aircraft CDP-calculated r_e of the minimum, median, and maximum 1-secr_e of the N cloud data seconds reported in this line.
Clouds LWC Mean, max: The aircraft CDP-calculated mean and 1-sec maximum liquid water content [g m^{-3}]
Precip LWC Mean, max: The aircraft CIP-calculated water from particles > 0.1 mm, assuming water spheres [g m^{-3}]. The calculation overestimates the precipitation water in case of ice hydrometeors, and fails when aggregates (snow) occurs. In such case "SNOW" is reported.

3.3.2. Quantitative Comparisons for March 4, 2005

The next day studied was March 4, 2005—a day on which there were two flights to study the clouds. As was the case during most of February and early March 2005, there was a low-pressure area well to the south of Sacramento, in this case near Santa Barbara. This put the Sacramento area into low-level easterly flow around this low with virtually no transport into the Sierra Nevada. Figure 25 documents the weather conditions at 0000 GMT on March 5, 2005, which is the time nearest the time of the afternoon flight. Only the second flight is discussed here.

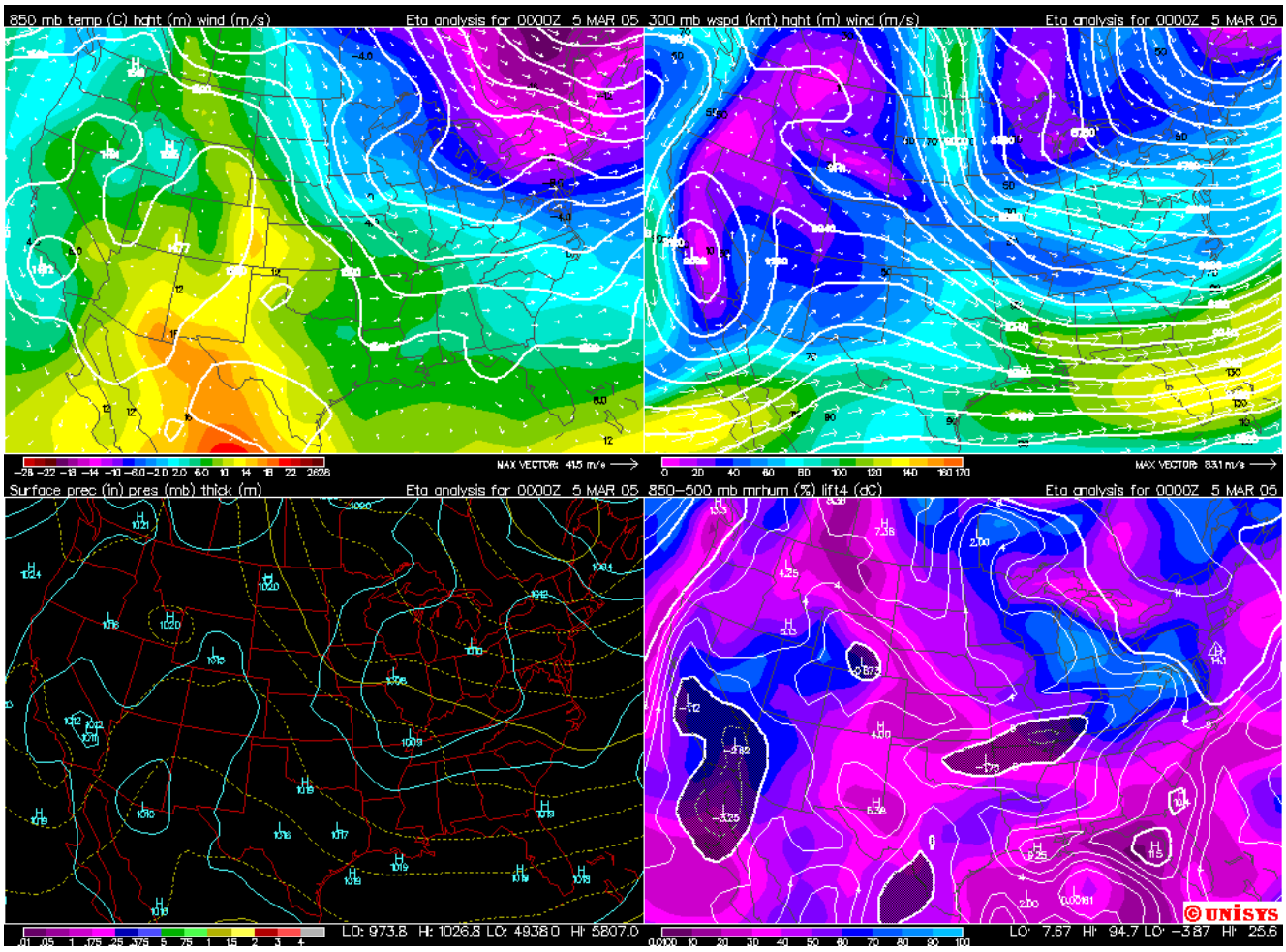

Figure 26. The initial weather conditions at 0000 GMT on March 5, 2005, that served to initialize the run of the Eta forecast model. The depicted weather conditions occurred about 3.5 hours after takeoff of the Cheyenne cloud physics aircraft.

Figure 27 illustrates the 850 mb wind field. In going from east to west across Northern and Central California, the 850 mb winds are easterly to the east of the Sierra Crest, zero at the portions of the mountains above the 850 mb pressure level, then northerly to the west of the divide and finally backing into the northwest over the Pacific. The wind speeds are strongest over the water. The closed cyclonic circulation can be seen in the far south of the figure. Thus, the portion of the Sierra of interest did not have any upslope flow from the west.

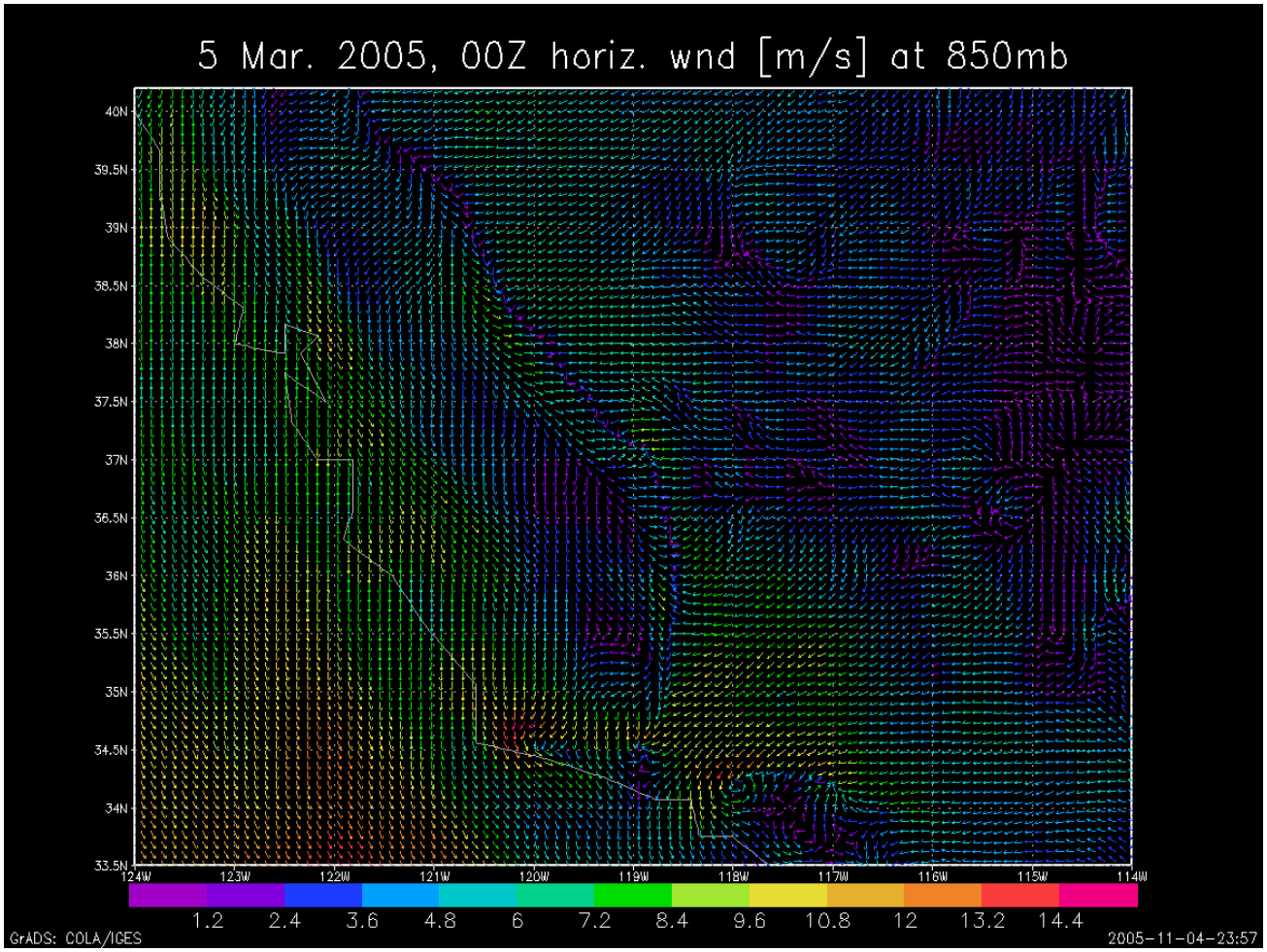

Figure 27. The 850 mb wind field (m s^{-1}) at 10 km resolution at 0000 GMT on March 5, 2005, as provided from the CaRD10 product by Dr. Masao Kanamitsu of the Climate Research Division of the Scripps Institution of Oceanography, at the University of California, San Diego

The aircraft took off at 2033 GMT (1200 PST) and passed through the very low polluted clouds in a layer between 800 and 1400 ft (240 and 430 m). It then penetrated an upper layer of cloud having a base at 4500 ft (1370 m) and climbed to 11,000 ft (3350 m) in rain, breaking out of the clouds while flying westward toward Point Reyes. The cloud tops in this area reached 5500 ft (1680 m), slightly lower than the clouds farther north near the coast. The clouds were microphysically continental with narrow spectra and > 200 droplets cm^{-3}, uncorrected. The aircraft was then flown to the southwest of San Francisco where the clouds became somewhat less continental. These clouds had the shape of shelf clouds wedging to the west, feeding the main cloud system to the east over the coast. The researchers on this aircraft saw developed convection with glaciated tops to the south over the ocean, and wanted to fly to there, but this could not be done because the flight plan called for flight to Salinas and Big Sur in order to study the clouds triggered by the coastal range. The low clouds ended towards Monterey, where the aircraft flew southwest to Salinas and crossed into the multilayer clouds, ascending to 7500 ft (2290 m) and then turning back westward through Big Sur. The layer clouds indeed intensified over the coastal range. The aircraft flew some 20 miles (32 kilometers, km) farther to the west over the ocean before breaking out of the layer clouds into convection that was just bounding the frontal cloud system. The aircraft was used to make detailed vertical profiles of the convection between 5,800 (1770 m) and 11,500 ft (3500 m) between 22:04 and 22:30 GMT. Some of the cloud tops were visibly glaciating, and some had nice capping pileus clouds, which were measured. These clouds were quite maritime, much more maritime than the clouds to the north over Point Reyes, but still significantly less maritime than the clouds studied during the early morning flight to the west of Mendocino. The aircraft then turned back to the east into the precipitating layer clouds. To the southeast of San Francisco there were good convective clouds developing in the rain into the layer clouds, which had much cloud water (> 1 g m^{-3} at 4500 ft, or 1370 m) and drop concentrations > 200 drops cm^{-3}. This was probably a pollution signature of San Francisco that overpowered the cleansing effect of the rain. The aircraft then passed through less developed convection that developed in the visibly hazy polluted air farther towards Sacramento and landed. The convective clouds on this flight had significant pollution signatures near San Francisco. Maritime clouds could be found only to the southwest and far to the northwest of San Francisco. The satellite and aircraft comparisons to be discussed next confirm this.

Figure 28 presents the NOAA-16 colorized image at 2224 GMT. As with the previous case, the flight track of the aircraft is shown on the image. Taking the long view of the image, one can see that the clouds in the San Francisco area have a green to pink tint, suggesting a pollution signature, whereas those to the south and southeast are predominantly red.

There were five cloud passes in the yellow box (#1) near Point Reyes. The aircraft-measured effective drop diameters ranged between 16 and 20 μm for the five passes, while the satellite values were 20 μm. These are small values that probably show the effect of the pollutants on the clouds. Again the agreement between the two is quite good.

The aircraft then moved to the south along the track and made four cloud passes within the magenta or purple box (#2) that contains clouds having a deeper magenta color relative to those in the initial yellow box. This means larger cloud drops and that proves to be the case. The range of the effective diameters for the aircraft passes is 19 to 22 μm while the range for the satellite inferences is 29 to 30 μm.

Moving still farther south to the yellow box shown in Figure 29, note that the cloud coloration is magenta to purple and the two cloud passes for clouds in this box (#3) shows larger drops only this time the effective diameters for the aircraft cloud passes of 30 to 32 μm exceed those inferred by the satellite for cloud pixels in the box of 24 to 26 μm. At the time of the flight it was recognized that the two clouds sampled in the magenta box were the most vigorous along the track and more representative of those seen farther to the west. It was decided, therefore, to examine the clouds in another box (#4) farther to the west. There were eight cloud passes along the track at the altitudes and times shown and these were compared to the satellite analysis for clouds in box #4, even though the cloud passes were not made through clouds in that box. The range of effective diameters for the cloud passes and the satellite inferences corresponding to the cloud passes are 27 to 35 μm for the aircraft cloud passes and 30 to 35 μm for the satellite analyses.

Upon moving back to the north later in the flight to box #5 (Figure 30) note that the clouds here have a yellow-green hue, meaning small particle sizes. This is verified by the aircraft cloud passes and the satellite analyses with aircraft and satellite-inferred effective diameters of 15 to 19 μm and 18 to 22 μm, respectively. This area is squarely in the region that appears to be a pollution cloud footprint in the San Francisco area. It is localized in its area of origin and offshore to the west and southwest because of the light offshore flow around the low-pressure well to the south.

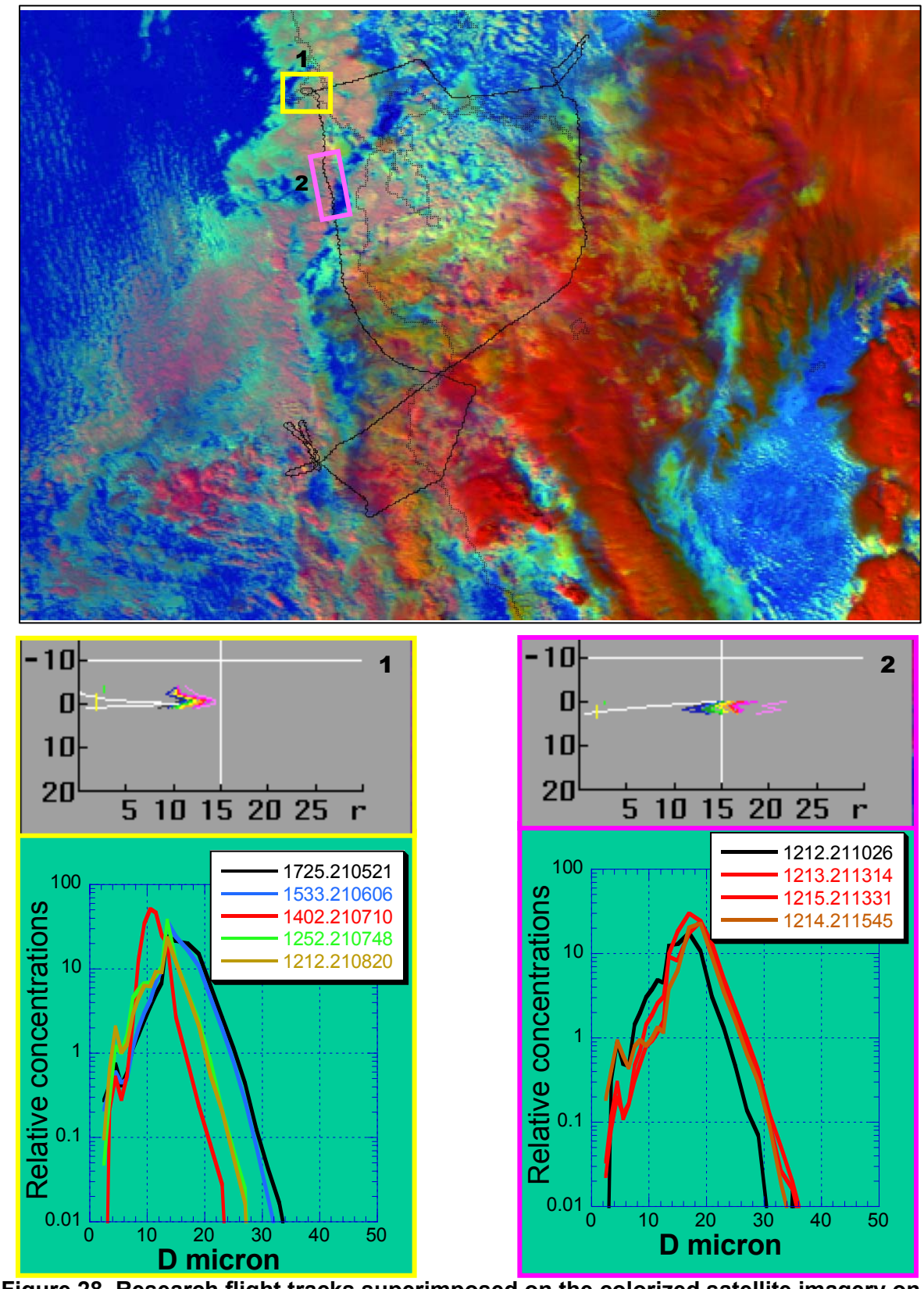

Figure 28. Research flight tracks superimposed on the colorized satellite imagery on 4 March 2005. Accompanying plots show the T-r_e plot (0–30 µm droplet radius) and the corresponding aircraft cloud penetration data (0–50 µm droplet diameter).

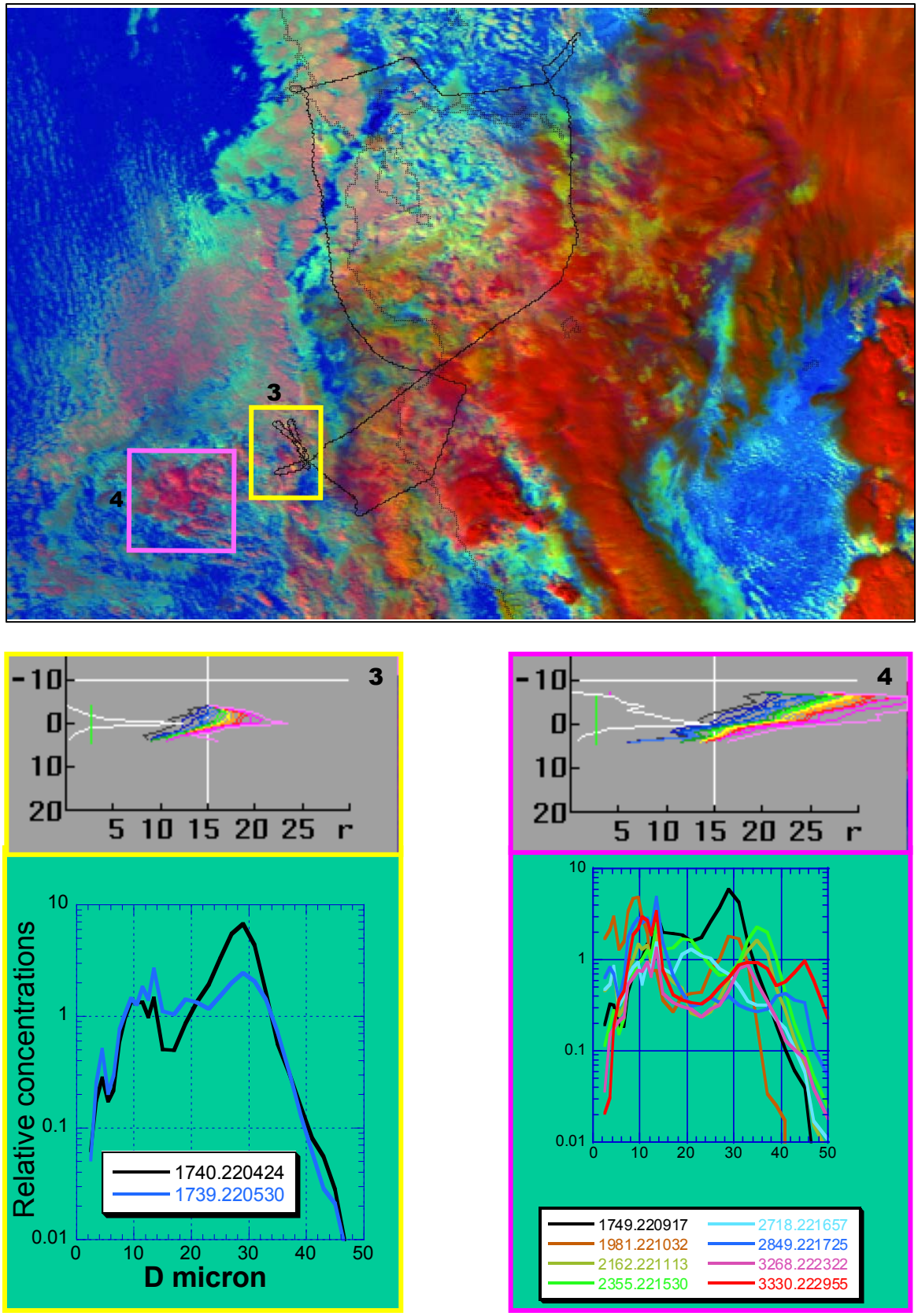

Figure 29. As in Figure 28, but for later cloud passes

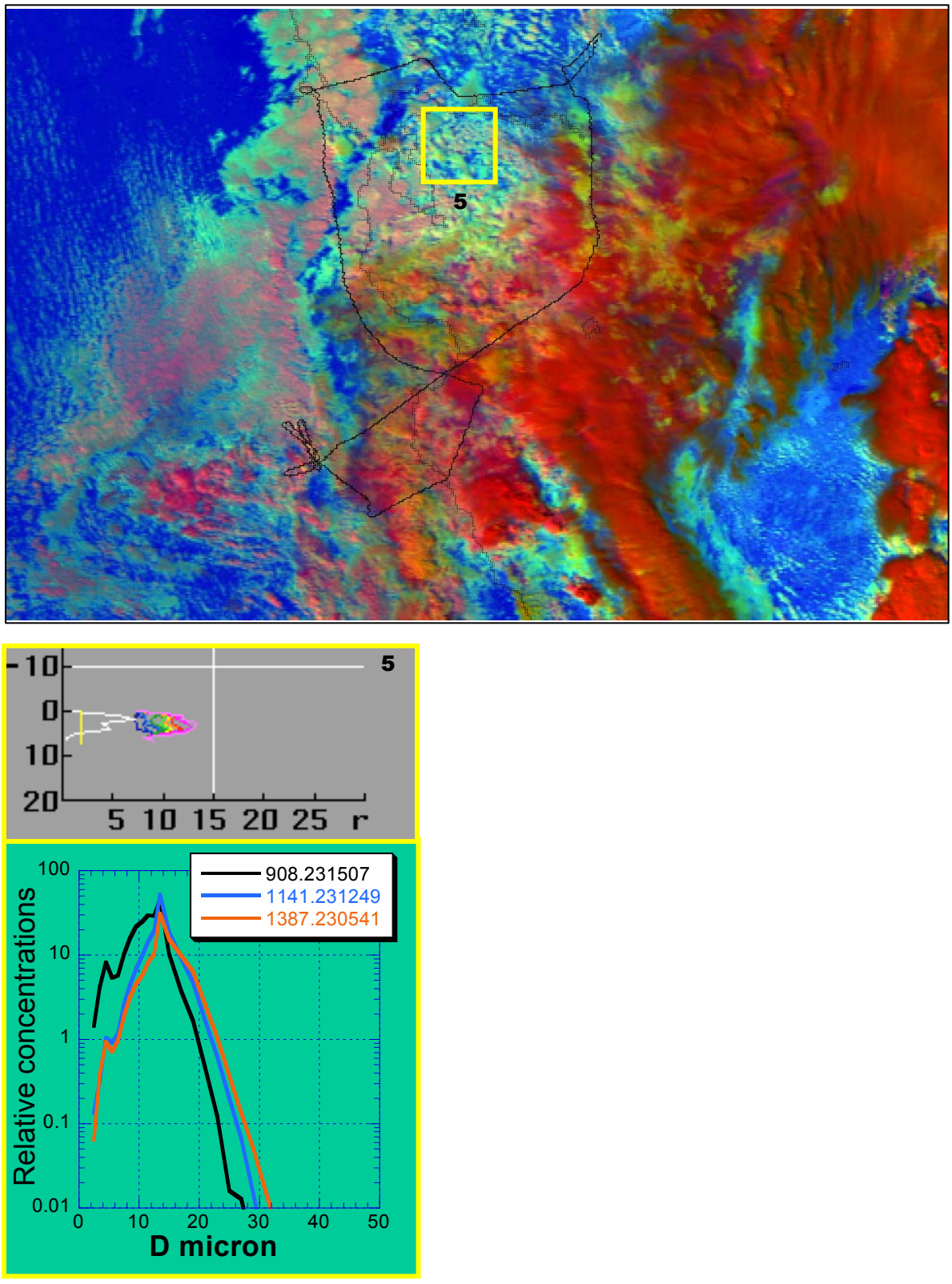

Figure 30. As in Figure 28, but for later cloud passes

3.3.3. Comparison of Overall Satellite and Aircraft Measurements

The satellite and aircraft inferences of cloud microstructure were made in terms of the effective radius. As described in the previous sections, the satellite inferences were made for all of the cloud pixels within a series of boxes along the flight track. Each box was defined such that it encompassed some of the individual aircraft cloud passes. This made it possible to compare the median effective radii for the cloud passes at the height and temperature of the pass with the satellite inferences of the effective radii at the 50th percentile for the composite cloud for all clouds in the box. The results are given in Figure 31, which shows a scatter plot of the cloud microphysical effective radii as measured by the cloud physics aircraft (Aircraft Reff, or effective radius) versus the inferences from the satellite imagery (Satellite median Reff) for the two days of study. Considering the differences in scale (i.e., individual cloud passes versus the composite cloud within a box that contains the cloud passes) and time, the agreement is remarkably good (linear correlation=0.73), giving increased credibility to the satellite inferences of suppressed precipitation-forming processes associated with pollution. For the purposes of this research effort, this is an important finding.

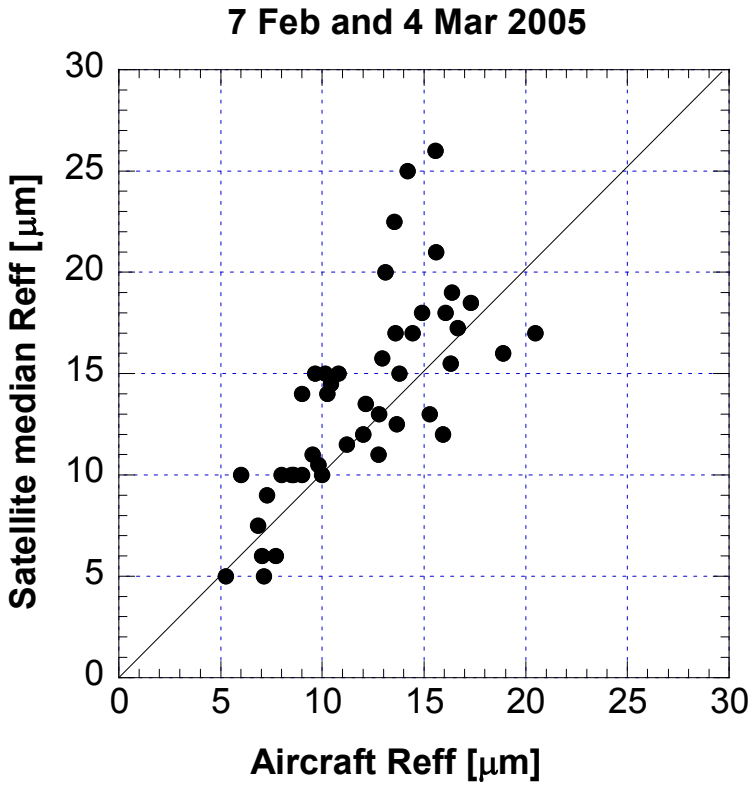

Figure 31. Scatter plot of the median effective radii determined by aircraft (Aircraft Reff) for individual cloud passes vs. the median effective radii inferred from the multi-spectral satellite imagery (Satellite median Reff) for the altitudes and temperatures of the aircraft cloud passes for clouds within boxes that contain the cloud passes. The comparisons were made for data obtained on February 7 and March 4, 2005.

3.3.4. The Status of Objective 2

The accomplishments in addressing Task 2 include the following:

- Validation of the satellite inferences of cloud microstructure using the in-cloud measurements from the cloud physics aircraft on two days of measurement (February 7 and March 4, 2005).
- Verification that pollution aerosols are instrumental in altering the internal structure of the clouds and their resultant precipitation.

Despite these accomplishments, Objective 2 under the contract was not reached fully because the sample was too small to justify claiming that the validity of the satellite inferences had been proven.

4.0 Conclusions and Recommendations

4.1. Conclusions

The research team working under the umbrella of Woodley Weather Consultants with the support of the California Energy Commission (Energy Commission) conducted a comprehensive scientific investigation, involving statistical analyses, quantitative satellite imagery, cloud and mesoscale modeling, and aircraft measurements, to address the loss of precipitation in the California Sierra Nevada as the result of pollution produced in upwind urban/industrial areas. The pollution aerosols are tiny CCN that result in a very narrow drop spectrum of small drops that inhibits droplet coalescence processes, the riming of ice crystals, and ultimately precipitation from the clouds. The Suppression of Precipitation (SUPRECIP) Experiment, was conducted with Energy Commission support to investigate these processes. The researchers documented the number, sizes, and concentrations of ingested aerosols and the resulting internal cloud microphysical structure using a cloud physics aircraft. Although much was accomplished in SUPRECIP, it is important not to "oversell" the effort as having accomplished more than it really did.

Realistically, it is our contention that this report validates the satellite inferences with respect to the following:

1. The retrieved satellite-indicated r_e represents an actual reduction in r_e, as validated by the in-cloud measurements.
2. The satellite inference that reduction of r_e is associated with suppression of the precipitation was validated by the in situ aircraft measurements.
3. There are some measurements showing that enhanced aerosol concentrations are associated with the decreased r_e and suppressed precipitation.

It is useful to summarize the results by objective here. In addressing Objective 1, the use of the cloud physics aircraft made possible the documentation of differences in cloud microstructure associated with differences in CCN, measured by the airborne CCN counter, that were visibly related to air pollution. With respect to Objective 2, it was determined further that these differences were related to the satellite retrievals, which were validated by the aircraft measurements. This is crucial since, previously, only the satellite retrievals were available as indicators of the apparent negative effect of pollution on Sierra precipitation. The new aircraft measurements have provided further "ground truth" for the satellite inferences. Thus, the aircraft component of the overall investigation showed the negative impact of pollutants on cloud processes and precipitation and made the linkages much more credible. Pollution is certainly affecting Sierra clouds and precipitation detrimentally. Through the aircraft and satellite measurements in SUPRECIP it has been noted that much of the Sierra precipitation was produced by surprisingly shallow pristine clouds. This observation suggests that pollution will act detrimentally on such clouds, if a mechanism, such as convective transport and/or orographic lift, is operative for the clouds to ingest the pollutants from the polluted boundary layer. This might help explain the long-term losses in Sierra orographic precipitation.

The results from SUPRECIP support the view that pollution is suppressing California orographic precipitation. Although much was accomplished, further investigation is needed, because it is impossible to characterize the problem in only a five-week measurement program. The weather was highly anomalous for the entire U.S. West Coast during the measurement program. Because of a high-pressure blocking pattern at the surface and aloft and the resulting split in the jet-stream flow, the usual Pacific storms were shunted far to the south of Sacramento. Thus, the typical Sierra orographic clouds thought to be most sensitive to the effects of pollution, produced by westerly winds into the Sierra, were rare during SUPRECIP, and the program was extended through the first week in March 2005 in an attempt to obtain additional orographic storm events.

Two papers of great relevance to SUPRECIP were prepared by members of the SUPRECIP research team and were being prepared for submission for publication while this final report was being prepared. These draft papers will be provided to interested parties by WWC upon request. The first paper is "Robust relations between CCN and the vertical evolution of cloud drop size distribution in deep convective clouds" by Eyal Freud, Daniel Rosenfeld, Meinrat O. Andreae, Alexandre A. Costa, and Paulo Artaxo.

The second paper, "The time-space exchangeability of satellite retrieved relations between cloud top temperature and particle effective radius," (Lensky and Rosenfeld 2005) is under review. Because of the great relevance of this paper to this report, the abstract for this paper is included below.

> A 3-minute 3-km rapid scan of the METEOSAT Second Generation geostationary satellite over southern Africa was applied to tracking the evolution of cloud top temperature (T) and particle effective radius (r_e) of convective elements. The evolution of T-r_e relations showed little dependence on time, leaving re to depend almost exclusively on T. Furthermore, cloud elements that fully grew to large cumulonimbus stature had the same T-r_e relations as other clouds in the same area with limited development that decayed without ever becoming a cumulonimbus. Therefore, a snap shot of T-r_e relations over a cloud field provides the same relations as composed from tracking the time evolution of T and r_e of individual clouds, and then compositing them. This is the essence of exchangeability of time and space scales, i.e., ergodicity, of the T-r_e relations for convective clouds. This property has allowed inference of the microphysical evolution of convective clouds with a snap shot from a polar orbiter. The fundamental causes for the ergodicity are suggested to be the observed stability of r_e for a given height above cloud base in a convective cloud, and the constant renewal of growing cloud tops with cloud bubbles that replace the cloud tops with fresh cloud matter from below. (Lensky and Rosenfeld, 2005, Abstract)

4.2. Recommendations

It is recommended that SUPRECIP be continued for a second year as SUPRECIP-2, in order to focus on the orographic storm events in the Sierra Nevada that were lacking in 2005. Specifically, it is crucial to document the ingestion of the pollution aerosols by the orographic clouds as they move uphill. The satellite imagery already shows that this is taking place and the precipitation measurements show the long-term effects of the pollution. Because it was nearly impossible in 2005 to "map" the pollution aerosols at low levels in urban areas with the cloud physics aircraft on an IFR flight plan, it is recommended further that a second aircraft be used to carry the CCN counter for the mapping of the pollution aerosols at low levels during VFR flight. More attention must be focused on the details of the pollution "footprint" as to the sources, kinds and concentrations of the pollution aerosols and on what portions of the Sierra should be most affected by them. With this plan the low-level aircraft will map the pollution aerosols while the cloud physics aircraft flies above to document their effects on the clouds ingesting them. More study of highly efficient Sierra precipitating clouds, the role that they play in the region's water budget and the effect of pollutants should also be examined. It is important also to obtain some insights as to the amounts of Sierra precipitation that are produced pre-frontally, frontally and post-frontally. The overall losses of annual precipitation are too large to ascribe all of the losses to suppressed post-frontal precipitation. The evidence from SUPRECIP-1 supports this view.

4.3. Benefits to California

This research effort already has been highly beneficial to California, because it has identified and quantified a significant problem for the regional water supply. The California Sierra Nevada is losing orographic precipitation and subsequent runoff, apparently because of the suppressive effects of fine pollution aerosols. If validated by continuing study, this suppressive effect ultimately will have serious consequences for California's water supply and hydroelectric power generation. The SUPRECIP effort has been very valuable because it has quantified the effect of the pollutants on the cloud microstructure and precipitation forming processes. Most importantly, SUPRECIP has validated the satellite inferences of the large-scale effects of pollutants on clouds and precipitation in California. As such, it has strengthened the scientific basis of the overall findings and it has provided the impetus for continuing study of this serious problem. Over the long term, resolving this issue will be highly beneficial to California, because it will be crucial to the development of informed public policy relating to future development in the state and to the pollution that results from that development. It will also influence priority setting at the state and federal levels.

4.4. Access to SUPRECIP-1 Data

Because of its great interest in sound science, Woodley Weather Consultants will make its SUPRECIP-1 data available to the scientific community for scientists interested in conducting their own analyses. WWC plans to develop a SUPRECIP-1 data CD or DVD and to make it available to reputable scientists upon their request. The contact person to request the data is Dr. William L. Woodley, President of Woodley Weather Consultants, at 303-979-7946 or williamlwoodley@cs.com. The content of the data CD or DVD is documented in Appendix E.

5.0 References

Bomar, G. A., W. L. Woodley, and D. L. Bates. 1999. "The Texas weather modification program: Objectives, approach and Progress." *J. Wea. Mod.* 31: 9–22.

Givati, A., and D. Rosenfeld. 2004a. "Quantifying precipitation suppression due to air pollution." *J. Appl. Meteor.* 43: 1038–1056.

Givati, A., and D. Rosenfeld. 2004b. "Separation between cloud seeding and air pollution effects." *Journal of Applied Meteorology.* 44: 1298–1314.

Kanamitsu, M. 2005a. *Scale Selective Bias Correction in Downscaling of Global Analysis Using a Regional Model.* CEC-500-2005-130.

Kanamitsu, M. 2005b. Insight into Regional Atmospheric Variability from Five Decades of High Resolution Model Simulation over California. Presented at the Second Annual Climate Change Research Conference, sponsored by the California Energy Commission and the California Environmental Protection Agency (CalEPA).

Nober, F., H.-F. Graf, and D. Rosenfeld. 2003. "Sensitivity of the global circulation to the suppression of precipitation by anthropogenic aerosols." *Global Planet. Change* 37: 57–80.

Rosenfeld, D. 1999. "TRMM observed first direct evidence of smoke from forest fires inhibiting rainfall." *Geophys. Res. Lett.* 26: 3105–3108.

Rosenfeld, D. 2000. "Suppression of rain and snow by urban air pollution." *Science* 287: 1793–1796.

Rosenfeld D., and G. Gutman. 1994. Retrieving microphysical properties near the tops of potential rain clouds by multispectral analysis of AVHRR data. *Atmospheric Research* 34: 259–283.

Rosenfeld D., and I. Lensky. 1998. "Spaceborne sensed insights into precipitation formation processes in continental and maritime clouds." *Bulletin of the American Meteorological Society* 79 (11): 2457–2476.

Rosenfeld D., Y. Rudich, and R. Lahav. 2001. Desert dust suppressing precipitation—a possible desertification feedback loop. *Proceedings of the National Academy of Sciences* 98: 5975–5980.

Rosenfeld D., R. Lahav, A. P. Khain, M. Pinsky. 2002. "The role of sea-spray in cleansing air pollution over ocean via cloud processes." Research Article in *Science* 297: 1667–1670. Highlighted and published online in "*Science Express*" on 15 August 2002.

Rudich Y., D. Rosenfeld, O. Khersonsky. 2002. "Treating clouds with a grain of salt." *Geophysical Research Letters* 29 (22): 2060. doi:10.1029/2002GL016055, 2002.

Sacramento Bee. 2004. "Cleaning up the air - Particulates a tough problem. Hundreds of U.S. counties don't meet new standards for tiny—and hazardous—air pollutants." December 18, page A1.

Woodley, W. L., D. Rosenfeld, and A. Strautins. 2000. "Identification of a seeding signature in Texas using multi-spectral satellite imagery." *J. Wea. Mod.* 32: 37–52.

Woodley, W. L., and D. Rosenfeld. 2004. "The development and testing of a new method to evaluate the operational cloud seeding programs in Texas." *J. of Applied Meteor.* 43: 249–263.

6.0 Glossary

ACRONYM	DEFINITION
BL	boundary layer
CaRD10	California Reanalysis Downscaling at 10 km
Cb	cumulonimbus cloud
CCN	Cloud Condensation Nuclei
CDP	Cloud Droplet probe (See Appendix B)
CEC	California Energy Commission
CIP	Cloud Imaging Probe
Cu	cumulus cloud
DMA/TDMA	Differential mobility analyzer/Tandem differential mobility analyzer
DMT	Droplet Measurement Technologies
DSD	Drop Size Distribution
FSSP	Forward Scattering Spectrometer Probe
GMT	Greenwich Mean Time
IFR	Instrument Flight Rules
LWC	Liquid Water Content
mb	millibar
MRF	Medium-Range Forecast Global Model
NOAA	National Oceanic and Atmospheric Administration
PCASP	Passive Cavity Aerosol Spectrometer Probe
PIER	Public Interest Energy Research
Reff	Effective Radius
SOAR	Southern Ogallala Aquifer Rainfall
SUPRECIP	Suppression of Precipitation Experiment
TAMU	Texas A&M University
UT	Universal Time
VFR	Visual Flight Rules
WWC	Woodley Weather Consultants

APPENDIX A

THE INFERENCE OF CLOUD PROPERTIES USING SATELLITE IMAGERY

1. Polar-Orbiting Satellites: The Foundation

The family of sensors on board recent polar-orbiting satellites covers a number of spectral bands in the solar and terrestrial portion of the radiation spectrum. Traditionally, the single visible and single IR channels on most satellites provided only very limited information about the cloud properties, such as visible reflectance, cloud top temperature, and a crude estimate of vertically integrated cloud water. Additional channels on NOAA/AVHRR and TRMM/VIRS in the solar IR (1.6 μm), mid-IR (3.8 μm) and far IR (10.8 and 12.0 μm), and many more on recently launched MODIS onboard AQUA and TERRA, now make it possible to obtain additional information about a wide range of cloud properties. Among them are cloud thickness and cloud composition, i.e., effective radius of cloud top particles, and whether they are composed of water or ice. The added multispectral information makes it possible to retrieve various properties of various types of clouds and surfaces.

The fundamental reason for the added capabilities is the differences in the interaction of the radiation with cloud particles at different wavelengths. A very important contribution of the added multispectral capability comes from the dependence of the absorption of water and ice on the wavelength. The absorption of the solar radiation by the cloud particles occurs within their volume (i.e., proportional to r^3), whereas the scattering of the radiation occurs at their surface (i.e., proportional to r^2). The absorption detracts from the overall back-scattered radiation. This results in net reflected radiation to the satellite (i.e., proportional to r^{-1}). Therefore, the reflected solar radiation in absorbing wavelengths is inversely proportional to the particle size. Taking into account the relative angles of the sun, object and sensor, it is possible to retrieve the effective radius of cloud particles, r_e. The effective radius is proportional to the sum of the volumes divided by the sum of the surface areas of the particles in the measurement volume of the satellite pixel. The large absorption in the 3.8 μm band makes it possible to use this channel for retrieving r_e, in contrast to the non-absorbing visible channel (Arking and Childs, 1985; Nakajima and King, 1990).

In reality, the calculations of the effective radius need to take into account effects such as multiple scattering within the clouds, correction for absorption by gases, upwelling radiation from the surface through the clouds, possible multiple layer clouds, and shadowing effects. Most of these errors increase with increasing solar zenith angles, limiting reasonably accurate retrievals only to times where the sun is more than about 20^o above the horizon, and satellite zenith angle < ~50^o.

Retrieval of r_e has been applied extensively to marine stratocumulus, in order to measure the impact of aerosols on cloud microstructure and through that on the earth's radiation budget. Attention was directed to this subject shortly after launch of the first NOAA orbiting satellites with the Advanced Very High Resolution Radiometer (AVHRR), revealing ship tracks consisting of polluted clouds with enhanced albedo and reduced droplet sizes (Coakley et al., 1987). The pollution particles emitted from the ship stacks act as cloud condensation nuclei (CCN), redistributing the fixed amount of cloud water that must condense into a larger number

of smaller droplets (Radke et al., 1989). It was recognized then that the reduced droplet size suppressed the coalescence and drizzle, thus preventing loss of cloud water. The effects of larger amounts of cloud water in smaller droplets are to increase the cloud reflectance of solar radiation. Similar effects were observed over land, where the impact of smoke on shallow tropical convective clouds was shown to decrease the droplets effective radius from about 15 microns to 9 microns (Kaufman and Fraser, 1997). The increased reflectance, mainly in the solar infra red, has been considered as a cooling mechanism partially counteracting global warming due to the increased greenhouse gases (Houghton et al., 1994). However, the potential applications of 1.6 μm and 3.8 μm reflectance go much beyond the important subject of cloud-aerosol impacts on the earth's radiative budget. The reported (Kaufman and Fraser, 1997) reduction of cloud droplets below the threshold of 14 μm, which is the minimum required size for effective coalescence (Rosenfeld and Gutman, 1994), means that in addition to the radiative effects, the smoke also had a suppressive effect on precipitation.

Much about cloud microstructure and precipitation forming processes in convective clouds can be obtained from analyses of complete cloud clusters, residing in areas containing thousands of satellite pixels. The underlying crucial assumption is that the microphysical evolution of a convective cloud can be represented by composition of the instantaneous values of the tops of convective clouds at different heights. This is based on the knowledge that cloud droplets form mainly at the base of convective clouds, and grow with increasing height or decreasing T. The form of dependence of r_e on T contains vital information about the cloud and precipitation processes, as described below. The T-r_e relations are obtained from an ensemble of clouds having tops covering a large range of T. Usually many pairs of T-r_e for each 1°C interval are observed in a region containing a convective cloud cluster. The points with smaller r_e for a given T are typically associated with the younger cloud elements, whereas the larger r_e for the same T are associated with the more mature cloud elements, in which the droplet growth had more time to progress by coalescence, and ice particles had more time to develop. Therefore, it is useful to plot not only the median value of T-r_e relation, but also, say, the 15th and 85th percentiles for representing the younger and more mature cloud elements within the measurement region, respectively.

Based on the shapes of the T-r_e profiles, Rosenfeld and Lensky (1998) defined the following five microphysical zones in convective clouds:

1) *Diffusion droplet growth zon*e: Very slow growth of cloud droplets with depth above cloud base, indicated by small $-dr_e/dT$.

2) *Droplet coalescence growth zon*e: Large increase of the droplet growth with height, as depicted by large $-dr_e/dT$ at T warmer than freezing temperatures, indicating rapid cloud-droplet growth with depth above cloud base. Such rapid growth can occur there only by drop coalescence.

3) *Rainout zon*e: A zone where r_e remains stable between 20 μm and 25 μm, probably determined by the maximum drop size that can be sustained by rising air near cloud top, where the larger drops are precipitated to lower elevations and may eventually fall as rain from the cloud base. This zone is so named, because droplet growth by coalescence is balanced by precipitation of the largest drops from cloud top. Therefore, the clouds seem to be raining out much of their water while growing. The radii of the

drops that actually rain out from cloud tops are much larger than the indicated r_e of 20–25 μm, being at the upper end of the drop size distribution there.

4) *Mixed phase zone*: A zone of large indicated droplet growth with height, occurring at T < 0°C, due to coalescence as well as to mixed phase precipitation-formation processes. Therefore, the mixed phase and the coalescence zones are ambiguous at 0 < T< -39°C. The conditions for determining the mixed phase zone within this range are specified in Rosenfeld and Lensky (1998).

5) *Glaciated zone*: A nearly stable zone of re having a value greater than that of the rainout zone or the mixed phase zone at T < 0°C.

These zones are idealizations. Not all clouds conform to this idealized picture. The transition between the coalescence and mixed phase zones, which are not separated by a rainout zone, cannot be determined, and are therefore set arbitrarily to –6°C in accordance with aircraft observations. The height of the glaciation zone can be overestimated in the cases of highly maritime clouds that grow through a deep rainout zone, because the scarcity of water in the supercooled portions of the clouds causes small ice particles, which sometimes can be mistaken for a mixed phase cloud. Addition of more spectral bands can help in separating the water from the ice, irrespective of the particle size. On the other hand, in vigorous clouds with active coalescence the height of the glaciation zone can be underestimated, because the high amounts of large ice hydrometeors dominate the radiative properties of the clouds, even when they co-exist with supercooled cloud water.

All of these microphysical zones are defined only for convective cloud elements. Multi-layer clouds start with small r_e at the base of each cloud layer. This can be used to distinguish stratified from convective clouds by their microstructure. Typically, a convective cloud has a larger r_e than a layer cloud at the same height, because the convective cloud is deeper and contains more water in the form of larger drops.

Examples of these zones are shown schematically in panels a through f in Figure 1 for a microphysically maritime cloud growing under conditions of increasing updraft. To the right of each T-r_e plot is the corresponding hypothetical cloud having the hydrometeors shown. Panel a shows a weak maritime cumulonimbus having zones (from bottom to top) of droplet coalescence growth, rainout, mixed phase and glaciation. With increasing updraft intensity the rate of droplet growth decreases, the rainout zone shrinks and disappears, the temperature at which r_e reaches 14 μm (the precipitation threshold) decreases and the temperature at which glaciation takes place decreases, reaching in the extreme the temperature of homogeneous nucleation (-39°C). Thus, powerful clouds have primarily diffusional droplet growth, a deep layer of supercooled water and little precipitation. Rosenfeld and Woodley (2000) and Rosenfeld et al. (2001) have observed such clouds with a jet cloud physics aircraft in Texas and Argentina, respectively.

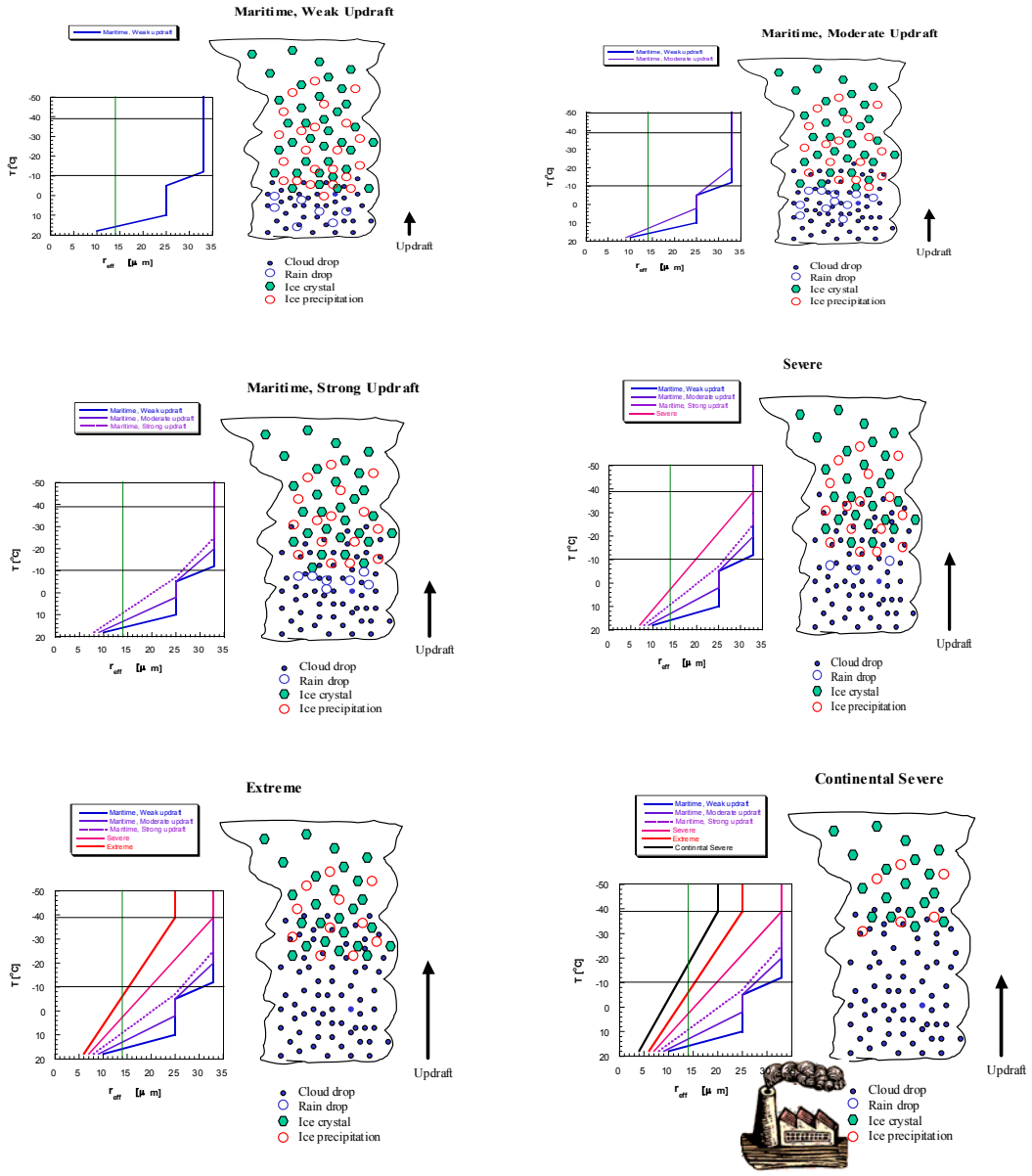

Figure 1. The classification scheme of convective clouds into microphysical zones, according to the shape of the T-r_e relations and hypothetical updraft intensity. In maritime clouds with weak updrafts r_e starts out relatively large at cloud base, crosses the precipitation threshold of 14 μm a short distance above the base. The deep rainout zone is indicative of fully developed warm rain processes in the maritime clouds. The large drops freeze at relatively warm temperatures, resulting in a shallow mixed phase zone and a glaciation temperature near -10°C. As the updraft increases, however, the hypothetical cloud becomes more continental in character with a deep zone of diffusional droplet growth, little coalescence, no precipitation, no rainout and delayed glaciation to very cold temperatures. The addition of small CCN changes the T-r_e relations in the same way as increasing the updraft velocity. Therefore, the polluted cloud in the last panel is illustrated with the most extreme T-r_e relation, although not with the strongest updraft.

The Rosenfeld satellite methodology has been put to many uses since its published documentation in 1998 (Rosenfeld and Lensky, 1998). Among the original motivations for its derivation was to provide a research component for the Texas operational cloud-seeding programs (Bomar et al., 1999) to identify seeding opportunities, to document microphysical seeding signatures (Woodley et al., 2000), and to quantify microphysical partitions for the analysis for seeding effects (Woodley and Rosenfeld, 2004).

It was not long, however, before the method was being used to document the worldwide suppressive effect of natural (Rosenfeld, 1999) and anthropogenic (Rosenfeld, 2000) pollution and desert dust (Rosenfeld et al., 2001) on cloud microstructure and rainfall. The method has been used also to document that, when salt from evaporating sea spray is ingested into polluted clouds, their rain-forming processes are restored gradually and they are cleansed ultimately of their pollution burden (Rosenfeld et al., 2002; Rudich et al. 2002). In addition, the focus now is on the climate implications of the suppressive effect of pollution on rainfall and the re-distribution of latent heating (Nober et al., 2003).

2. Geosynchronous Satellites

For many years satellites in orbits synchronous with the earth (i.e., geosynchronous) have been used by the United States and around the world. These geostationary satellites (GOES) have been "parked" at various locations above the equator such that they provide a view of the earth from the same position in space relative to a point on the ground. The early GOES satellites provided views in both the visible and infrared portions of the electromagnetic spectrum at a resolution of roughly 4 km. The main advantage of a GOES satellite is its continuous temporal resolution such that large cyclonic storms, hurricanes and severe convective weather can be followed continuously for their complete life histories.

Within the past decade, however, a second series of GOES satellites, beginning with GOES-8, was launched with additional sensors that permitted sensing through a broader portion of the electromagnetic spectrum, including the water vapor window near 3.7 microns. This sensing package is very similar in many respects to that on the polar-orbiting satellites that give great spatial resolution, approaching 1 km, on the earth's surface, but poor temporal resolution for any cloud system of interest because the satellite over flights are limited to one to two per day. Even so, this series of GOES satellites has provided a highly useful data stream of high interest to this proposal.

Figures 2, 3, and 4 are provided here to illustrate the differences. Figure 2 gives the superposition of the image from the Aqua polar-orbiting satellite and the NEXRAD radar mosaic at 2104 GMT on February 7, 2005. This image has been processed according to the method of Rosenfeld that was discussed in the previous section. The gold line on the satellite image is the track of the cloud physics aircraft that was flying for cloud measurements prior to and immediately after the satellite overpass. The radar echoes are shown in green within the image. Lake Tahoe can be seen clearly in the right-center of the image. There is obviously a lot of information spatially in this image. Further, the method of Rosenfeld allows one to infer the properties of the clouds as a function of height or temperature as was discussed earlier. These products have been excerpted from an ongoing research effort that Woodley Weather Consultants is doing for the California Energy Commission to document the effects of pollutants on clouds and precipitation over the Sierra Nevada.

A broader view from the NOAA-16 polar orbiting AVHRR satellite is given in Figure 3 at 2209 GMT for the same day (February 7, 2005) as shown in Figure 2. In this instance all of California, most of the western United States and the eastern Pacific can be seen in the image, which again has been processed according to the method of Rosenfeld. A magenta-colored cloud band can be seen sweeping in from the Pacific to the south of San Francisco and then curling northeastward and northward into the Sierra. This cloud band, which can be seen in both Figures 2 and 3, has clouds with large effective radii and some precipitation (see the superimposed echoes in Figure 2.)

Figure 4 gives a view of the same area from the GOES-10 satellite. The product shown is a map of the cloud effective radius, where the definition is the same as in Rosenfeld's work. It was obtained from the website of the NASA Langley Cloud and Radiation Research Group headed by Dr. Patrick Minnis (http://angler.larc.nasa.gov/satimage/products.html). Dr. Minnis and his associate Mr. David F. Young lead a team that has major research responsibilities for the development and application of advanced data analysis techniques to interpret satellite measurements of clouds and radiative characteristic of the Earth. This includes developing a globally robust technique for retrieving cloud parameters and microphysical properties. Some of the products, (calculated using Visible Infrared Solar-Infrared Split Window Technique (VISST) and Solar-Infrared Infrared split Window Techniques, SIST) that are available include: (a) estimates of the water phase (ice or liquid), (b) temperature at cloud top, (c) the effective drop radius, (d) the existence of supercooled liquid water, and (e) the albedo of cloud tops. This information is available for the daylight hours from the latter half of 2003 to the present day. Much of the information is available in real time.

The presentation in Figure 4 agrees at least qualitatively with that in Figure 3, which is the superior product spatially. The cloud band sweeping from the Pacific into California to the south of San Francisco and then into the Sierra is shown to have larger effective radii, indicative of precipitation, whereas the circular area of clouds to the northeast of San Francisco and to the north of Sacramento has much smaller effective radii. This is an area that appeared to have been affected by pollution emanating from these urban areas.

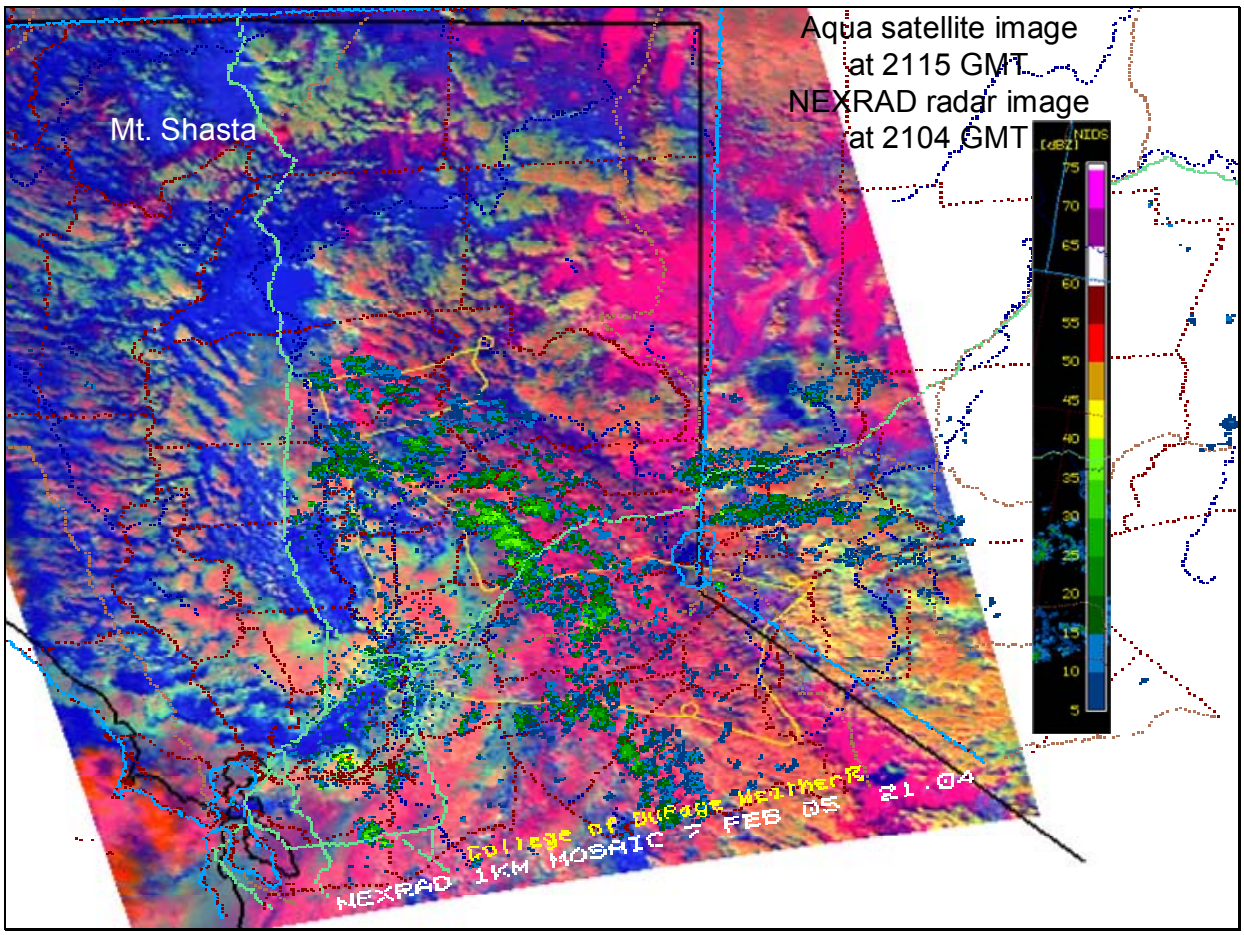

Figure 2. Superposition of the processed Aqua satellite image and the NEXRAD radar mosaic at 2104 GMT on February 7, 2005. The gold line on the satellite image is the track of the cloud physics aircraft that was flying for cloud measurements prior to and immediately after the satellite overpass. The radar echoes are shown in green within the image.

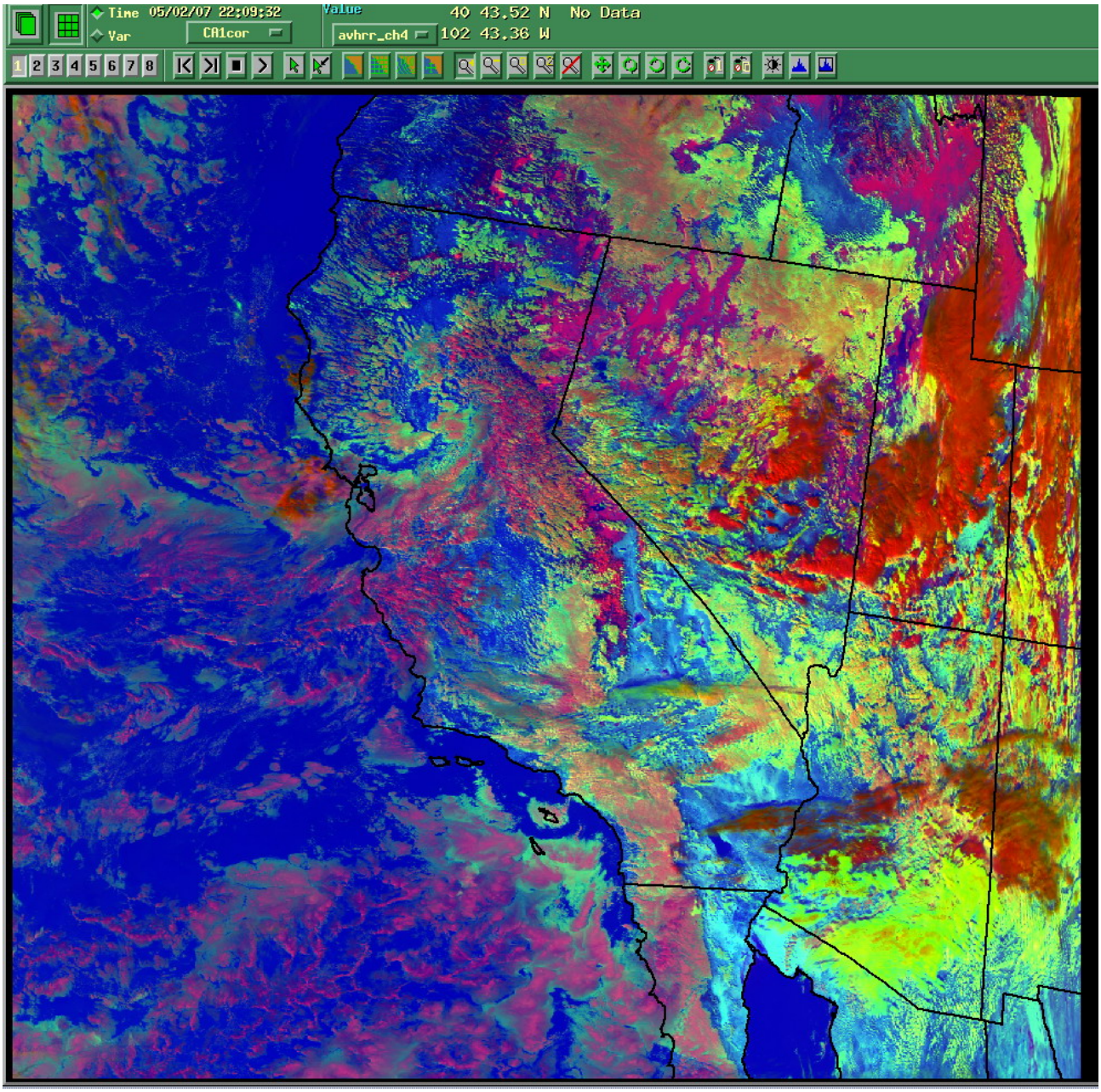

Figure 3. The NOAA-16 AVHRR satellite image at 2209 GMT on February 7, 2005. The image has been colorized according to the method of Rosenfeld (Rosenfeld and Lensky, 1998), where dark red clouds are visibly bright clouds with large particles, yellow and yellow-green clouds have small particles, and dark pink to magenta clouds may have precipitation-sized particles.

Although the high-resolution data from the polar orbiters is the preferred product, the value of these GOES products should not be underestimated. Whenever possible, the orbiter data will have the highest priority for the proposed studies. Even so, heavy use will be made of existing satellite products for the documentation of the spatial and temporal patterning of supercooled liquid water on those days when validation ("groundtruth") data exist. The planned validation effort is discussed in the next section of this proposal.

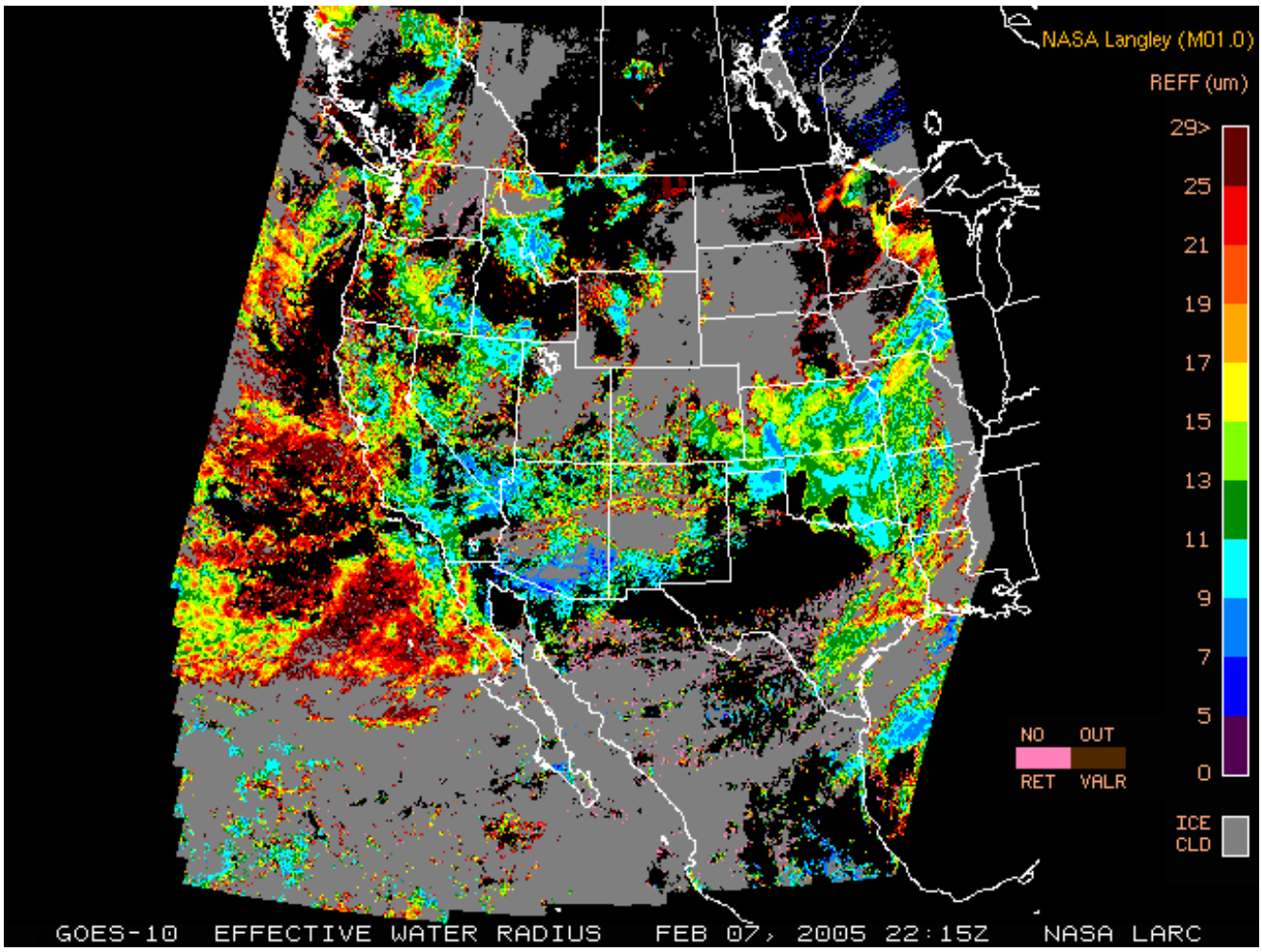

Figure 4. A map of effective water radius derived from the GOES-10 satellite image at 2215 GMT on February 7, 2005. The effective radii were derived from VISST and SIST algorithms by the NASA Langley Cloud and Radiation Research Group.

References

Arking, A., and J. D. Childs. 1985. "Retrieval of cloud cover parameters from multispectral satellite images." *Journal of Climate and Applied Meteorology* **24** (4): 322–333.

Bomar, G. A., W. L. Woodley, and D. L. Bates. 1999. "The Texas weather modification program: Objectives, approach and Progress." *J. Wea. Mod.* 31: 9–22.

Coakley, J. A., R. L. Bernstein, and P. R. Durkee. 1987. "Effects of ship-stack effluents on cloud reflectivity." *Science,* **237:** 1020–1022.

Houghton, J. T., L. G. Meira Filho, J. Bruce, Hoesung Lee, B. A. Callander, E. Haites, N. Harris, and K. Maskell. 1994. *Climate Change 1994 – Radiative forcing of climate change and an evaluation of the IPCC IS92 Emission Scenarios.* Reports of working groups I and II of the Intergovernmental Panel on Climate Change. Cambridge University Press, 339p.

Kaufman Y. J., and R. S. Fraser. 1997. "The effect of smoke particles on clouds and climate forcing." *Scienc*e **27**7 (5332): 1636–1638.

Nakajima, T., and M. D. King. 1990. "Determination of the optical thickness and effective particle radius of clouds from reflected solar radiation measurements. Part I: Theory." *J. Atmos. Sci.* **47:** 1878–1893.

Nober, F., H.-F. Graf, and D. Rosenfeld. 2003. "Sensitivity of the global circulation to the suppression of precipitation by anthropogenic aerosols." *Global Planet. Change* **37**: 57–80.

Radke, L. F., J. A. Coakley, and M. D. King. 1989. "Direct and remote sensing observations of the effects of ships on clouds." *Science* 246 (4934): 1146–1149.

Rosenfeld, D., and G. Gutman. 1994. "Retrieving microphysical properties near the tops of potential rain clouds by multispectral analysis of AVHRR data." *J. Atmos. Res.* 34: 259–283.

Rosenfeld D., and I. Lensky. 1998. "Spaceborne sensed insights into precipitation formation processes in continental and maritime clouds." *Bulletin of the American Meteorological Society* **79** (11): 2457–2476.

Rosenfeld, D. 1999. "TRMM observed first direct evidence of smoke from forest fires inhibiting rainfall." *Geophys. Res. Lett*. **26**: 3105–3108.

Rosenfeld, D. 2000. "Suppression of rain and snow by urban air pollution." *Science* **287**: 1793–1796.

Rosenfeld D., and W. L. Woodley. 2000. "Convective Clouds with Sustained Highly Supercooled Liquid Water Down to –37.5°C." *Nature* **405**: 440–442.

Rosenfeld D., and W. L. Woodley, and T. Krauss. 2001. Satellite Observations of the Microstructure of Natural and Seeded Severe Hailstorms in Argentina and Alberta. *15th Conference on Planned and Inadvertent Weather Modificatio*n. AMS, 14–18 January 2001, Albuquerque, New Mexico, p. 68–74.

Rosenfeld D., R. Lahav, A. P. Khain, M. Pinsky. 2002. "The role of sea-spray in cleansing air pollution over ocean via cloud processes." Research Article in *Science* 297: 1667–1670. Highlighted and published online in "*Science Express*" on 15 August 2002.

Rosenfeld, D., and W. L. Woodley. 2002. Closing the 50-year circle: From cloud seeding to space and back to climate change through precipitation physics. Chapter 6 of *Cloud Systems, Hurricanes, and the Tropical Rainfall Measuring Mission (TRMM),* edited by Drs. Wei-Kuo Tao and Robert Adler, Meteorological Monographs, Amer. Meteor. Soc. p.59–80.

Rudich Y., D. Rosenfeld, O. Khersonsky. 2002. Treating clouds with a grain of salt. *Geophysical Research Letters* **29** (22), doi:10.1029/2002GL016055, 2002.

Woodley, W. L., D. Rosenfeld, and A. Strautins. 2000. "Identification of a seeding signature in Texas using multi-spectral satellite imagery." *J. Wea. Mod.* 32: 37–52.

Woodley, W. L., and D. Rosenfeld. 2004. "The development and testing of a new method to evaluate the operational cloud seeding programs in Texas." *J. of Applied Meteor.* 43 (2): 249–263.

Appendix B

1. Specifications for the SOAR Cheyenne II cloud physics aircraft

1.1 The SOAR Cheyenne II cloud physics aircraft

The SOAR Cheyenne II research aircraft airborne platform for atmospheric research consists of instrumentation that has the capability of measuring in-situ microphysical properties of clouds and their thermodynamic environment, documenting the composition of clouds and diagnosing the physical processes within them.

For adequate sampling of particles in and around clouds, the research aircraft has the capability of measuring the size distribution of particles ranging from 0.1 μm to 1.55 mm in diameter. This dynamic range is achieved by the permanent platform of the SOAR research aircraft which consists of the Passive Cavity Aerosol Spectrometer Probe (PCASP SPP-200), the Cloud Droplet Probe (CDP), and the Cloud Imaging Probe (CIP) which are described below. This range gives the scientists a spectrum of measurements in the temporarily suspended aerosol range and in the cloud hydrometeor range. In addition, inferences on the cloud composition and the particles that act as surfaces or embryos for water to condense on can be achieved by cloud condensation nuclei counters.

1.2 Passive Cavity Aerosol Spectrometer Probe (PCASP SPP-200)

Atmospheric particles in the temporarily suspended aerosol range are measured by the Passive Cavity Aerosol Spectrometer Probe (PCASP SPP-200). The PCASP-SPP200 (Figure 3) is configured with a sampling cone that extends out from the forward end cap that is always oriented into the direction of flight. The PCASP is designed to sample air isokinetically in a laminar stream as it intersects a high-powered laser beam. All particles entrained in the sample flow are aerodynamically focused to interact with the laser beam in a controlled sampling zone location in the center of the beam. Light scattered by a particle entering the laser beam is collected and focused onto a photodetector where it undergoes three stages of amplification to cover the range between 0.1 μm and 3.0 μm.

1.3 The cloud droplet probe (CDP: 2 μm to 50 μm)

The Cloud Droplet Probe (CDP) (Figure 2) is a new forward light-scattering spectrometer that can measure cloud particles in the range of 2 μm to 50 μm. For the past 28 years, Particle Measuring Systems' (PMS) Forward Scattering Spectrometer Probe (FSSP) has been used widely and the capabilities and limitations of this probe have been published frequently. However, the FSSP weighs 40 pounds and little improvements have been made to the FSSP electronics over the years. The Droplet Measurement Technologies (DMT) CDP is similar in operation to the FSSP. The instrument counts and sizes individual droplets as they traverse a laser beam. Droplets that hit the laser beam within the sample volume scatter light and the forward scattered light is collected onto an optical beam splitter and then onto a pair of photo detectors, the sizing detector and the qualifying detector. The CDP accepts and sizes only particles that

pass through a uniform power region of the laser beam since the scattered light is focused through an optical mask that defines the depth of field (DOF). Different voltage pulses from the sizing detector are compared with the voltage pulses from the qualifying detector, and a digital flag is raised if the masked detector's output exceeds that of the signal to be sized, hence rejecting the particle (DOF rejected). The DOF qualified photon pulse is then converted, amplified and digitized into a sizing bin. The range of the CDP is fixed and the output is distributed in 30 size channels. The CDP is mounted external to the aircraft below the right wing and adjacent to the Cloud Imaging Probe (CIP). The probe is quite compact and aerodynamic compared to the FSSP and weighs only 4 pounds. The CDP electronics are mounted in the wing and weigh 2 pounds.

1.4 The Cloud Imaging Probe (CIP: 25 μm to 1.55 mm)

The DMT Cloud Imaging Probe (CIP) (Figure 2) is very similar in technical operation to the 2D-OAP developed by PMS. A linear array of laser beams is focused on a sampling area where the particles' shadows are optically magnified to provide the imaging data. Whenever a detector diode is shadowed by a passing particle, the on-board digital electronics begin storing diode information at the true airspeed (TAS) frequency. The TAS is determined using an on-board pitot tube mounted just adjacent to the sampling area, providing accurate airspeed at the instrument itself. On the SOAR aircraft, the AIMMS-20 provides more accurate TAS data, so the TAS clock is provided from the AIMMS-20 air data probe. The CIP incorporates a 64-element photo-diode array and has a 25 μm size resolution. The data output is distributed in 62 channels making the minimum detectable particle size at 12.5 μm and the largest particle at 1562.5 μm. Particles that shadow the two end diodes (1 and 64) are end rejected.

The CIP incorporates a Liquid Water Content (LWC) detector. The LWC is a hot-wire sensor. The sensor head of the LWC holds a hot wire element. The temperature of the wire is maintained constant at 125°C. The more liquid water present in the immediate environment, the greater the number of cloud droplets impinging on the heated sensor element that is exposed to the airflow outside the aircraft. This causes a cooling effect that increases the power needed to maintain the sensor temperature constant. The additional power needed to react to the drop in the temperature is a function of the liquid water content and the true airspeed.

1.5 The DMT Cloud Condensation Nuclei (CCN) counter

The DMT Cloud Condensation Nuclei (CCN) (Figure 5) counter samples aerosols from outside the aircraft to measure their capability to act as cloud condensation nuclei. An air sample is introduced in the CCN chamber via a 0.25-inch diameter inlet on top of the aircraft fuselage and non-conductive tubing that is plumbed from the CCN instrument to the aircraft fuselage. The air enters the top center of the vertical cylindrical column and is surrounded by an aerosol-free humidified uniform supersaturation flow environment. As the air sample flows down through the chamber, CCN activate in response to the exposed supersaturation and grow to droplets. An optical particle counter at the base or outlet of the chamber detects all particles with diameters larger than 0.5 μm. The heart of the instrument is the 50 cm long cylindrical column which provides the environment to activate and grow aerosol particles. The column is mounted

vertically with the ambient aerosol entering at the top, and the increase in supersaturation takes place down the column.

The unit operates at a single supersaturation. The supersaturation depends on the temperature difference between the top and bottom of the column as well as the flow rate in the column. The supersaturation can be varied between 0.1% and 1.2%. The column has three temperature control zones, for rapid shifting between supersaturation. Approximately 30 seconds are required for a shift from one supersaturation to another, although operation in the field shows that shifting from a high supersaturation (1.0%) to a low supersaturation (0.1%) may take more than a minute since the temperature controllers are more efficient at warming the column than at cooling.

The data output is distributed in 20 bins of resolution over the sizing range of 0.75 μm to 10 μm. The particle sizing data is updated at 1-second intervals. At a sample flow rate of 60 vccm, 6000 particles per cubic centimeter can be counted with a maximum of a 10% coincidence. The CCN counter is mostly operated at supersaturation steps of 0.1%, 0.25%, 0.5%, and 1.0%. Particles that exit the base of the column and are in bin 1 through bin 20 comprise the measured CCN concentration.

1.6 The Differential mobility analyzer (DMA)/tandem differential mobility analyzer (TDMA)

Texas A&M University owns and operates a DMA/TDMA system that measures aerosol size distributions and size-resolved hygroscopic growth (Figure 6). A DMA uses an electric field to separate particles within a narrow range of electrical mobility. If the voltage is fixed, a monodisperse aerosol may be separated from a polydisperse population. If the voltage is varied, the distribution of aerosol particles may be obtained. Since the electrical mobility is related to the diameter of the particle and the amount of charge on the particle, aerosols are neutralized prior to classification so that the relationship between size and electrical mobility is unique. The TDMA uses two DMAs in tandem to measure the hygroscopic growth of particles exposed to a controlled relative humidity (RH). The first DMA is used to select particles of a single dry size, which are then exposed to a controlled RH. The distribution of humidified particles is then scanned by the second DMA to determine the fraction of those particles that grew in response to the change in RH. The particles containing hygroscopic material will grow according to the amount and type of hygroscopic material they contain, and those that are non-hygroscopic will remain the same size. Most often, size distributions of the ambient aerosol from 0.010 μm to 0.500 μm and hygroscopic growth distribution at 85% RH are measured for particles with dry sizes from 0.013 μm to 0.300 μm.

1.7 Aircraft Integrated Meteorological Measurement System (AIMMS-20)

Aircraft Integrated Meteorological Measurement System (AIMMS-20) (Figure 3) gives up-to-the-second, real-time, three-dimensional wind conditions evaluated using the Kalman Filter Digital Signal Processing (DSP) technique. Wind Vector Software provides a real-time display of the horizontal wind component. The AIMMS-20AQ consists of four components: an Air Data Probe (ADP), a carrier-phase Geostationary Positioning Satellite (GPS) measurement module,

an Inertial Measurement Unit (IMU), and a Central Processing Module (CPM). The ADP is mounted below the lower wing surface, while the other three modules are located in the cockpit. The system gives position and velocity information from the GPS with six-axis inertial rates from the IMU's three rate gyros and accelerometers and aerodynamically corrected 3-D aircraft-relative flow vector data from the ADP. The CPM then processes this sensor data at 20 times per second, combines the differential GPS carrier-phase data with the inertial data to determine accurate aircraft attitude, and then combines these data with the raw air-motion data to precisely determine the wind solution to better than 0.5 m/s accuracy. In addition, the AIMMS-20AQ measures the flow direction, true heading, barometric pressure, altitude, temperature, and relative humidity. This makes the AIMMS-20AQ a suitable instrument to measure research-grade atmospheric soundings close in time and space to the intended cloud studies. The AIMMS-20AQ is also suitable for cloud draft measurements, since the ADP on the SOAR aircraft is a de-iced version.

Figure 1: The SOAR Cheyenne II cloud physics aircraft.

Figure 2: The DMT CIP probe and the DMT CDP probe.

Figure 3: Aventech Research AIMMS-20 and PMS PCASP.

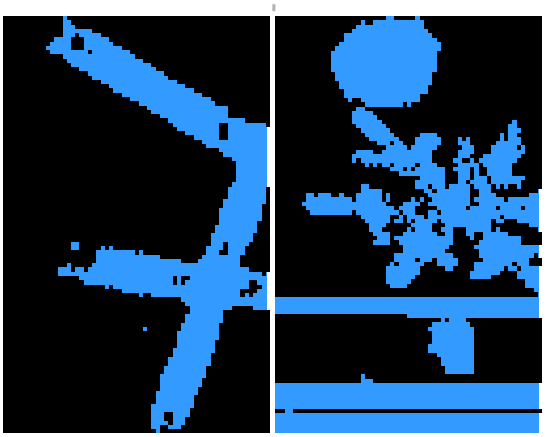

Figure 4: Needles, spherical graupel and a dendritic crystal imaged by the CIP probe east of Midland TX in a cold front on 25 Sep 2004.

Figure 5: The cloud condensation nuclei (CCN) counter developed by Georgia Tech Assistant Professor Athanasios Nenes and Gregory Roberts at the Scripps Institution of Oceanography. The instrument measures how many cloud droplets form and how long they take to form.

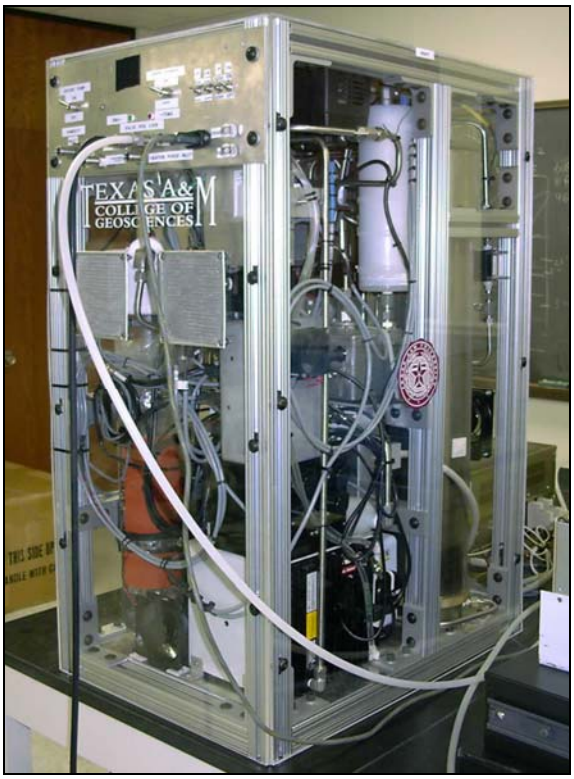

Figure 6: The aircraft-based high flow DMA / TDMA measures aerosol size distributions for particles between about 0.01 and 1.0 micrometers, and measures size-resolved hygroscopic growth of particles between about 0.015 and 0.6 micrometers.

2. Variables measured on the SOAR Cloud Physics research platform

Table 1: Summary of parameters and measuring devices used on the SOAR Cheyenne II

VARIABLE	INSTRUMENT	RANGE	ACCURACY	RESOLUTION	FREQUENCY
Air temperature (reverse flow)	0.038" DIA. Bead Thermistor	-30°C to +50°C	0.05°C/0.3°C incl DHC	0.01°C	< 1 s TC
Relative humidity (reverse flow)	Thermoset Polymer RH Sensor	0 to 100% RH	2% RH	0.1% RH	5 s TC @ 20°C
Barometric pressure	MEMS Pressure Sensor	0 to 110000 Pa	100 Pa	10 Pa	20 Hz
u wind component (+ North)	Extended Kalman Filter (EKF)		0.50 m/s @ 75 m/s TAS	0.01 m/s	5 Hz
v wind component (+ East)	Extended Kalman Filter (EKF)		0.50 m/s @ 75 m/s TAS	0.01 m/s	5 Hz
w wind component (+ Down)	Extended Kalman Filter (EKF)		0.50 m/s @ 75 m/s TAS	0.01 m/s	5 Hz
Position (Latitude/Longitude)	WAAS DGPS		2 m (2 σ)	< 1 m	5 Hz
Altitude	WAAS DGPS	-300 to 18000 m	5 m (2 σ)	< 1 m	5 Hz
Geometric Altitude	King KRA 405 Radar Altimeter	0 to 2000 ft	3% < 500 ft 5% > 500 ft	0.48 ft (0.15 m)	
Roll Attitude (ϕ)	MEMS IMU/GPS/EKF	-60 to +60°	0.1°	0.01°	5 Hz
Pitch Attitude (θ)	MEMS IMU/GPS/EKF	-60 to +60°	0.2°	0.01°	5 Hz
Yaw Attitude (ψ)/ Heading	MEMS IMU/GPS/EKF	0 to 360°	0.1°	0.01°	5 Hz
Angle of attack (α)	MEMS Pressure Sensor	-15 to +15°	0.03° @ 150 m/s	0.001° @ 150 m/s	20 Hz
Side-slip (β)	MEMS Pressure Sensor	-15 to +15°	0.03° @ 150 m/s	0.001° @ 150 m/s	20 Hz
True Air Speed	MEMS Pressure Sensor	0 to 150 m/s	0.1 m/s	0.01 m/s	20 Hz
Video record	Sony DCR-DVD 201				
Logging, telemetry & event markers	ESD DTS (GPS)				1 Hz
Cloud droplet spectra	DMT CDP	2 to 50 µm		1 to 2 µm, 30 bins	1 Hz
Cloud particle spectra	DMT CIP	25 to 1550 µm		25 µm, 62 bins	1 Hz
Cloud particle image	DMT CIP	25 to 1550 µm		25 µm	
Liquid water content	DMT LWC-100	0 to 3 g/m^3	0.05 g/m^3	0.01 g/m^3	1 Hz
	CDP calculated	> 3 g/m^3			1 Hz
Aerosol spectrometer	PMS PCASP SPP-200	0.1 to 3 µm		0.02 µm, 30 bins	1 Hz
Aerosol properties	TAMU DMA/TDMA	See text			1 Hz
CCN	DMT CCN counter	0.5 to 10 µm 0.1 to 1.2 % SS	see text	0.5 µm, 20 bins	1 Hz

3. Upgrades installed on the standard package of the SOAR Cheyenne specifically for the SUPRECIP program

3.1 Terrain Awareness and Warning System (TAWS)

The SUPRECIP program brings challenges to the field measurement program that needed special attention. One of these challenges was measurement of cloud microphysical properties using the SOAR Cheyenne research aircraft in the proximity of mountainous terrain. The addition of Terrain Awareness and Warning System (TAWS) on the SOAR Cheyenne enables the SOAR crew to interpret terrain features when flying in low visibility or in clouds. This is achieved by the installation of the TAWS-enabled Garmin GNS 530 to graphically display the surrounding terrain and obstacles in bright yellow and red, relative to the aircraft's current altitude (Figure 7). Yellow is used to depict conflicts 1,000 to 100 vertical feet below the aircraft. Red is used to depict conflicts 100 vertical feet below the aircraft's current altitude and above. Working in tandem with the aircraft's audio system, the TAWS-certified GNS 530 provides audible cautions and warnings to alert the pilot of a possible terrain and obstacle conflict. Audible and graphical alerts include forward-looking terrain avoidance, imminent terrain impact, premature descent during approach, altitude loss after takeoff, 500-foot callout, and excessive rate of descent.

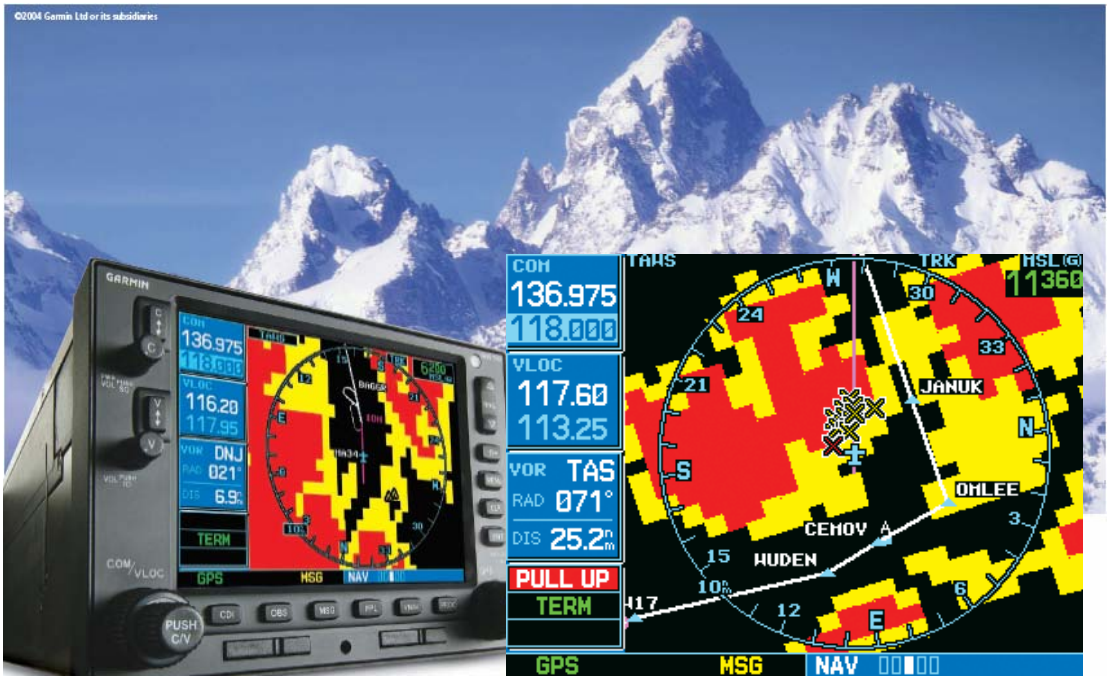

Figure 7: Terrain Awareness and Warning System (TAWS) on the Garmin 530

The GNS 530 is an integrated system with IFR oceanic-approved GPS, VHF navigation with instrument landing system, and VHF communication with 8.33-kHz channel spacing. Its five-inch (diagonal) color TFT display features an electronic map with a built-in database of cities, highways, rivers, lakes, and coastlines—as well as a complete TAWS database. The TAWS data include:

- Terrain Database: 30 arc-second resolution coverage of the world (75 N-60 S).
- Obstacle Database: Consists of all obstacles higher than 200′ within the U.S.
- Airport Terrain Database: 9 arc-second resolution in 12 nm by 12 nm coverage around every U.S. airport.

3.2 Traffic Collision Avoidance System (TCAS)

Another challenge in SUPRECIP is flying in conditions when other aircraft are maneuvering in close proximity. Traffic Collision Avoidance System (TCAS) consists of a radio transmitter and receiver, directional antennas, computer and cockpit display. It sends out signals, called *interrogations*. When another airplane's transponder receives an interrogation, it transmits a reply. The TCAS computer uses the time between interrogation and reply to calculate distance. It uses information from the directional antennas to determine direction. If the other aircraft has a transponder that provides altitude data, TCAS displays its relative altitude and whether it is climbing or descending. For example, if the other airplane is 1,400 ft below the interrogating airplane and climbing, "14" and an arrow pointing upward will appear above the aircraft's symbol.

The TCAS gives you Tas (Traffic Advisories) and Ras (Resolution Advisories climb and descent commands). To review briefly, the system provides a map-like display of surrounding traffic, and a TA whenever another aircraft is within about 48 seconds of its closest point of approach. During a TA, a synthesized voice announces, "Traffic, traffic," and the symbol for the intruder aircraft changes from a white diamond shape to a solid yellow round dot. During an RA, the other aircraft symbol changes to a solid red square block, and the system will demand a maneuver such as "Climb, climb" or "Descend, descend," or it may tell the pilot not to maneuver. When a TCAS issues an RA involving another TCAS-equipped aircraft, it coordinates with the other aircraft's TCAS to avoid mirror-image maneuvers, such as having both airplanes climb.

Figure 8: Using standard TCAS symbols, easily identified by their color and shape, the range, bearing and altitude of each intruder is shown relative to the aircraft.

4. Data Acquisition and Quality Control

4.1 The Aircraft Data Acquisition System

The main aircraft data acquisition system is a software called DAQFactory. DAQFactory provides all the tools needed to acquire data, log it, display it, graph it, and analyze it. DAQFactory includes an advanced serial driver that can be easily set up to communicate with most serial devices.

The features of the DAQFactory system are the following:

a) Data acquisition from different instrument inputs at 1Hz. The DAQFactory system logs data from the CIP, CDP, AIMMS-20, and PCASP.

b) Continuous data logging to an ASCII file for each instrument. During the data logging process, one data file is created for each instrument per hour.

c) User-definable screens for different measurement objectives during the research flight.

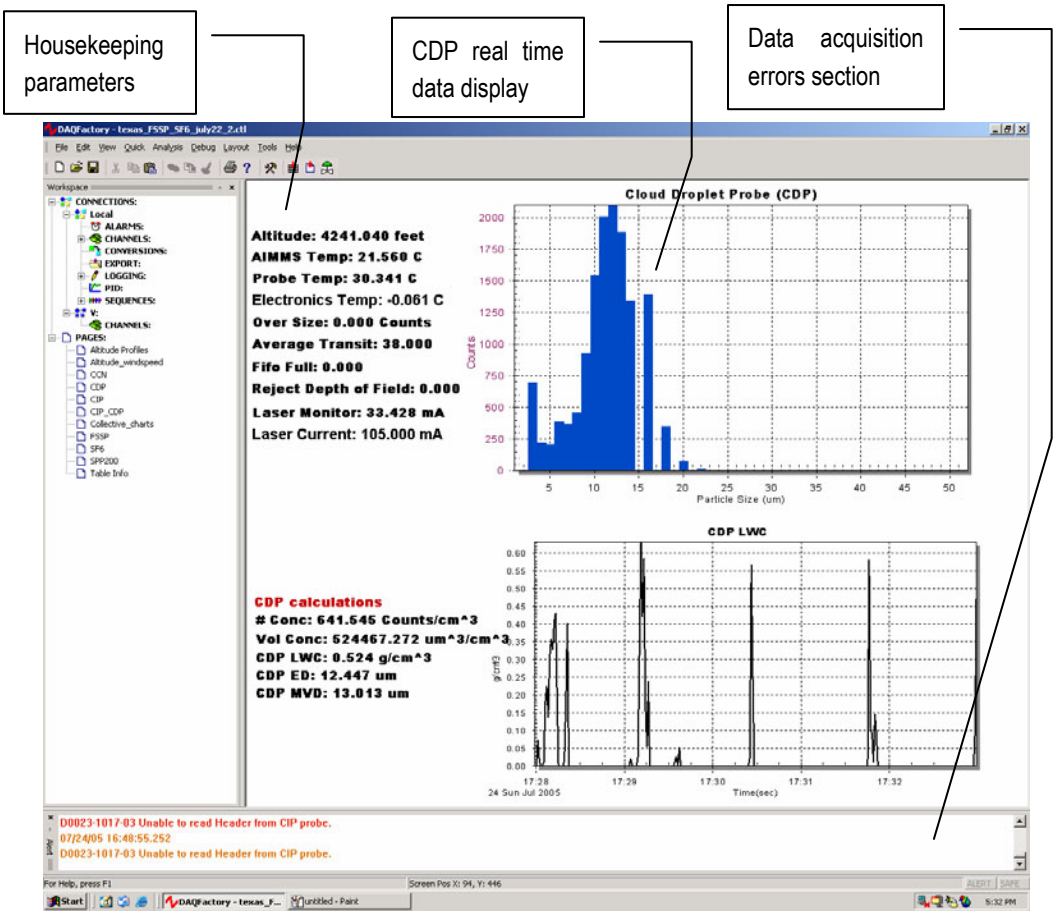

Figure 9: DAQFactory screen shot in-flight during a cloud penetration

Figure 9 shows the DAQFactory screen shot during a cloud penetration. The data are displayed in real time as shown. The housekeeping parameters are data that are specific to the operation of the instrument. If the housekeeping parameters fall within known unreliable values, the instrument operator can diagnose the operation of the instrument. With this feature, the instrument operator can maintain a certain level of quality assurance in real time operation of the instruments.

4.2 Post processing of the data and quality control

The post processing of the aircraft data is performed using LabVIEW. National Instruments LabVIEW delivers a powerful graphical development environment for signal acquisition, measurement analysis, and data presentation. After each flight, the research meteorologist collects the DAQFactory data from each instrument and processes this data using LabVIEW. The LabVIEW software checks for errors in each data file, synchronizes all the data from all the instruments, performs calculations, and creates data files for further analysis.

Figure 10 shows a screenshot from the CCN counter playback software. Using this software, the research meteorologist plays all the data for each instrument for all the flight or for portions of the flight. Quality control of the data can be assured during the playback after each flight.

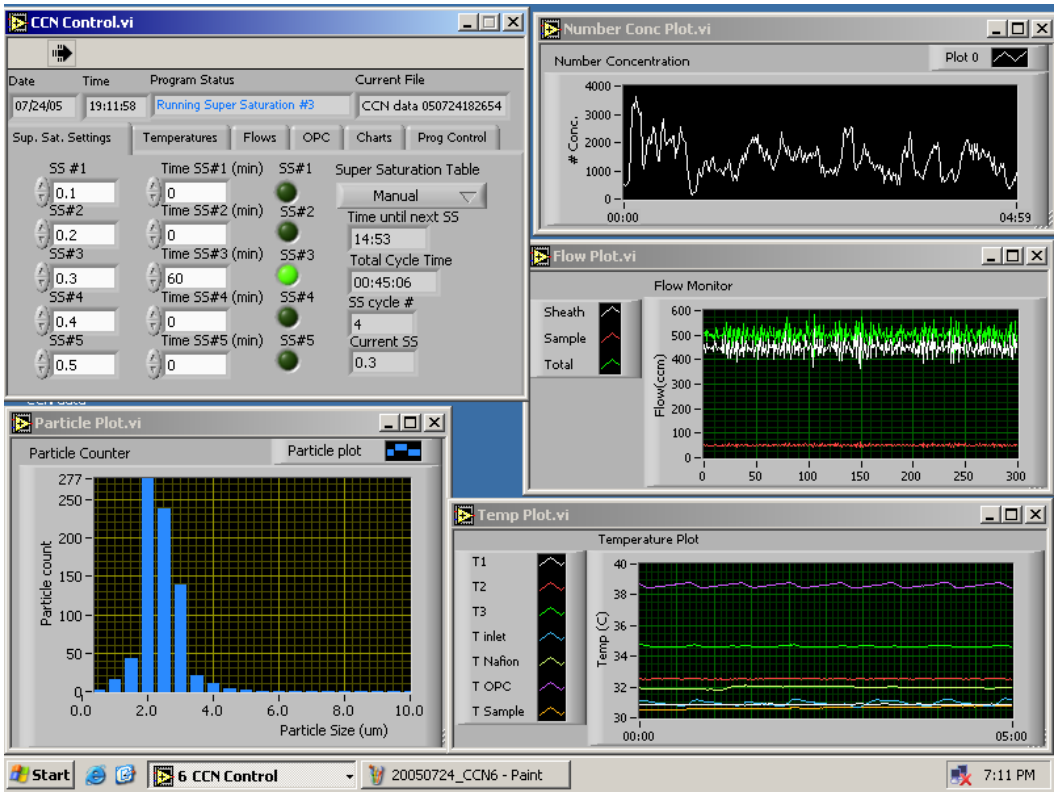

Figure 10: LabVIEW playback software

5. Instrument Considerations (See Table 1 for instrument sensitivities)

5.1 General Comments

The instrumented package on the Piper Cheyenne II is composed of wing probes and cabin instruments. Although these instruments are fairly new and the design of the electronics is quite modern, these instruments have known sensitivities that are inherent to the instrument. Most of the instrument errors are caused by:

a) the physical principle by which the instrument measures,

b) the way the environment is disturbed by the mounting location of the instrument before the measurements are taken, or

c) erroneous alignment and calibration.

The FSSP, CDP, and PCASP are calibrated using glass beads of different known sizes. Both are cleaned and calibrated regularly. The CCN counter is calibrated in the laboratory before each field deployment and is known to maintain its calibration throughout a field campaign. The CIP probe can be checked for calibration by collecting data from a spinning disc to simulate particles streaming through the viewing area. The CIP is also known to remain in good calibration. The AIMMS probe is calibrated before a field campaign by conducting specific flight profiles. These flight profiles are analyzed by the manufacturer and correction factors are entered in the AIMMS firmware. The AIMMS is also calibrated by flying in coordination with a sounding launch to calibrate the winds, the temperature and the relative humidity.

In the following sections, instruments with known errors or issues are discussed.

5.2 Aerosol Measurements

During the SUPRECIP field campaign, the DMT CCN counter and the Texas A&M TDMA were operated for the duration of the program. The DMT CCN counter is a very new instrument (built in 2003 and marketed in 2004) and its limitations are still somewhat unknown. Although the instrument is a newcomer, the DMT CCN counter is quickly becoming the industry standard in aerosol and CCN research. TDMA instruments have been used for the last decade and it is well known that their greatest limitation is the 3- to 5-minute resolution to conduct one DMA cycle for the desired range.

During SUPRECIP, the aerosol sampled by the CCN counter and the TDMA entered the research aircraft via a heated pitot tube inlet. This inlet is shown in Figure 11. For the measurement requirements of SUPRECIP, where the aircraft was required to conduct consecutive cloud penetrations followed by aerosol measurements, a heated inlet was desired to prevent a reduction on the airflow caused by aircraft icing. This presented a problem with the inlet desired for this application. The easiest solution for SUPRECIP was to use an off-the-shelf heated pitot tube. The inlet was located along the top centerline of the research aircraft, 45.5 inches aft of the windshield (as shown in Figure 12). All of the aerosol measurements were made inside the research aircraft at a temperature at least 10°C warmer than the ambient values. Hence, it was assumed that most of the chemically bound water was evaporated prior to detection by the CCN counter.

A pitot tube is not equipped with a velocity diffuser to allow for isokinetic or quasi-isokinetic sampling. A key concern, as in any other aircraft aerosol inlet, became the particle losses in the inlet. Another concern is the enhancement in submicron aerosol due to non isokinetic sampling. In SUPRECIP, it was observed that a 100 mb pressure drop was apparent between the ram air pressure at the inlet and the instruments in the aircraft cabin. This indicated that the pitot tube was restricting flow from the ram air entering the nose of the pitot. Although the passing efficiency of the pitot inlet is uncharacterized, and the aerosol cut off size is unknown, the concern becomes the loss of particles with dry sizes larger than 1μm. The latter should not be too serious of a sensitivity for pollution aerosol with a peak in submicrometer mass but would result in underestimates of dust aerosol aspirated into the aircraft. It was concluded that aerosol measurements during SUPRECIP are not sensitive to the exact values of the size-cut diameters.

Figure 11: Heated aerosol 'pitot' inlet used in SUPRECIP

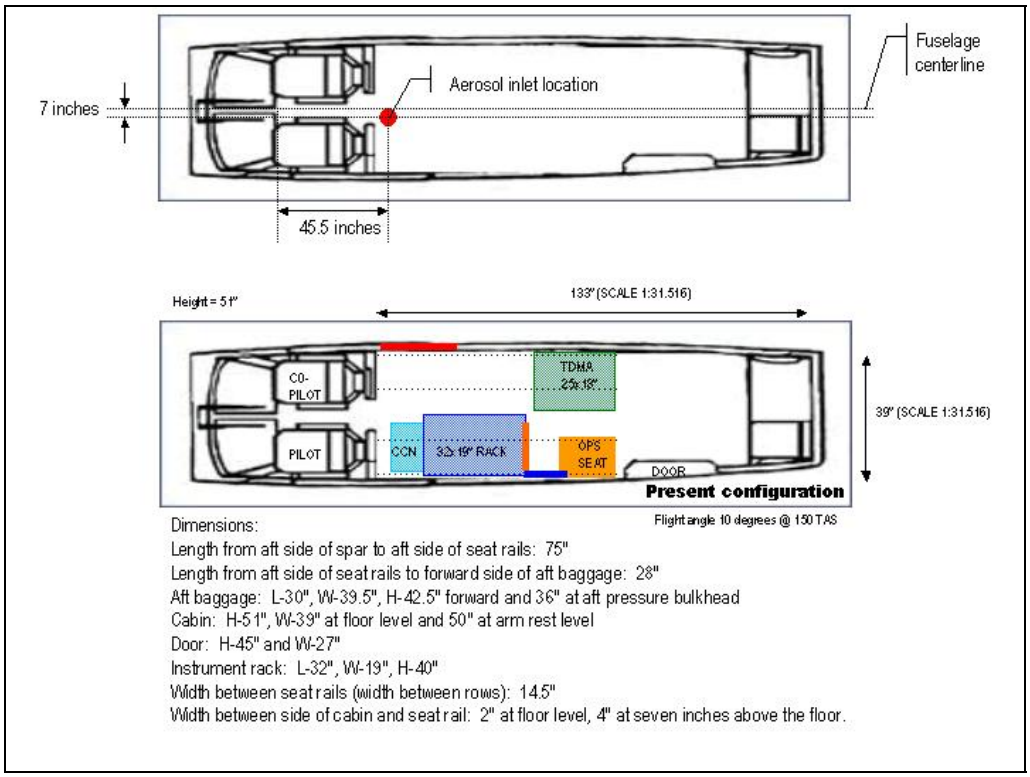

Figure 12: Aircraft configuration during SUPRECIP

Another uncertainty in the measurements are instances when the aircraft was in-cloud and when the aircraft attitude was not straight and level. Aerosol measurements in-cloud are not well understood, and aerosol/CCN concentrations are usually enhanced due to droplet shatter at the inlet. During the data analysis, aerosol measurements in-cloud are ignored. Another problem is when the aircraft is climbing or descending. These measurements are also ignored since flow at the inlet may become turbulent, creating a loss of flow or an enhancement in small aerosol concentration.

To summarize, it is well established that aircraft aerosol sampling is dependant on the passing efficiency of the inlet, and the upper cut-off diameter of the sampled aerosol. During SUPRECIP, the aerosol of interest was pollution aerosol that is not highly sensitive to these above mentioned factors. During the analysis, the data in-cloud and during climb or descent was ignored. It is believed that the CCN/DMA data presented in the report can be viewed as scientifically representative of the environmental aerosol during the measurement program.

During SUPRECIP 2, it is recommended that the aircraft inlet be improved to sample quasi-isokinetically or isokinetically. The current thinking is that a de-iced inlet is not required as the limitations imposed by providing de-icing to the inlet far exceed the basic requirements for aerosol sampling. Ultimately, the aerosol inlet used should be well characterized so that aerosol measurements can be interpreted within the limitations imposed by the inlet.

5.3 The CDP and the FSSP

During the SUPRECIP field campaign, both the CDP and the FSSP SPP-100 where flown on selected flights. The CDP was flown on all flights. DMT's CDP is a miniaturized version of the FSSP. Both probes collect and measure scattered light from a particle passing through a laser beam. The practical size range is very close: CDP is 2–50 microns, FSSP is 2–47 microns. The CDP electronics are modern, and programmable. The CDP has window-protected optics, while the FSSP has optics open to the environment. The FSSP probe that was operated for a few flights during SUPRECIP had DMT upgraded electronics.

The maximum concentration measurable by the FSSP and the CDP are limited by the speed of the electronics in processing a droplet. It will also depend on how many of the droplets actually pass though the beam within the depth of field of the instrument.

The counting accuracy of the FSSP is mainly determined by uncertainties in the sample volume, although laser inhomogeneities and coincidence of droplets in the beam also affect the measurement accuracy. The same can be said for the CDP, except that the laser distribution is known and of a "gaussian" distribution. Also, the FSSP and the CDP are different in the way they "accept" or "reject" a droplet as it crosses an inhomogeneous portion of the beam. Several papers have been written characterizing the performance of the FSSP, but none so far have characterized the performance of the new CDP. Although these differences cannot be ignored, an attempt is made here to compare the CDP to the FSSP during one SUPRECIP flight.

During one calibration test flight on 2 March 2005, the CDP and the FSSP SPP-100 were flown in fair weather Cu, from base at 3000 ft up to top at 7000 ft. First impressions show that with respect to the FSSP SPP100 the CDP undercounts by a factor varying between 2 to > 4, and over-sizing by about 2 bins. The cloud droplet distributions seem to be shifted respectively. This is shown in Figure 13, where 12 cloud pass data for the CDP and the FSSP SPP-100 are analyzed.

Additional analysis was conducted on this data and presented in Figure 14. A cloud-by-cloud comparison of the CDP and FSSP data was conducted after performing an airspeed correction for the FSSP. The FSSP is an early model with electronics that cause an intensity roll-off above airspeeds of 50 m/s. The channel-by-channel sample areas for the CDP were derived, and corrections applied to each channel (or sizing bin). Figure 14 shows the distributions of the number concentrations as a function of size for the same data set in Figure 13. The blue curves in the size distribution graphs are the airspeed corrected SPP spectra, the black curves are CDP spectra calculated using the nominal, constant sample area, and the red curves are the CDP with sample areas that vary with particle size. The correction for the sample area with particle sizes was necessary because in Figure 13 the CDP underestimates the concentration of the smaller sizes (< 8 μm) and overestimates the concentration of larger sizes (> 16 μm).

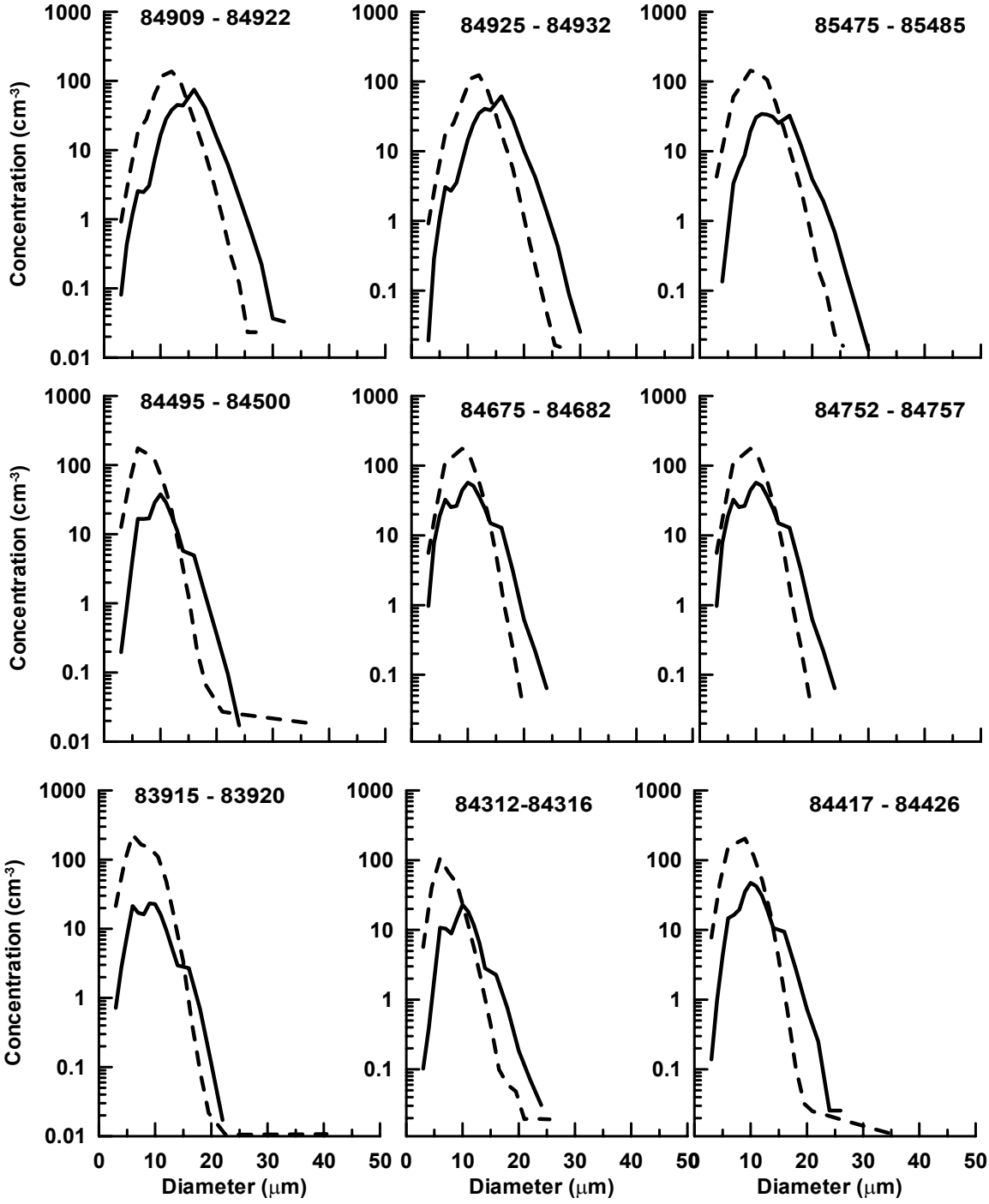

Figure 13: Cloud droplet spectra comparisons from 12 cloud passes on 2 March 2005. The solid line is the CDP, the dashed line is the FSSP SPP-100.

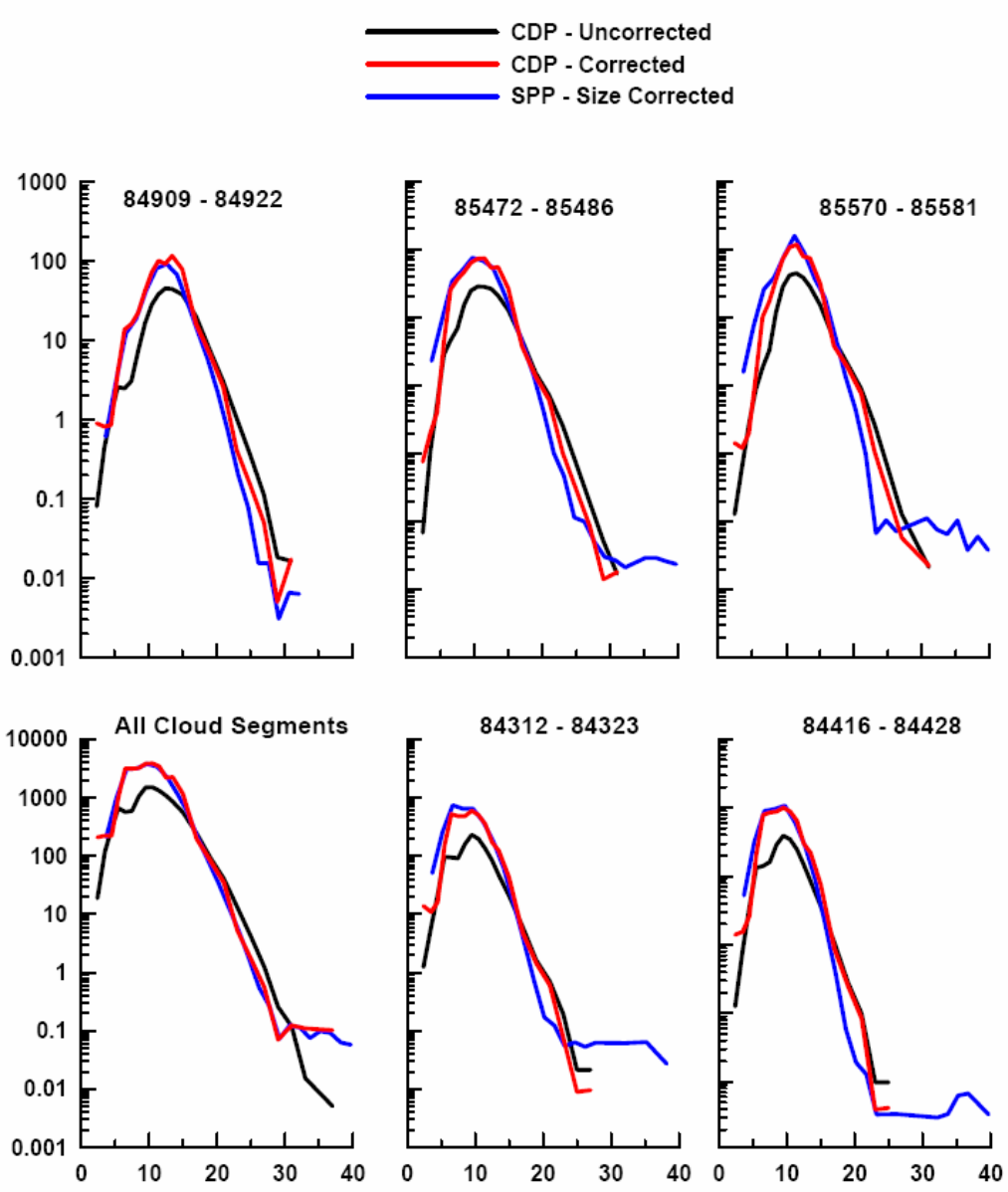

Figure 14a: Cloud droplet spectra comparisons from 5 cloud passes on 2 March 2005. The blue curves in the size distribution graphs are the airspeed corrected FSSP SPP-100 spectra, the black curves are CDP spectra calculated using the nominal, constant sample area, and the red curves are the CDP with sample areas that vary with particle size.

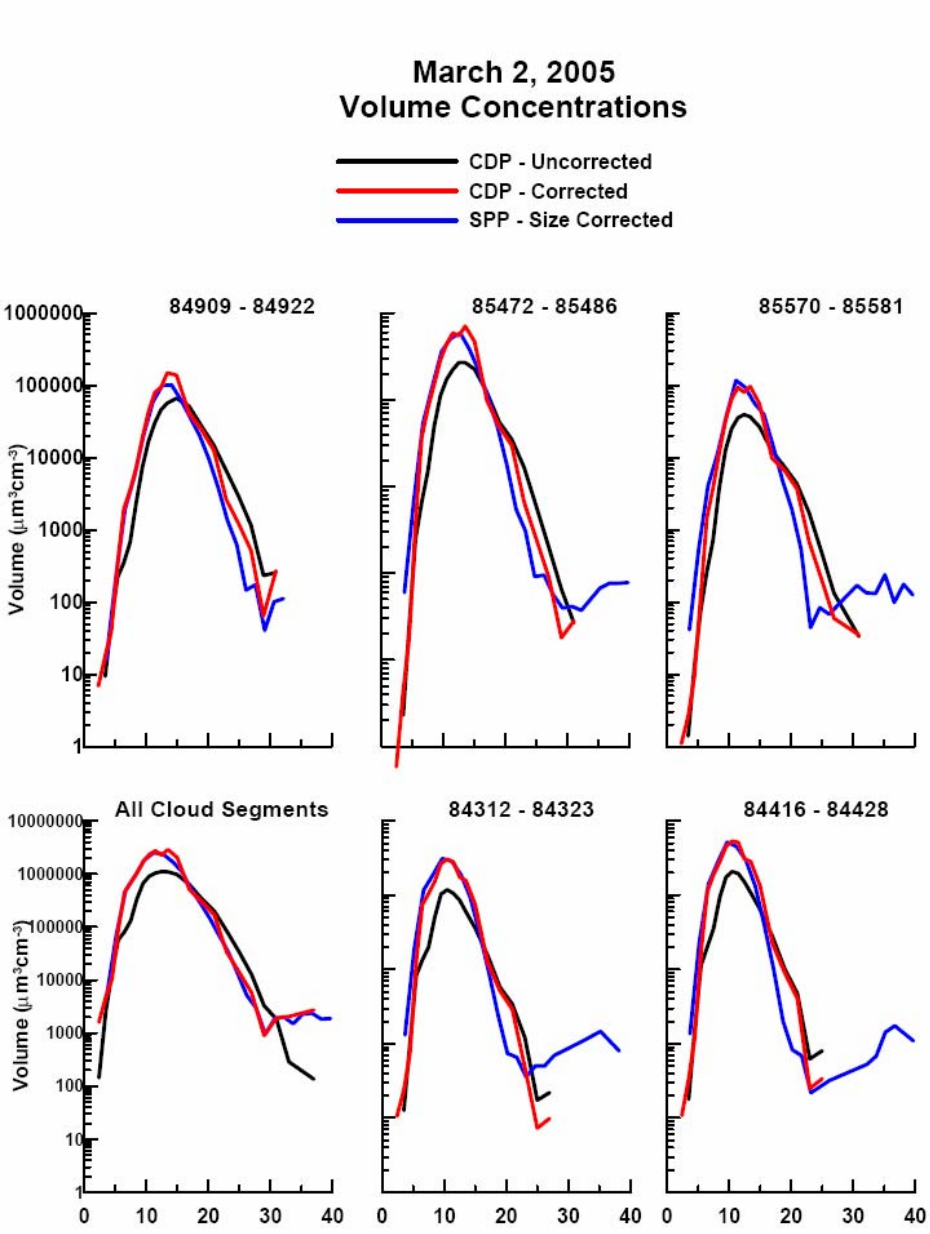

Figure 14b: Cloud droplet spectra comparisons from an additional 5 cloud passes on 2 March 2005. The blue curves in the size distribution graphs are the airspeed corrected FSSP SPP-100 spectra, the black curves are CDP spectra calculated using the nominal, constant sample area, and the red curves are the CDP with sample areas that vary with particle size.

This leads to the conclusion that the sample area for the CDP should be much smaller for sizing bins < 8 μm and somewhat larger for sizing bins > 16 μm. The sample areas are also sensitive to particle velocity, but no correction has been applied to these data in figures 14a and b.

In the graphs of size distribution, the first panel at the bottom left is the average over all clouds. The other distributions are clouds where the aircraft spent at least 10 seconds in cloud at droplet concentrations greater than 100 cm^{-3}. In this analysis, the airspeed corrected FSSP is in good agreement with the CDP corrected with sample areas that vary with particle size. In the 2–3 μm range the discrepancy is sometimes greater than seen in the average comparisons.

Additional analysis with corrections for airspeed for each FSSP and CDP channel showed that both the FSSP and the CDP were very sensitive to airspeed. The plots in Figure 15 show how the CDP and the FSSP droplet spectra data for 2 March 2005 differ at airspeeds ranging from 70 to 100 ms^{-1}. This data analysis led to the development of refined correction factors for both probes.

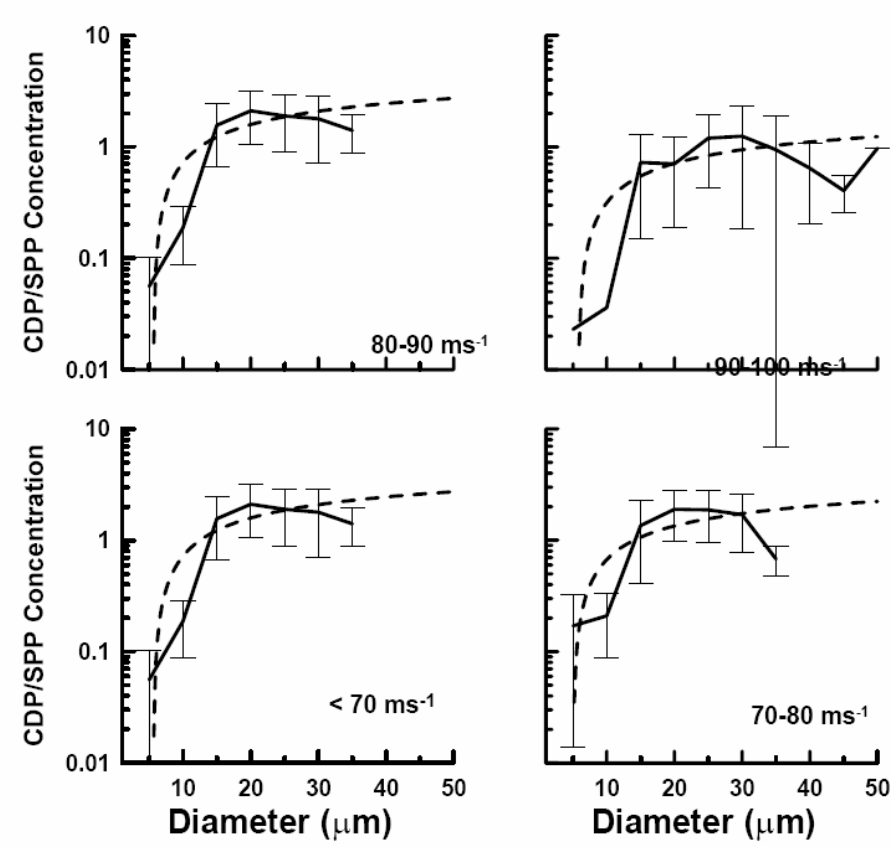

Figure 15: Correction factors as a function of TAS and size for the CDP (solid line) and the FSSP SPP-100 (dashed line)

In summary, the comparison between the CDP and SPP-100 on 2 March 2005 could provide sufficient data for reprocessing the CDP data with size dependent sample areas and arrive at size distributions and cloud microphysical parameters that are consistent with the FSSP SPP-

100. In the SUPRECIP final report, the CDP uncorrected data is used. In these data, the large drops (> 25 μm) are thought to be accurate, but the small drops (< ~14 μm) are increasingly underestimated with decreasing size, and therefore the drop counts are underestimated by a factor of 2 to 4. The effective diameter is also affected, because the large drops dominate them. Therefore, the decision was made to use differential concentrations in the final report, since this analysis would minimize the errors associated with the CDP and FSSP comparisons.

Ultimately, the CDP and the FSSP are expected to perform differently within a certain range of expected uncertainty that is typical in forward scattering spectrometer probes. During SUPRECIP 2, it is recommended that the SOAR research aircraft be equipped with both the CDP and FSSP. This should provide an excellent data set for probe comparison and for the collection of cloud microphysical data.

APPENDIX C

SUPRECIP Flight Summary

Date	Flight #	CLOUD PHYSICS Flight Duration	CLOUD PHYSICS Cum. Hours	FERRY TIME Flight Duration	FERRY TIME Cum. Hours	Comments (purpose of flight)	Analysis Priority (Low 1-5 High)	Weather conditions & areas flown
1/27/2005	1	0:00	0:00:00	2:00	2:00	Ferry to Texas A&M University College Station to pickup DMA/TDMA.		
1/28/2005	2	0:00	0:00:00	2:00	4:00	Ferry from Texas A&M University College Station.		
2/1/2005	3	1:35	1:35:00	0:00	4:00	First calibration flight for AIMMS-20 Air Data Probe in the SUPRECIP area of study. Conducted flight profiles to calibrate the dynamic heating affect on the temperature sensor at a low and high altitude and the acceleration gyro sensors.	2	
2/2/2005	4	2:00	3:35:00	0:00	4:00	Second calibration flight for AIMMS-20 Air Data Probe in the SUPRECIP area of study. Conducted flight profiles to calibrate the heater bias affect on the temperature sensor at a low and high altitude, the relative humidity dry bias and confirm that aerodynamic coefficients converge.	2	
2/3/2005	5	1:11	4:46:00	0:00	4:00	First instrumented flight in the SUPRECIP area of study. During this flight all the instrumentation was on except for the DMA/TDMA. The main objective of this flight was to conduct a similar flight profile that is expected to be flown in orographic clouds. The TAWS and TCAS systems on the aircraft were checked.	2	SKC
2/6/2005	6	1:14	6:00:00	0:00	4:00	Instrumented flight. Conducted cloud top penetrations on the windward side of the Sierra Nevada Mountains east of Sacramento. The main objective was to test the cloud physics package.	2	Orographically induced clouds developed over the windward side.

2/7/2005	7	3:22	9:22:00	0:00	4:00	Instrumented flight. Conducted various cloud penetrations on the windward and lee side of the Sierra Nevada Mountains east and northeast of Sacramento. The main objective was to conduct microphysical measurements of orographic clouds.	5	Frontal & orographic clouds. Windward & lee side from South of Lake Tahoe to Lake Almanor.
2/7/2005	8	0:40	10:02:00	0:00	4:00	Cloud Droplet Probe failed.		
2/11/2005	9	2:20	12:22:00	0:00	4:00	DMA/TDMA testing and CDP testing. Flight through continuous supercooled cloud on the windward side of the Sierra.	4	
2/13/2005	10	1:01	13:23:00	0:00	4:00	Instrumented flight. Testing of collective data system and flight through thick cloud layer over the Central Valley south of Sacramento.	4	
2/14/2005	11	2:15	15:38:00	0:00	4:00	Instrumented flight. Emphasis on CCN/TDMA measurements. Flight through cloud layers from the surface up to crest level on the windward side. Vertical profile through a visibly polluted "brown" cloud of convective cumuliform structure.	5	
2/18/2005	12	0:52	16:30:00	0:00	4:00	Instrumented flight. Flight through layered cloud with snow precipitation.	4	
2/20/2005	13	3:19	19:49:00	0:00	4:00	Instrumented flight. Conducted various cloud penetrations on the windward and lee side of the Sierra Nevada Mountains east and northeast of Sacramento. The main objective was to conduct microphysical measurements of clouds associated with a low pressure that moved onshore.	5	
2/20/2005	14	1:10	20:59:00	0:00	4:00	Instrumented flight. Conducted cloud penetrations on the windward side of the Sierra Nevada Mountains northeast of Sacramento.	4	
2/21/2005	15	2:42	23:41:00	0:00	4:00	Instrumented flight. Conducted cloud penetrations through convective clouds from cloud base to 20000 feet in the vicinity of the foothills of the Sierra Nevada.	5	

2/25/2005	16	3:48	27:29:00	0:00	4:00	Instrumented flight. Conducted extensive cloud penetrations in a shallow stratiform cloud deck in the central valley, cloud penetrations over the water west of San Francisco and cloud penetrations over orographic cumulus that developed over the coastal range.	5
2/27/2005	17	1:43	29:12:00	0:00	4:00	Instrumented flight. Conducted cloud penetrations in layered cloud on the lee side of the Sierra Nevada and through mountain wave clouds over the high Sierra crest. Conducted CCN DMA/TDMA measurements below the boundary layer in the central valley.	4
2/28/2005	18	2:40	31:52:00	0:00	4:00	Instrumented flight. Conducted cloud penetrations in precipitating thin layered cloud on the lee side of the high Sierra Nevada peaks and conducted CCN DMA/TDMA measurements from the crest down to the central valley.	5
2/28/2005	19	2:16	34:08:00	0:00	4:00	Instrumented flight. Conducted cloud penetrations in cumulus clouds over the coastal range, over the foothills and the Sierra crest. Emphasis on drop size distributions of the sampled clouds and on CCN DMA/TDMA measurements.	5
3/2/2005	20	2:58	37:06:00	0:00	4:00	Instrumented flight. Conducted cloud penetrations in post frontal clouds over the foothills and convective towers over the Sierra crest. Clouds were sampled extensively on the windward (west) side of the Sierra. Conducted CCN DMA/TDMA measurements.	5
3/2/2005	21	1:12	38:18:00	0:00	4:00	Instrumented flight. Conducted cloud penetrations in shallow cumulus clouds to the east of Sacramento and over the foothills. The main objective of this flight was to document the cloud droplet concentrations using two different probes, the Cloud Droplet Probe (CDP) and the Forward Scattering Spectrometer Probe (FSSP-100).	5
3/4/2005	22	1:53	40:11:00	0:00	4:00	Instrumented flight. Conducted cloud penetrations in layered cloud west of Sacramento, over the coastal range, north of San Francisco and over the coast.	5
3/4/2005	23	3:15	43:26:00	0:00	4:00	Instrumented flight. Conducted cloud penetrations in layered and cumulus cloud over the central valley, the coastal range and maritime cumulus clouds off the coast.	5

APPENDIX D

Documentation of Cloud Structure during Two Flights on February 28, 2005

The first flight on February 28, 2005 was made in the dry slot after the cold front but before the arrival of the post frontal convection. The tail of the cold front was receding to the SE. The purpose of the flight was to make morning measurements in the tail of the front. The pollution was trapped in the BL (boundary layer) within the stratus and Sc. The frontal cloud band of this very weak weather system was shallow, but disconnected from the surface, so that the clouds remained pristine and acted as Hawaiian orographic clouds. Documentation of this is presented here. There are good pictures documenting the looks of these clouds, as well as good in situ and satellite documentation, all supporting the same impressions.

A photograph of the drizzling clouds is given in Figure 1. Cloud tops were only 2,100 m. The plotted droplet spectra are given in the inset. The first number in the legend is the aircraft altitude in meters and the second number is the GMT time of the cloud pass. Note that the droplet spectrum is very wide, as is typical of highly maritime clouds. The droplet images at

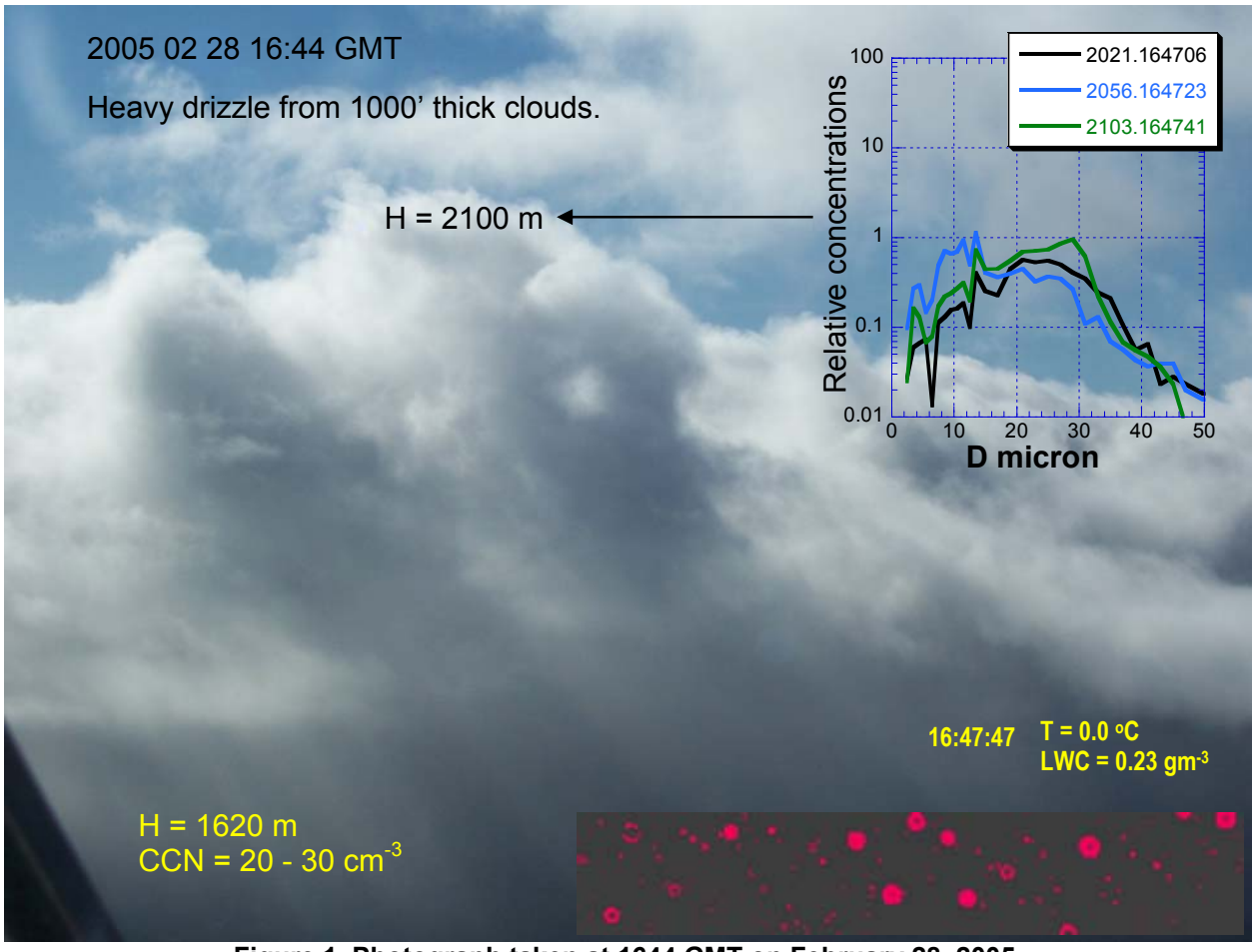

Figure 1. Photograph taken at 1644 GMT on February 28, 2005.

164747 GMT from the CIP probe at roughly 0°C at an altitude of about 2,100 m are shown in the lower right inset. To size the drops note that the vertical width of the strip is 1,500 mm, so the largest drop is roughly one-tenth the strip width or roughly 150 µm. The maximum cloud water content during this pass was 0.23 gm m^{-3}. The CCN counts were on the order of 20 to 30 cm^{-3}.

A larger view is given in Figure 2. The precipitation from the elevated shallow clouds can readily be seen in the image. The cloud thickness was only about 500 m. Clouds were growing also in the boundary layer, where the CCN counts were much higher, beneath the precipitating clouds. It is important to note that if the precipitating clouds had ingested the pollution aerosols from the boundary layer, it is doubtful that they would have produced any precipitation.

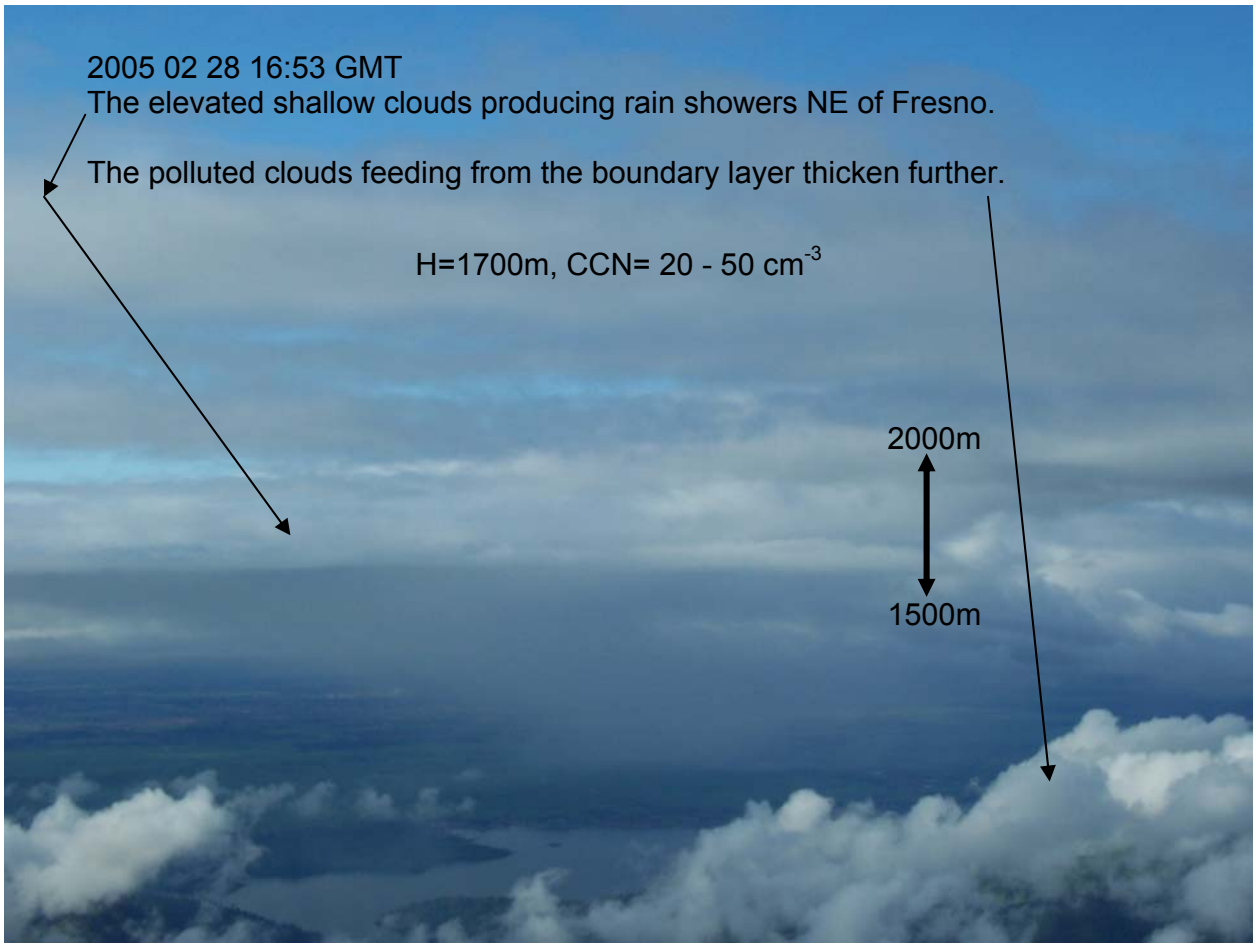

Figure 2. Photograph taken at 1653 GMT on February 28, 2005

Figure 3 gives an additional view of the clouds from 1,700 m. The inset plot in the lower right corner of the figure shows a very broad droplet spectrum, indicating large drops. Indeed, this is supported by the droplet images and by the weak rainbow in the left-center of the picture.

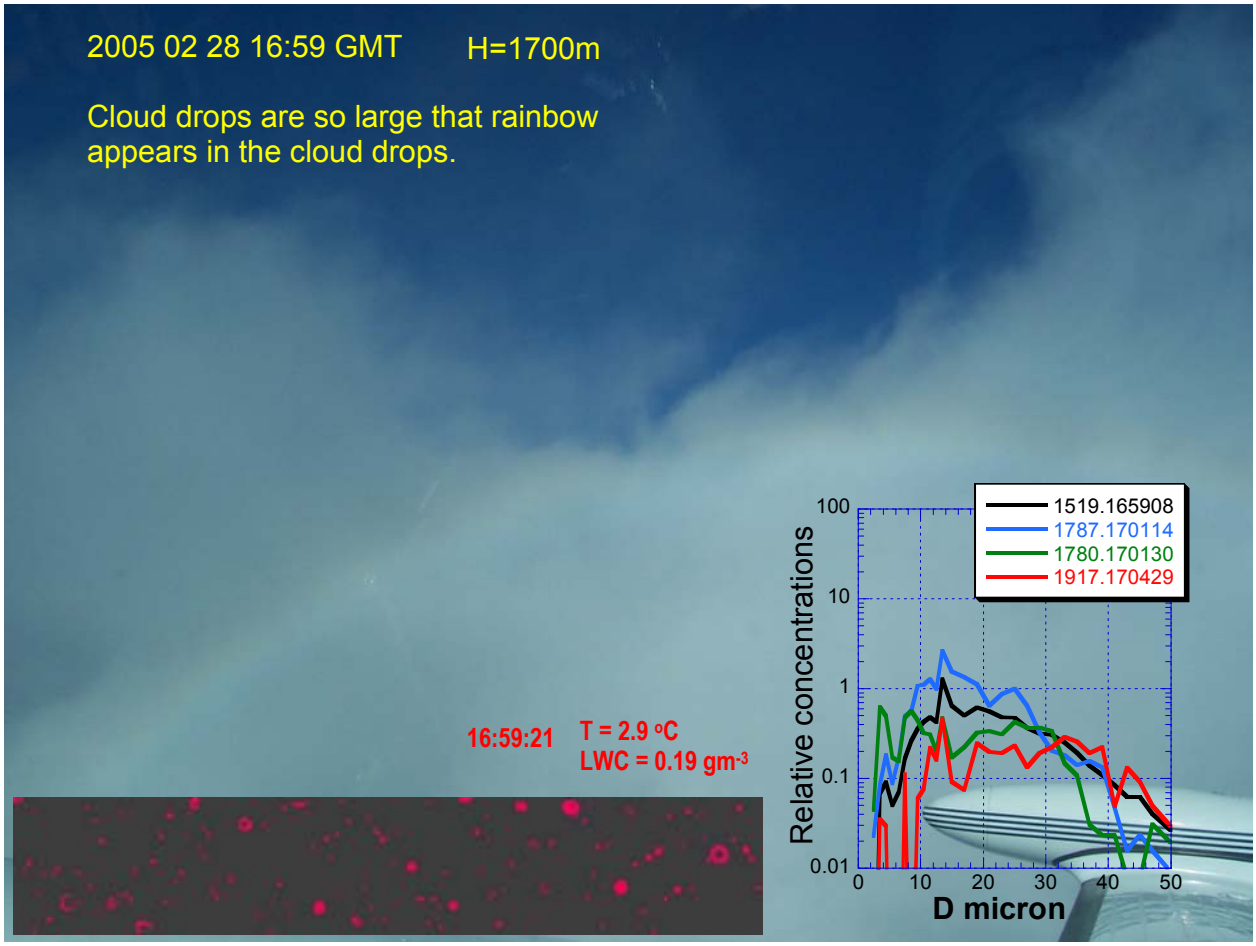

Figure 3. Photograph taken at 1659 GMT on February 28, 2005

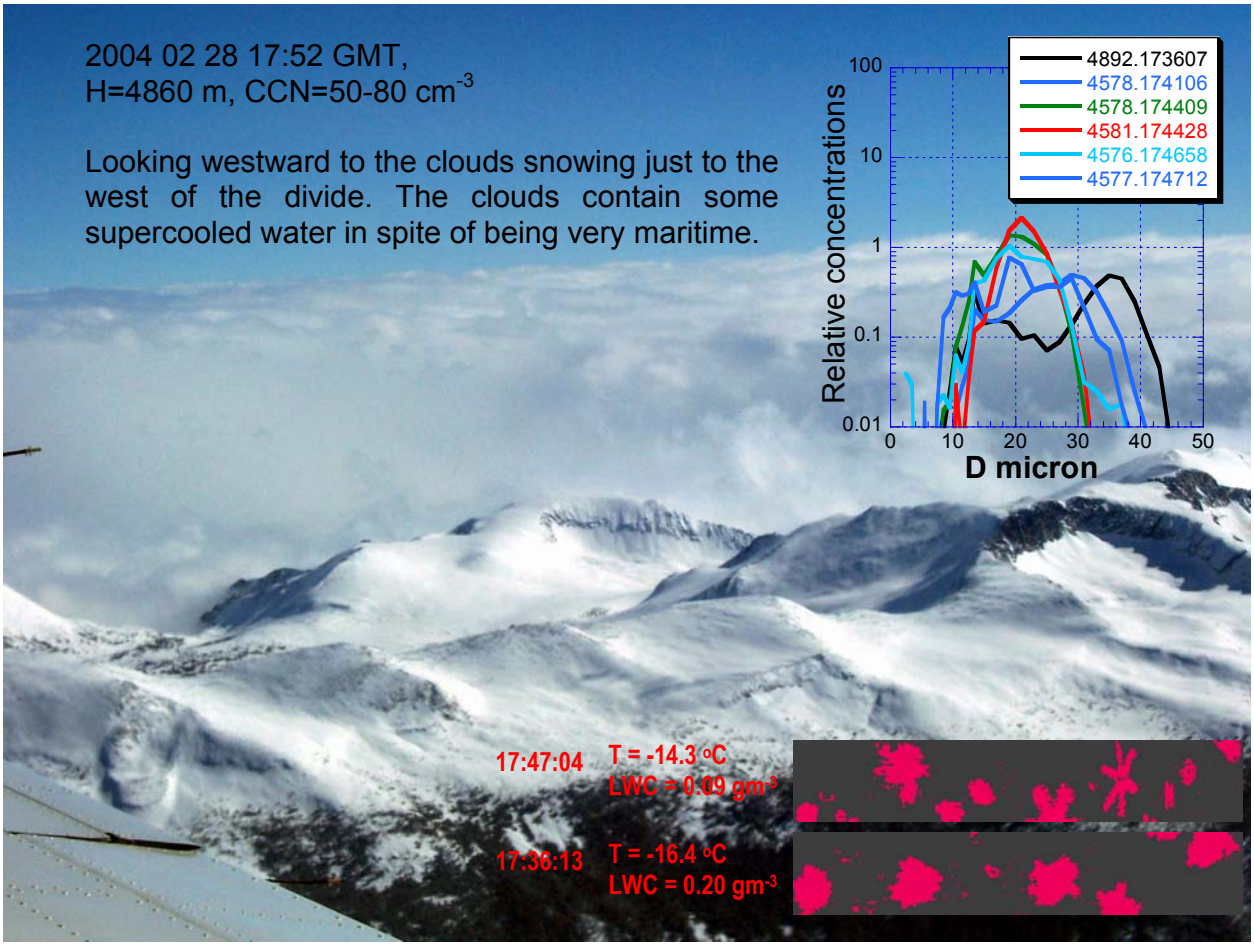

Figure 4. Photograph taken at 1752 GMT on February 28, 2005

Figure 4 shows that by 1752 GMT, the aircraft had climbed above 4,000 m while flying to the east toward the Sierra crest. Note that there were six cloud passes during the climb (see right insert). Again, the spectra are quite broad. The particle images in this instance are ice crystals at temperatures as cold as -16°C. The view in the picture is looking back to the west from just east of the Sierra crest. Note that the wall of cloud ends right at the crest with cloud dissipation and evaporation occurring on the east side. These clouds appear to be highly efficient precipitators, as would be expected, since the precipitating clouds farther to the west readily precipitated, even though they were quite shallow.

By 1822 GMT the aircraft had returned to the boundary layer near Sacramento and was preparing to land, as shown in Figure 5. Note that the CCN counts at 600 m were around 100 cm^{-3} but at 400 m above the ground the CCN counts ranged from 600 to 1,000 cm^{-3}. The inset plot in the right corner for the clouds growing in the boundary layer shows high concentrations of small drops, as would be expected from the CCN counts.

During the afternoon the front continued to recede to the SE as it dissipated. Weak post frontal convection developed during the day over the northern Sierra and coastal ranges and produced some cellular radar echoes (see Figure 6). The cloud droplet concentrations were clearly higher in the vicinity of San Francisco and Sacramento, becoming less than half the urban values some 30 miles to the north. The background concentrations were not maritime,

because of the general regional haze that occurred also over the ocean. Evidently the weak front that passed last night did not flush the surface layer. There was a huge contrast between the morning clouds that precipitated very readily; whereas the afternoon clouds over the Sierra did not reach mature precipitation processes, even though they were much thicker (Figure 7). Although the clouds belonged to a very weak system, the contrast in the microphysical and precipitation properties was highly evident, and clearly related to the differences in the aerosols that these clouds were ingesting. From that standpoint this is a very important illustration of the crucial role that aerosols play in determining cloud structure and precipitation.

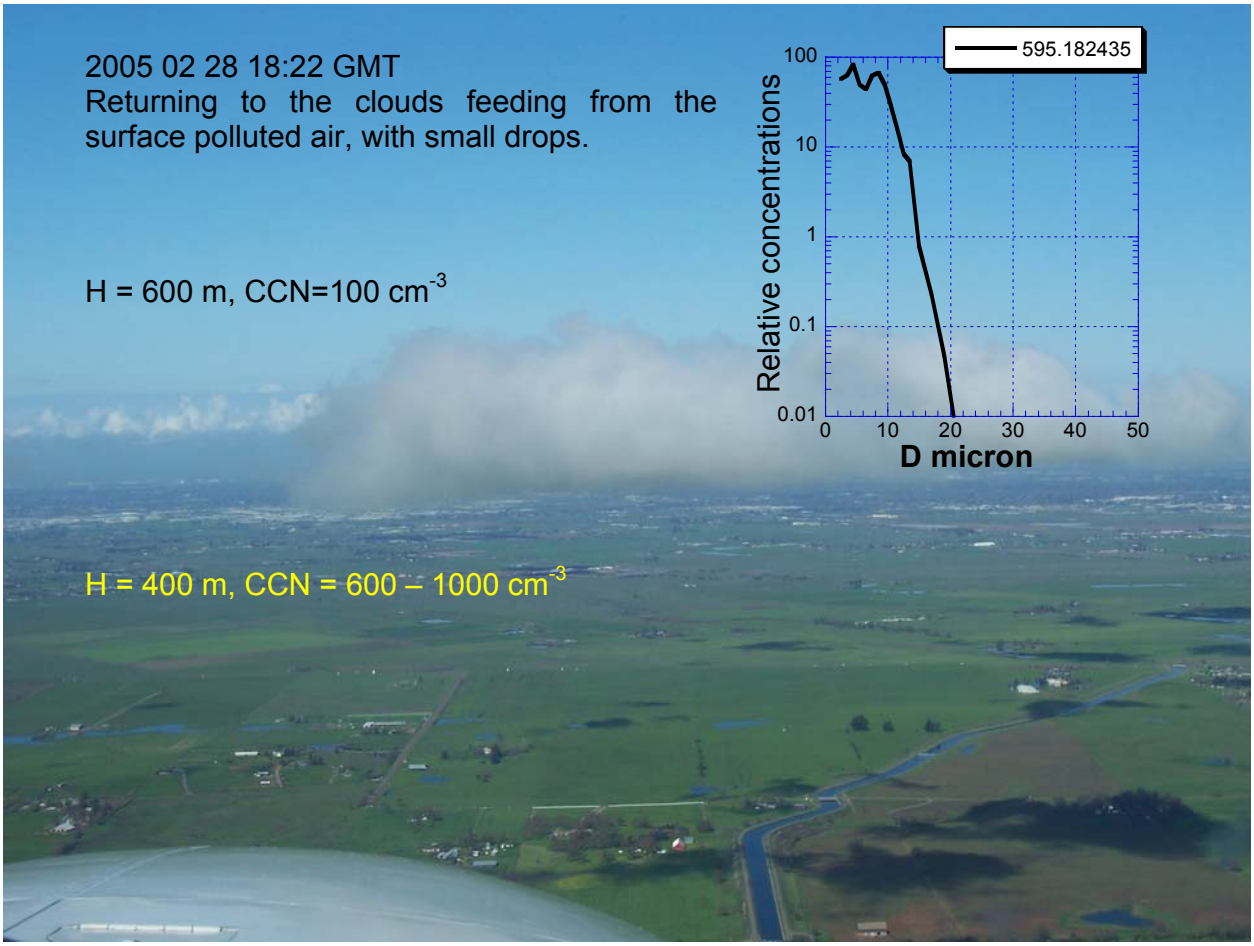

Figure 5. Photograph taken at 1822 GMT on February 28, 2005

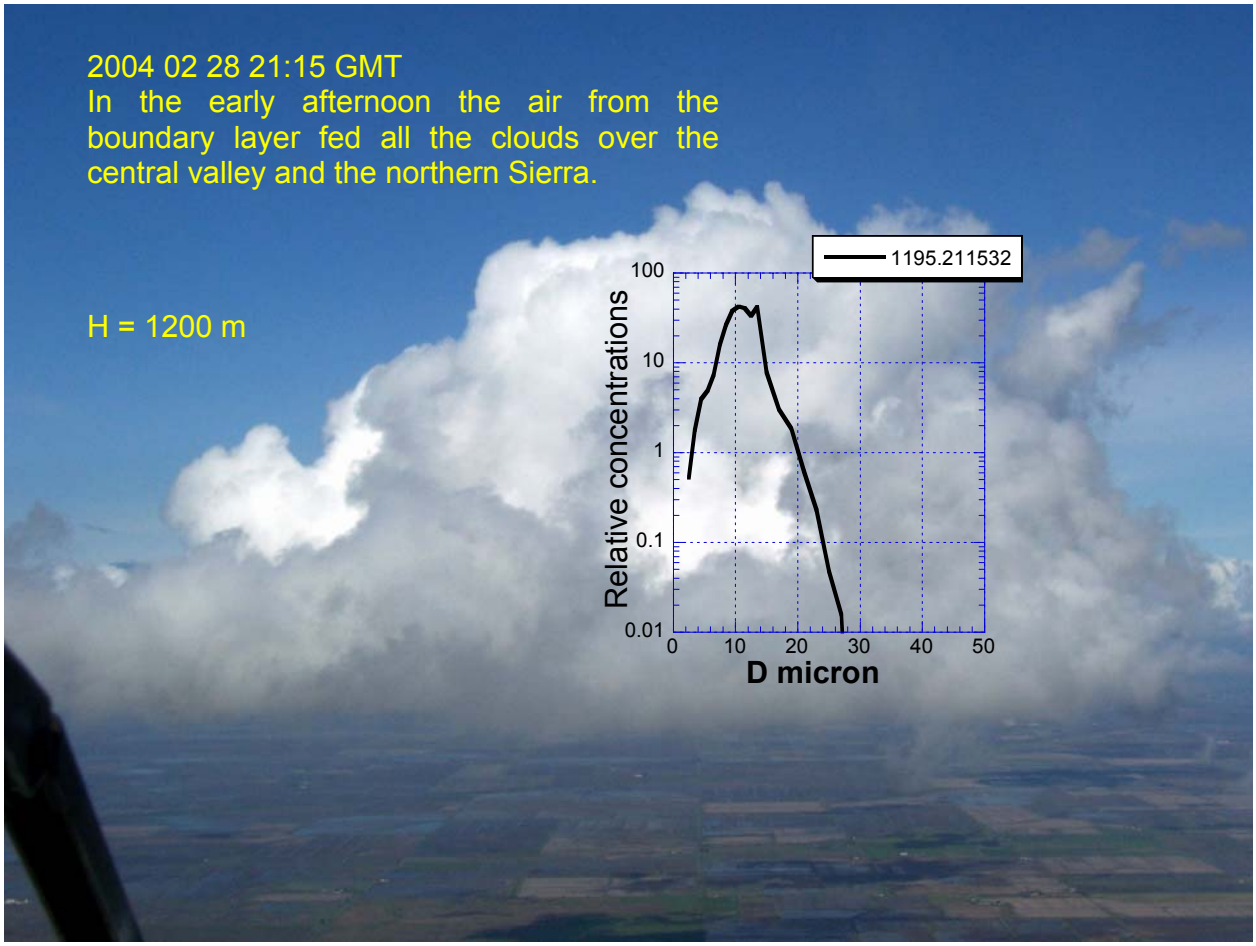

Figure 6. Photograph taken at 2115 GMT on February 28, 2005

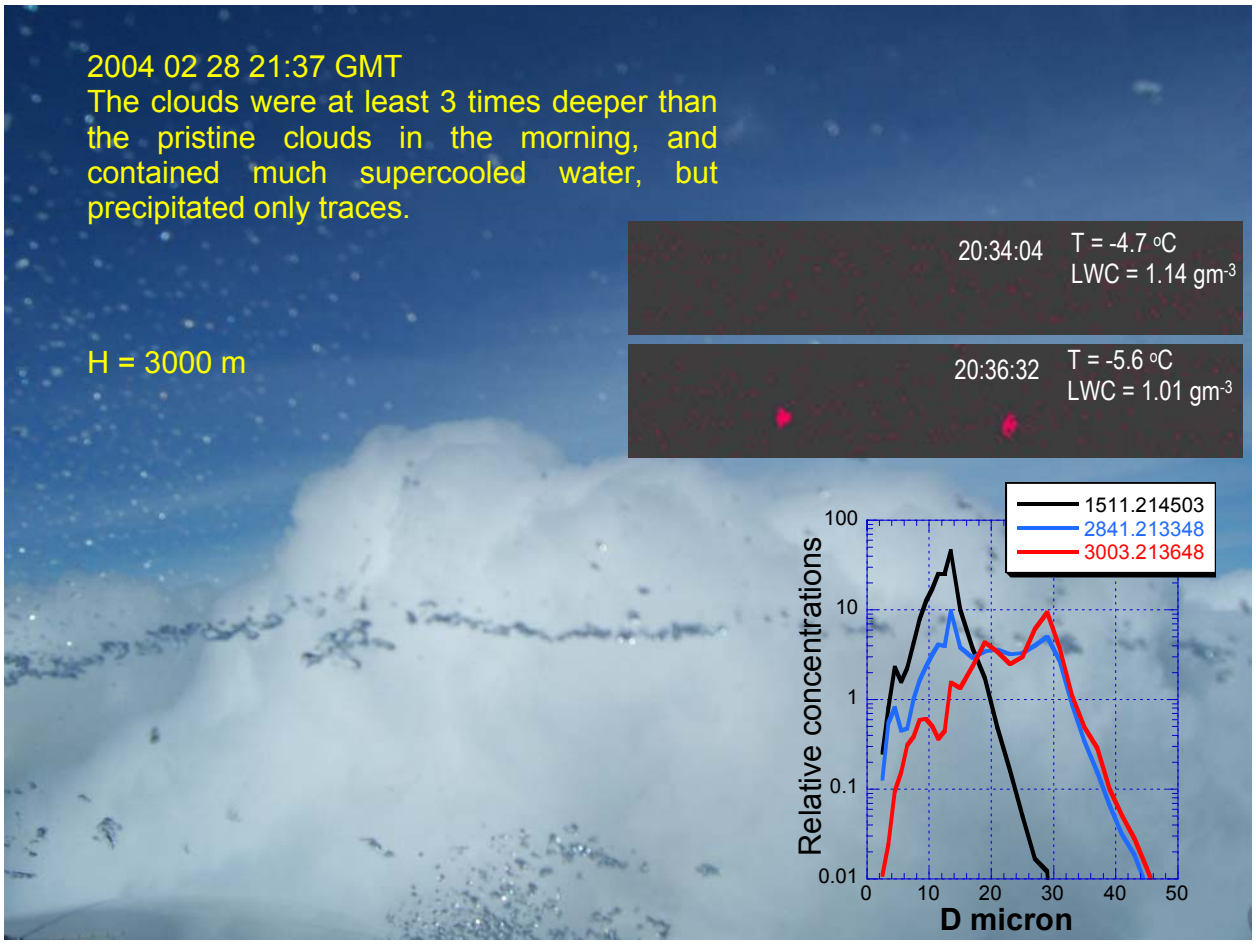

Figure 7. Photograph taken at 2137 GMT on February 28, 2005. See the text and the figure inserts for details.

APPENDIX E

DATA INVENTORY FOR SUPRECIP 1

Because of its great interest in sound science, Woodley Weather Consultants will make its SUPRECIP-1 data available to the scientific community for scientists interested in conducting their own analyses. WWC plans to develop a SUPRECIP-1 data CD or DVD and to make it available to reputable scientists upon their request. The contact person to request the data is Dr. William L. Woodley, President of Woodley Weather Consultants, at 303-979-7946 or williamlwoodley@cs.com. The content of the data CD or DVD is documented in this appendix.

Each flight has a folder that contains:

1. Document file FlightReportyyyymmddn n.doc

A document containing the flight report as written by the flight scientist at the end of the day.

2. Folder Pics

A folder containing the pictures taken during the flight.

3. Folder Sat

A folder containing the satellite images for the flight.

4. Folder ACFT

A folder containing the aircraft instruments raw data for the flight.

The data file types are:

4.1 SACyyyymmddnASC.txt

A summary file of all the main flight and instrument data.

4.2 SACyyyymmddnCDP.txt

The cloud drop spectra measured by the CDP instrument.

4.3 SACyyyymmddnCIP.txt

The precipitation particle spectra measured by the CIP instrument.

4.4 SACyyyymmddnPCA.txt

The aerosol spectra measured by the PCASP instrument.

4.5 CCN data yymmddhhmmss.txt

5. Folder CN_CCN_CDP

Summary graphs of the time and height march of the DMA, CCN and CDP data. This is for obtaining quick looks on the relations between the aerosols and cloud drop concentrations at the various segments of the flights. The data are provided with the height and geographic context. Each flight segment is shown on a flight trajectory map.

6. Folder H_CIP_CDP

Summary graphs of the time and height march of the CCN and CDP and CIP data. This is for obtaining quick looks on the relations between the CCN, cloud drop concentrations and precipitation at the various segments of the flights. The trajectory maps are provided in folder CN_CCN_CDP.

7. Folder DSD_txt

Summaries of combined CDP and CIP particle size distributions for automatically divided individual cloud passes. There are three kinds of files:

7.1 DSDyyyymmdd_hhmmss.txt

Each file represents data from one cloud pass. The individual 1-sec distributions and overall pass summary are provided.

7.2 DSDyyyymmdd_hh.txt

There is one such file, which contains one data column for each cloud pass, that contains the averaged DSDs and their integral DSD properties.

7.3 PASyyyymmdd_hh.txt

There is one such file, which contains a table with one row for each cloud pass, that contains the integral DSD properties.

8. Folder DSD_Plots

Plots of the CDP and CIP particle averaged size distributions for the automatically divided cloud passes.

9. CIP_Images

Selected CIP images.

10. Radar

Selected radar images.